1·0

2·8   2·5

5·0   3·15   2·2

5·6   3·5

1·1   4·0   2·0

4·5

1·8

1·25   1·4   1·6

NATIONAL BUREAU OF STANDARDS
MICROCOPY RESOLUTION TEST CHART

ARO 12680.6-E

LEVEL

COLLEGE
OF
ENGINEERING

DDC
OCT 17 1978
F

VIRGINIA
POLYTECHNIC
INSTITUTE
STATE
UNIVERSITY

78 10 16 068

(9) Final rept. 15 Nov 74-31 May 78,

(11) Aug 78   (12) 138p.

(18) ARO   (19) 12680.5-E

DDC
OCT 17 1978
F

(6) UNSTEADY LAMINAR SEPARATION
-AN EXPERIMENTAL STUDY.

by

(10) D. P. Telionis and C. A. Koromilas
August 1978

Report No. (14) VPI-E-78-24

Virginia Polytechnic Institute and State University
Department of Engineering Science and Mechanics
Blacksburg, VA 24061

404 722

78 10 10 065

REPORT DOCUMENTATION PAGE		READ INSTRUCTIONS BEFORE COMPLETING FORM
1. REPORT NUMBER	2. GOVT ACCESSION NO.	3. RECIPIENT'S CATALOG NUMBER
4. TITLE (and Subtitle) UNSTEADY LAMINAR SEPARATION -AN EXPERIMENTAL STUDY		5. TYPE OF REPORT & PERIOD COVERED Final, 15 NOV 1974- 31 MAY 1978
		6. PERFORMING ORG. REPORT NUMBER VPI-E-78-24
7. AUTHOR(s) D. P. Telionis and C. A. Koromilas		8. CONTRACT OR GRANT NUMBER(s) DAHC04-75-G-0067
9. PERFORMING ORGANIZATION NAME AND ADDRESS Virginia Polytechnic Institute and State Univ.		10. PROGRAM ELEMENT, PROJECT, TASK AREA & WORK UNIT NUMBERS
11. CONTROLLING OFFICE NAME AND ADDRESS U.S. Army Research Office Post Office Box 12211 Research Triangle Park, NC 27709		12. REPORT DATE August 1978
		13. NUMBER OF PAGES
14. MONITORING AGENCY NAME & ADDRESS(if different from Controlling Office)		15. SECURITY CLASS. (of this report) Unclassified
		15a. DECLASSIFICATION/DOWNGRADING SCHEDULE NA

16. DISTRIBUTION STATEMENT (of this Report)

Approved for public release; distribution unlimited.

17. DISTRIBUTION STATEMENT (of the abstract entered in Block 20, if different from Report)

NA

18. SUPPLEMENTARY NOTES

The findings in this report are not to be construed as an official
Department of the Army position, unless so designated by other authorized
documents.

19. KEY WORDS (Continue on reverse side if necessary and identify by block number)

Laminar   Reversing Flows
Boundary Layers
Separation
Unsteady
Oscillatory

20. ABSTRACT (Continue on reverse side if necessary and identify by block number)

The design of most aerodynamic surfaces, as for example the heli-
copter rotor, is based essentially on quasi-steady theories. However
the dynamics of a rotating blade introduce unexpected fluctuations and
overshoots of properties like lift, drag, etc. The phenomenon of un-
steady stall is intimately connected with the development of an
oscillating boundary layer and separation. Experimental investigation
of such flows was undertaken by a method of visualization developed

DD FORM 1473 1 JAN 73   EDITION OF 1 NOV 65 IS OBSOLETE

especially for the study of laminar or turbulent boundary layers and separation. The method captures the instantaneous 2-D flow field, including regions of separated flow and provides accurate quantitative information. Laser doppler anemometer measurements complement the optically received data. Results reveal that separation responds with time-lag to external disturbances, in agreement with unsteady stall data. Oscillating outer flows result in displacement of the point of separation and under certain conditions, the Despard and Miller criterion was found to hold. Earlier theoretical models of separation are confirmed qualitatively and for the early stages of the transient phenomena. The findings provide physical insight and quantitative data that may help understand the phenomenon of unsteady stall and unsteady separation.

ABSTRACT

The design of most aerodynamic surfaces, as for example the helicopter rotor, is based essentially on quasi-steady theories. However the dynamics of a rotating blade introduce unexpected fluctuations and overshoots of properties like lift, drag, etc. The phenomenon of unsteady stall is intimately connected with the development of an oscillating boundary layer and separation. Experimental investigation of such flows was undertaken by a method of visualization developed especially for the study of laminar or turbulent boundary layers and separation. The method captures the instantaneous 2-D flow field, including regions of separated flow and provides accurate quantitative information. Laser doppler anemometer measurements complement the optically received data. Results reveal that separation responds with time-lag to external disturbances, in agreement with unsteady stall data. Oscillating outer flows result in displacement of the point of separation and under certain conditions, the Despard and Miller criterion was found to hold. Earlier theoretical models of separation are confirmed qualitatively and for the early stages of the transient phenomena. The findings provide physical insight and quantitative data that may help understand the phenomenon of unsteady stall and unsteady separation.

i

ACKNOWLEDGMENTS

TABLE OF CONTENTS

viii

INTRODUCTION

Potential-flow theory has been an invaluable tool for the designer in a variety of engineering applications of aerodynamics. It is well known, however, that this has been possible only via appropriate heuristic assumptions, as for example the Kutta-Joukowski condition, which replace the catalytic role played by viscosity. Alternatively, potential theory may be supplemented with a boundary-layer calculation. Today it is widely accepted that viscous effects, although very often confined to small areas, control and regulate basic features of the flow field, as for example, circulation. As a result, aerodynamic character-istics of significant engineering importance, like lift and drag, depend on the development of a viscous layer and its downstream fate which may or may not experience transition to turbulence and separation to a wake.

In unsteady aerodynamics viscosity has again reserved for us some unexpected surprises. It is the agent responsible for phenomena that cannot be predicted or explained with potential theory and quasi-steady viscous models. Some typical examples: dynamic stall of lifting sur-faces, stall flutter of helicopter rotor blades, rotating stall in engine compressor blades, etc. Most of such phenomena can be attributed to the nonlinear character of the viscous layers that generate space and time phase differences, non-linear steady streaming, separation delay, viscous damping, etc.

Some of the most spectacular dynamic effects that clearly demonstrate the futility of quasi-steady solutions are connected with unsteady separation. Experimental evidence has indicated, for example,

1

that the stalling characteristics of airfoils in unsteady flow deviate
substantially from the quasi-steady case. The phenomenon is well known
in literature as "unsteady stall" and is due to the fact that for a
sharp increase of the angle of attack the upstream propagation of
separation appears to be delayed. As a result, the airfoil remains
unstalled for a while, at angles of attack that are well beyond the
static stall angle of attack.

An experimental study of unsteady separation was undertaken a few
years ago at VPI & SU. This is the first complete report of the
experimental findings. The work was confined essentially to laminar
flows. All the facilities described here were constructed especially
for this project. These are: one open channel, a small water tunnel
with a free surface and a medium speed water tunnel.

The main efforts of this work were directed towards the immediate
neighborhood of separation. Flow-visualization methods and laser-doppler
velocimetry were used. Numerous difficulties were encountered in the
design of the facilities and the appropriate models to exhibit the
dynamic characteristics of separation encountered in common Aeronautical
applications. It is a very unfortunate and difficult task for experi-
mentalists to search for phenomena described earlier by theoreticians.
The present results shed some more light to the problem revealing
clearly some features of the flow that were predicted theoretically
but also indicating the need to reconsider and reframe the theory.

This report includes only a small portion of the data received
throughout the period of the last few years. Reduction and interpretation
of the data is presented here as well. However, due to the difficulty

of the problem, it is very possible that alternative interpretations

may be offered which may in fact prove eventually to be more reasonable.

CHAPTER 1

REVIEW OF LITERATURE AND PRESENT EXTENSIONS

Separation is usually defined in aerodynamics as the breakaway of
the flow from a bounding surface and the initiation of a wake. For
the case of steady two-dimensional or axisymmetric flow over fixed
walls, a criterion for separation was suggested by Prandtl [1] (see
Fig. 1.1)

$$\frac{\partial u}{\partial y} = 0 \text{ at } y = 0 \qquad (1.1)$$

where u is the velocity component parallel to the wall and y is the
coordinate perpendicular to the wall. This criterion proved to predict
the phenomenon correctly and it has been used extensively by both
theoreticians and experimentalists for over fifty years. However,
Sears [2], Moore [3] and Rott [4, 5] demonstrated that Prandtl's
criterion (Eq. (1)) is inadequate for cases other than steady flow
over fixed walls and indicated the need for a generalized definition
and a convenient criterion for separation. They also suggested in-
dependently a more appropriate criterion for the case of steady flow
over moving walls, namely (see Fig. 1.2)

$$\frac{\partial u}{\partial y} = 0 \text{ at } u = 0 \qquad (1.2)$$

Sears [2] and Moore [3] proposed a definition of unsteady sepa-
ration which is essentially equivalent to the above condition, Eq. (1.2),
expressed in a coordinate system moving with the point of separation.

4
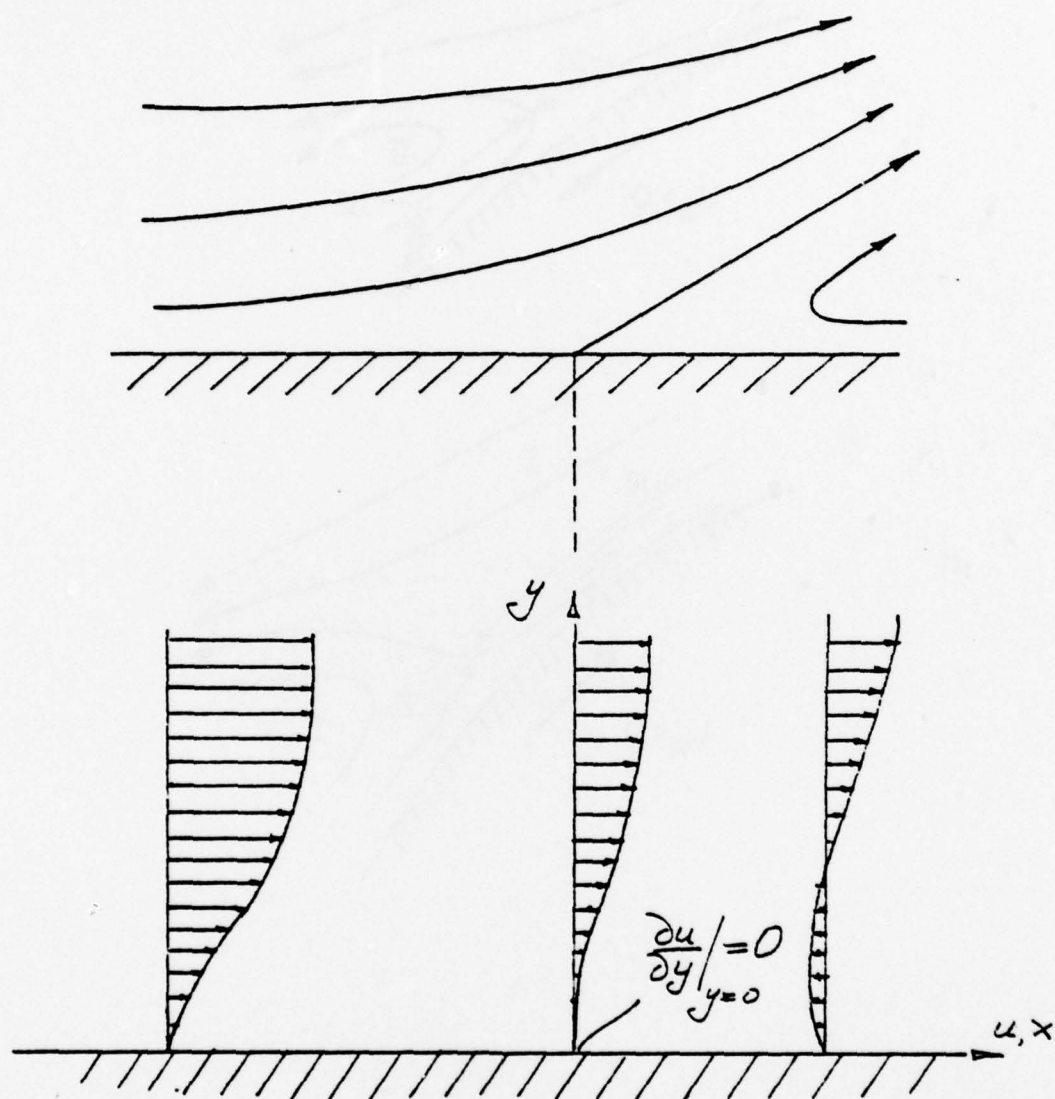
Fig. 1.1   Separation over a fixed wall

6
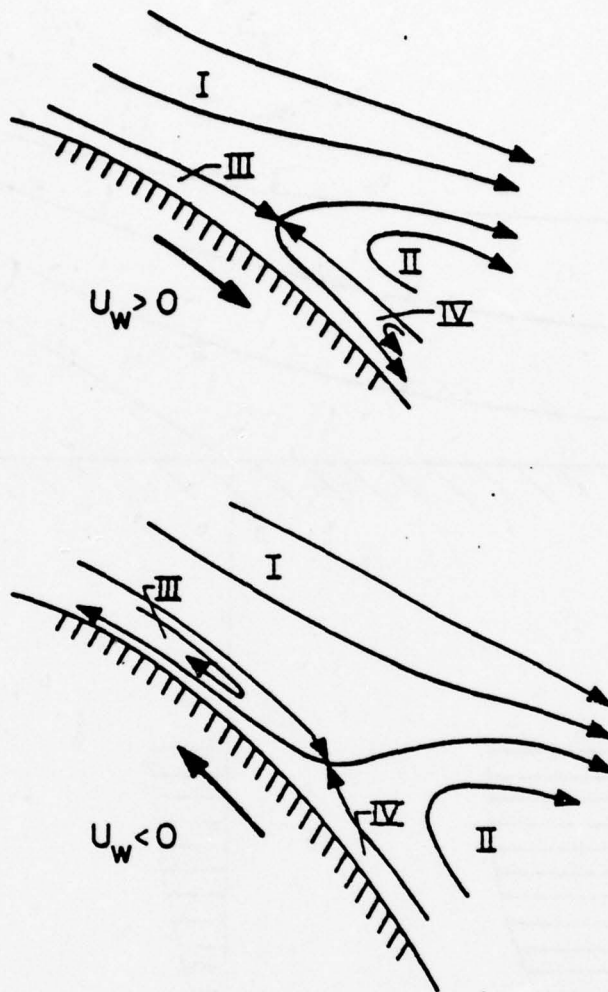
Fig. 1.2   Separation over moving walls

Vidal [6] and later Ludwig [7] performed experiments with a cylinder rotating in the test section of a wind tunnel. Using hot-wire anemometers, they were able to verify the theoretical model of equation (2) at least for the case of downstream moving walls. Tennant and his associates (Tennant [8]; Tennant and Yang [9]) also performed experiments with moving boundaries for both laminar and turbulent flow. Their findings pertain to skin velocities much larger than the free stream and always downstream motion of the skin. Despard and Miller [10] again inspired by the analytical work of Moore [3] for laminar flow and the experimental work of Sandborn [11] for turbulent flow, considered the problem of an oscillating outer-flow velocity and proposed a definition for a mean location of separation. Working with air and using hot-wire anemometers, they were also able to verify that in unsteady flow the location of zero skin friction is not necessarily related to the phenomenon of separation. In a very recent effort, Simpson [12] and Kenison [13] investigated experimentally the neighborhood of separation of an oscillating turbulent boundary layer. Kenison reports that as separation is approached, fluctuating velocity overshoots and phase angles indicate sharp changes. However, the basic features of oscillating turbulent separation are similar to those of laminar separation.

Telionis and Werle [14] showed analytically that for steady boundary-layer flow over moving walls, the location of zero skin friction is nonsingular, while a typical separation singularity appears at the station where Moore, Rott and Sears predict separation. A substantial number of analytical investigations on the topic have

already appeared as reviewed recently by Sears and Telionis [15] and Williams [16]. However, the available experimental data up to now is inadequate to validate the models of unsteady separation.

The work of Vidal and Ludwig pertains only to steady flow and the work of Despard and Miller is confined to oscillatory flows with high frequencies and Reynolds numbers. Our knowledge, therefore, about this complex phenomenon is remarkably narrow and seriously in need of more intensive investigation. This can be accomplished both by methods of flow visualization and by hot wire or laser anemometery techniques. Visualization methods were employed by Schraub et. al. [17], Werle [18], Ruiter, Nagib and Fejer [19], McCroskey [20] and McAlister and Carr [21] to study unsteady viscous flow phenomena, but the specific cases considered and the scale of the models were designed for a study of the entire flow field. There was no emphasis on the features of the unsteady boundary-layer and in particular separation.

In a more recent effort Carr, McAlister and McCroskey [22] employed a variety of sensing devices ranging from flow-visualization methods (tufts, smoke) to pressure and velocity measuring methods (pressure transducers, hot wire anemometers etc.) to study the phenomenon of unsteady stall. In this study some basic features of unsteady separation were verified. In particular, pressure and velocity signatures throughout a period of oscillation are given for different stations on the airfoil and compared with flow-visualization data. A more complete account of this work is reported in Ref. 23 in which the authors also present estimates of the unsteady drag force and the characteristics of

the pressure response which are intimately connected with unsteady

separation and symptomatic of the occurence and relative severity of

moment stall.

In the present report the results of experimental investigations

of unsteady separation are reported. In an effort to receive

an overall picture of the phenomenon, we decided to magnify and

visualize the immediate neighborhood of separation. To this end a

lowspeed water tunnel was designed and constructed. Flow visualization

was accomplished by dispersion of solid particles with density very

close to the density of water. The method developed and described in

this report can capture approximately the instantaneous velocity

field. Boundary layer velocity profiles were obtained in this manner

for transient and oscillatory velocity fields. Glycerin-water mixtures

were used to achieve low-Reynolds-number flows with measureable magni-

tudes of velocity.

In earlier visualization studies of separation it was attempted

to generate information about the whole flow field. As a result, the

details and the mechanism of unsteady separation were not adequately

revealed. In the present study, special effort is directed towards

the amplification of the neighborhood of separation. In most of the

flows visualized the frame of visualization is of the same order of

magnitude as the boundary-layer thickness. Except for the work of

Despard and Miller [10], quantitative boundary-layer data in the

neighborhood of unsteady laminar separation are presented here for the

first time. Despard and Miller concentrated on oscillatory flows. In

the present report we compare our data with those of Despard and
Miller and reconfirm the validity of their definition for separation
in oscillatory laminar boundary layers. The present study proceeds
further in the area of transient and impulsive flows to provide data
that appear useful to numerical analysts.

CHAPTER 2

STEADY FLOWS OVER MOVING WALLS

The experimental evidence up to now seem to support the M.R.S.

criterion (Eq. 1.2) at least for the case of a downstream moving wall.

However, the saddle-point-streamline pattern suggested by Moore, Rott

and Sears has not been verified analytically. This is due to the fact

that for moderate Reynolds numbers, the wake is turbulent. In this

chapter we report on our experimental efforts to visualize streamline

patterns in the neighborhood of separation over downstream and up-

stream moving walls. "Saddle-point" patterns are captured for the

first time. Some interesting new information is also included about

the overall validity of the M.R.S. criterion in the case of an upstream

moving wall. This work was performed in an open channel designed and

constructed especially for this project.

The flows considered here are steady. However there is a very

strong similarity between steady separation over moving walls and un-

steady separation over fixed walls as Moore and Sears have pointed

out.

2.1 The Open Channel

Open-channel-flow facilities offer some distinct advantages over

closed tunnels, essentially because it is very convenient to insert

and secure the models in the proper position. In our case

the models or other auxiliary equipment are required to perform some

type of dynamic motion, and this is particularly difficult to achieve

in water tunnels. The open facility appeared further to be very

11

attractive in the initial phase of our project, when a large number of models and shapes had to be tested until the optimum combination could be chosen.

The flow is driven in this facility by a centrifugal pump (Fairbanks, Morse Co., 1160RPM, 4"ϕ) which discharges into a 18 cm diameter plastic pipe (see Fig. 2.1). This pump is certainly not ideal for such a facility because it generates an unwanted head, but it was available in the Engineering Science and Mechanics shop and its use appeared satisfactory for the initial steps of this work. Artificial head loses were provided by a valve connected at the discharge of the pump. The pipe directs the flow into an open container where perforated sheets and screens eliminate the large-scale vorticity. After a small converging section, the flow goes through a honeycomb and into the test section which is an open rectangular section 47 x 31 cm.

Models were inserted in the middle of the open section and the flow was visualized at the free surface or at horizontal planes beneath the free surface. Surface-flow visualization is straightforward and does not require any special lighting facilities or particles with special buoyancy properties. For visualization beneath the surface, it is necessary to generate a flat sheet of light. This is accomplished by a system of lenses and a narrow slot on the wall of the channel (see Fig. 2.2). The photographic equipment is mounted above the channel as shown in Fig. 2.2. A 16 mm movie camera with speeds up to 80 frames per second (AROFLEX-S) and a 35 mm motor-drive still camera (NIKON-F2) with a MICRO-NIKKOR 55 mm lens were used to record the flow.
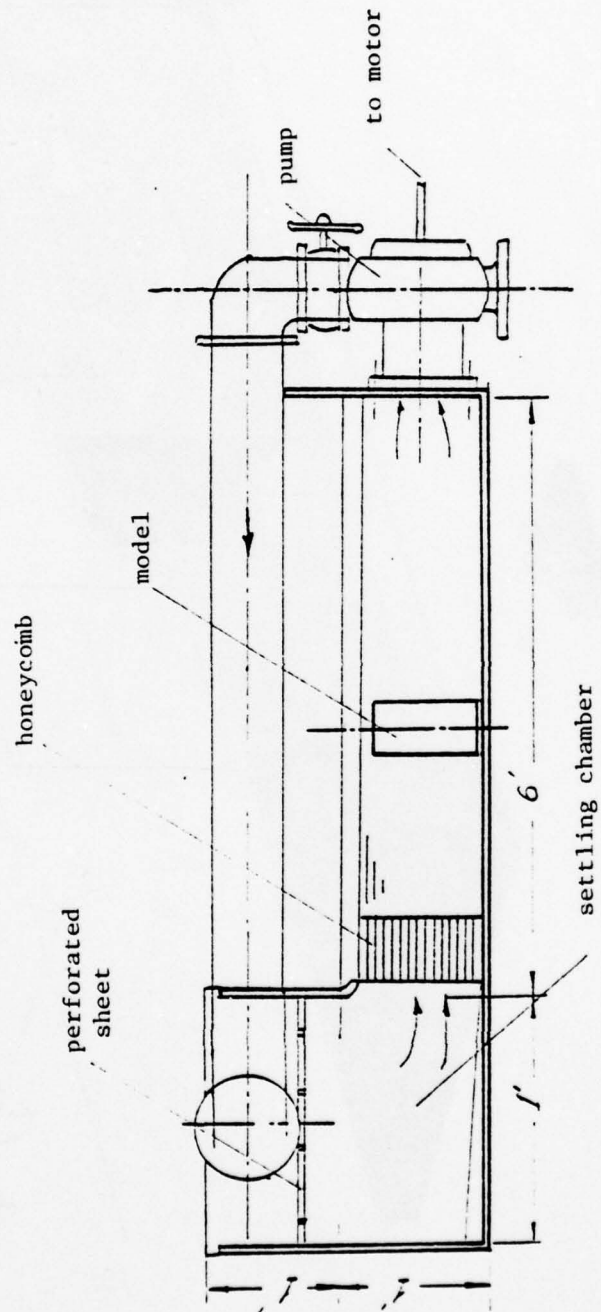
Fig. 2.1 The open recirculating tank
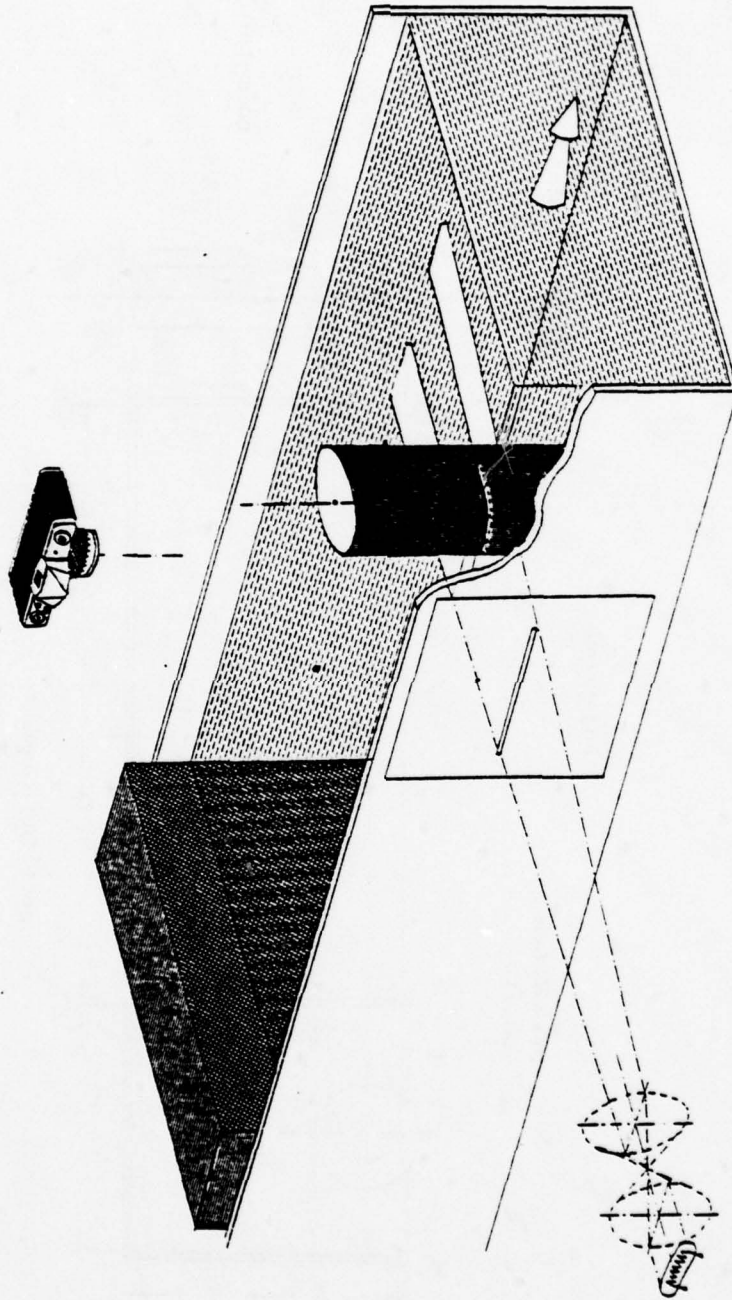
Fig. 2.2   Schematic representation of the optical
arrangement and the test section

Flow visualization was achieved at first with hydrogen bubbles and pliolite particles. These methods did not prove convenient for our open-channel facility: the first, due to the necessity of special designs for locating wires next to moving walls, the second due to problems with proper lighting and visualization across the free surface of the medium.

In this phase of our work we were interested mostly in low Reynolds number flows and such flows were produced with water-glycerin mixtures. However it was discovered that such mixtures quickly become milky if they are subjected to violent turbulent motion. Indeed the flow goes through a region of strong forced mixing in the pump and the valve that follows and this makes it very hard to visualize the flow beneath the free surface. Most of the experiments with glycerin-water mixtures were performed with surface pellets and surface visualization.

The flow over a circular cylinder was chosen for two basic reasons. On one hand the flow about a fixed circular cylinder is well documented and comparison with earlier analytical and numerical results is possible. On the other hand rotation of the cylinder about its axis of symmetry leaves the potential flow undisturbed, at least if the secondary effects of wake distortion are ignored. The skin motion is then the only disturbance of the flow. Any other configuration would require a system of belts on the skin of the body in order to achieve boundary motion with no disturbance of the outer flow.

The flow was visualized on the surface with dyes injected upstream of the cylinder. Black buoyant pellets were also used to visualize particle paths. Still photographs of the flow were taken with exposure

times of 1/2, 1/4 sec. and 1/8 sec. In these photographs established
dye paths appeared, clearly marking the wake region as shown in Fig.
2.3. Moreover, the pellets appear as shaded segments on the film.
These segments are proportional to the average velocity of the particle,
provided the streamline curvature effects are not very strong. All
the experiments were performed with a 50-50% water-glycerin mixture
which achieves a viscosity of 7 centipoise.

Experiments were performed with a fixed cylinder of 11 cm in
diameter, in order to compare with earlier experimental data. It
should be noted that for the low Reynolds numbers tested, the wake is
made up of two finite closed recirculating bubbles. In Fig. 2.4 we
compare the length of the wake as measured in our flow-visualization
pictures with theoretical results compiled by Pruppacher et. al [29]
and the experimental data of Homann [30], Fage [31] and Taneda [32].
Figure 2.5 shows the location of separation for different Reynolds
numbers. The present results are in good agreement with earlier
analytical and experimental results.

2.2 Separation Over Moving Walls

The flow over a rotating cylinder was studied for Reynolds numbers
ranging from 35 to 600 and velocity ratios u_w/U_∞ = 0.4 to 1.4 where u_w
is the velocity of the cylinder skin and U_∞ is the velocity of the
undisturbed flow. This corresponds to velocity ratios of approximately
u_w/U_e = 0.2 to 0.7 where U_e is the outer flow velocity in the neighbor-
hood of separation, that is at $\Theta = 90°$. The wake of the rotating
cylinder for u_w/U_∞ = 0.8 with separation over the downstream moving wall,
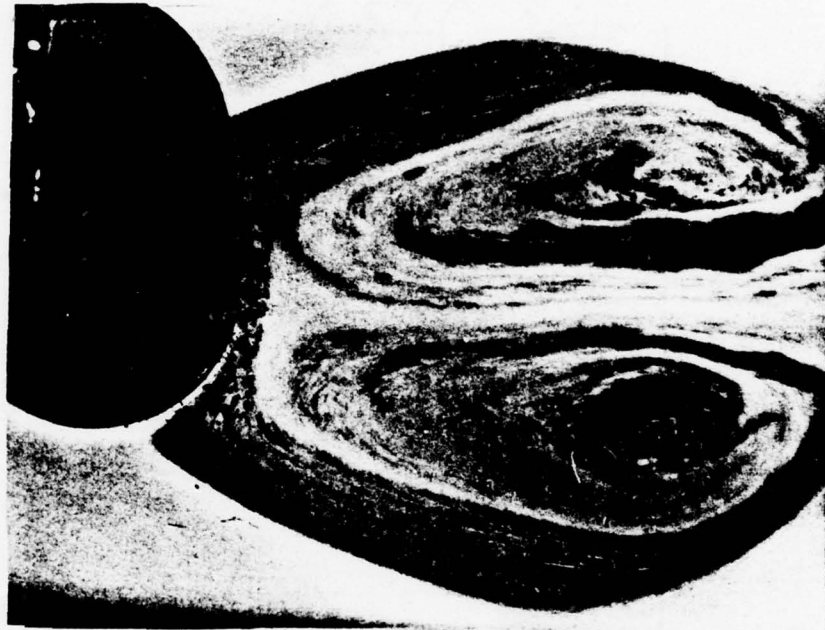
Fig. 2.3   The wake of a circulat cylinder for R_e = 40
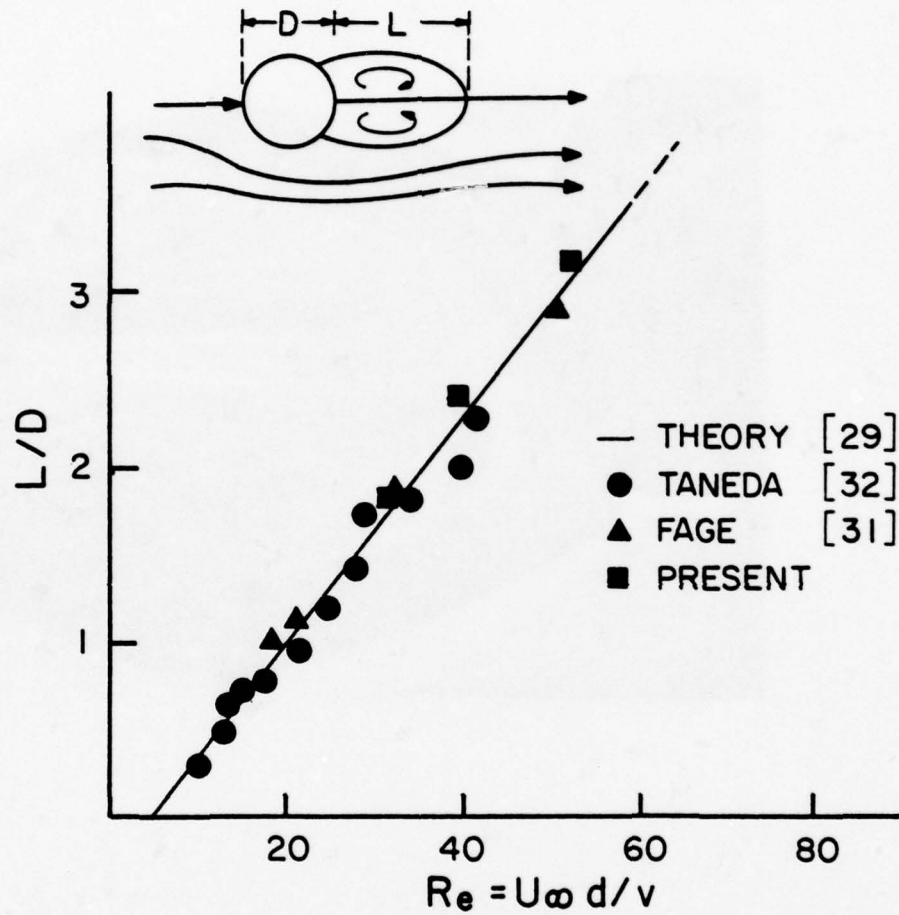
Fig. 2.4   The length of the wake as a function of the
            reynolds number
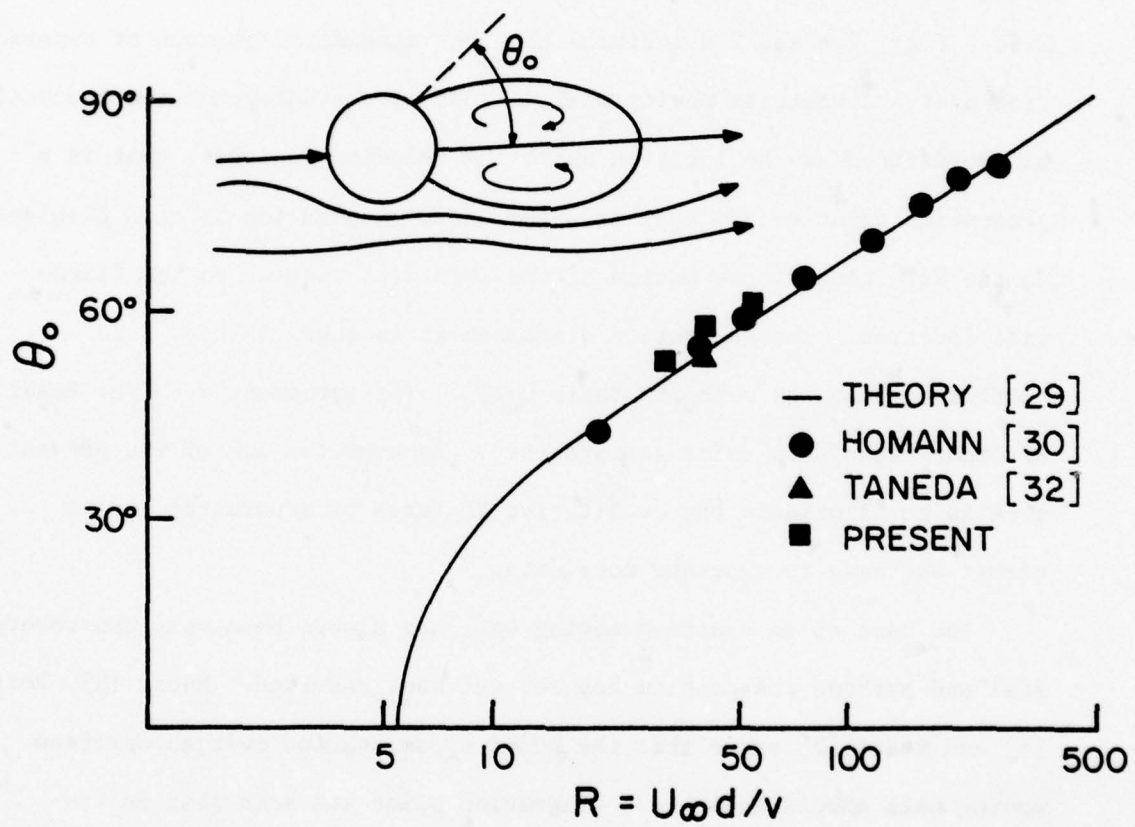
Fig. 2.5   The angle to separation as a function of the
            Reynolds number

is shown in Fig. 2.6. Fig. 2.7 shows the other side where the flow is opposed by the motion of the skin. The immediate neighborhood of the points of separation is visualized better by shorter film exposures and larger magnification.

Figs. 2.8b and 2.9b show the streamline pattern in the neighborhood of separation as received from the flow visualization of Figs. 2.8a and 2.9a. Figs. 2.6 and 2.8 indicate that the streamline pattern of separation over a downstream moving wall is that of a saddlepoint and separation may be defined as the location where the velocity vanishes, that is a stagnation point exists away from the wall. Separation is then displaced in the direction of the motion of the skin with respect to its fixed-wall location. The separation displacement is shown in Fig. 2.10 plotted against the velocity ratio u_w/U_∞. The agreement with the results of other methods is quite satisfactory. However the aim of the present work is to illucidate the qualitative features of separation and no effort was made to generate more data.

The case of an upstream moving wall has always been very controversial and perhaps the problem has not yet been resolved. Moore [3], Rott [4] and Sears [2] argue that the point of separation over an upstream moving wall should again be a stagnation point and such that in its neighborhood, the same criterion is met (Eq. [1.2]). The streamline configurations suggested, however, are not in agreement as Sears and Telionis [15] emphasize. Earlier experimental evidence on the topic is inconclusive [7]. In this work it is explained that the thickness of the boundary layer on the side of an upstream moving wall is very large and a sublayer is present which appears to be coming from the

Fig. 2.6   Separation over a downstream moving wall
for $u_w/U_\infty = 0.8$ and $R_e = 50$
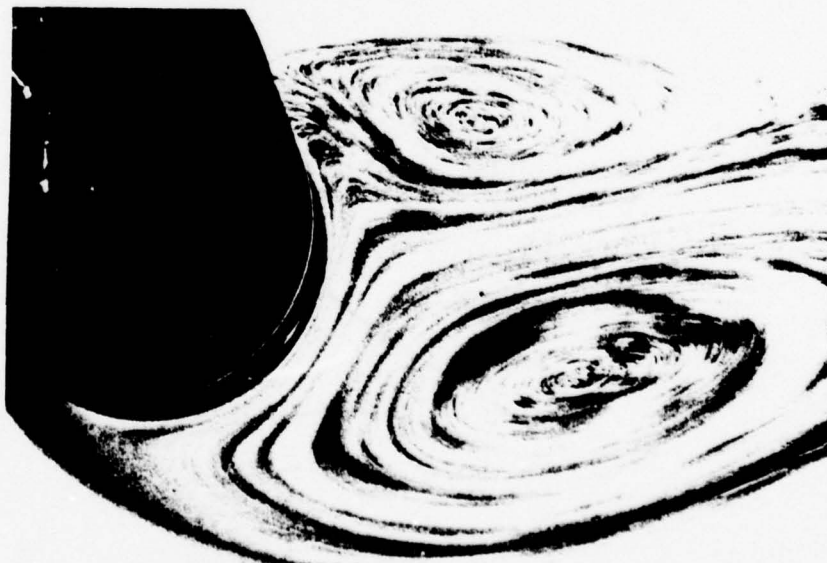
Fig. 2.7   Separation over an upstream moving wall
for $u_w/U_\infty = 0.8$ and $R_e = 50$

Fig. 2.8a   Detail showing the saddle-point pattern for a downstream
            moving wall ($u_w/U_\infty = 0.8$, $R_e = 50$)
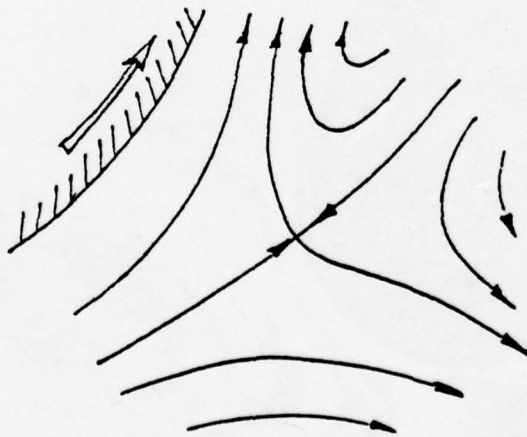
Fig. 2.8b   Streamlines obtained from Fig. 2.8a

Fig. 2.9a   Detail showing the saddle-point pattern for an upstream moving wall ($u_w/U_\infty = 0.8$, $R_e = 50$)
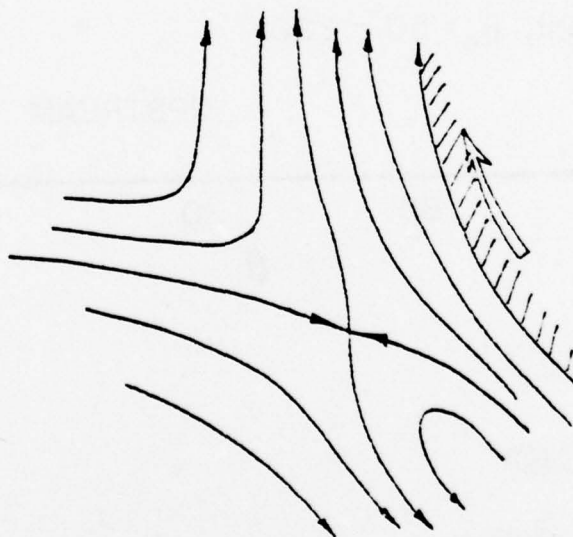
Fig. 2.9b   Streamlines obtained from Fig. 2.9a
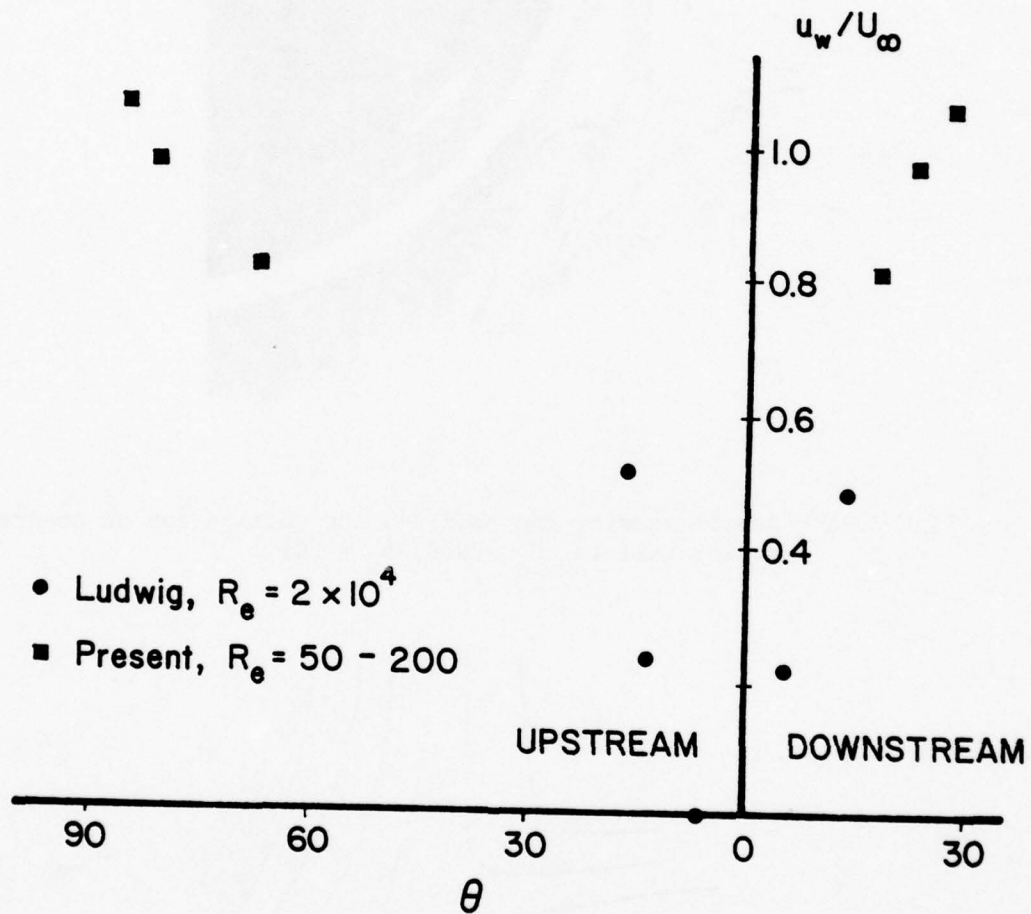
Fig. 2.10   Displacement of separation with the wall velocity ratio, u_w/U_∞.

wake. As a result, it was not possible to check the singular profile assumed by Moore, Rott and Sears. It is clear that the boundary layer equations do not accept a solution that meets the M.R.S. criterion (Fansler and Danberg [33]). However this does not exclude the possibility that the M.R.S. condition is actually met and therefore that the Navier Stokes equations could capture it. In fact Tsahalis' [34] numerical calculations indicate that, for the case of an upstream moving wall, it appears that M.R.S. conditions are approached with the same rate with which the Goldstein singularity is approached.

The present experimental evidence indicates that a saddle-point configuration exists on the side of the cylinder where the wall is moving upstream. This is shown clearly in Fig. 2.9. Therefore, the fluid in one of the four areas defined by the critical streamlines is moving with the wall in a direction opposite to the outer flow. This is in agreement with the observation of Ludwig who describes it as "a sublayer which appears to be coming from the wake." In fact it is felt that Ludwig's discovery should not at all be considered an anomaly. Such a layer would be necessary if a saddle-point pattern were to exist in this neighborhood, as Sears and Telionis [15] point out. An overall flow pattern emerges now which together with the distorted separation bubbles is shown in Fig. 2.11. The streamline pattern shown in this figure was always observed during our experiments. It was not convenient to capture it in one photograph but piecing together the information received from smaller frame pictures we arrived at the sketch of Fig. 2.11. The geometry of this figure may not be very accurate but on the other hand this is more than just a schematic of the flow field. The
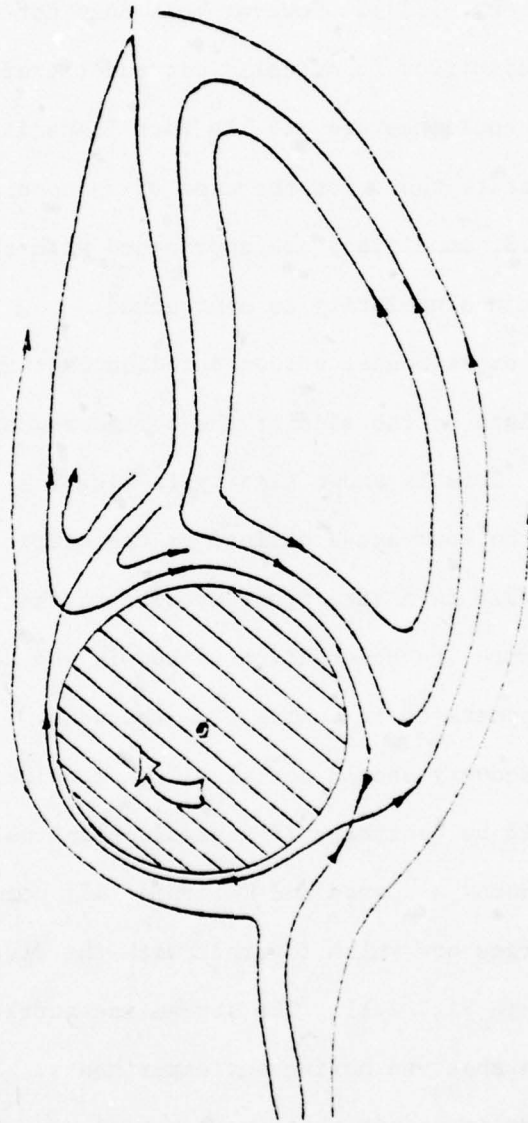
Fig. 2.11 Approximate streamline pattern for $u_w/U_\infty = 0.8$, $R_e = 50$ obtained from flow visualizations.

error involved in sketching these streamlines, that is their sidewise

displacement, was estimated to be less than 10% of the diameter of the

cylinder. The streamline pattern shown in Fig. 2.11 has only two

critical points. It appears that the upper point of separation has

merged with the rear stagnation point and the lower point of separation

has merged with the front stagnation point in agreement with earlier

conjectures of Telionis [24, 35].

CHAPTER 3

THE EXPERIMENTAL LAY-OUT

In order to eliminate the effects of free surfaces on the pressure
and velocity variations, it is necessary to work with closed test sec-
tions. In fact for larger speeds the pressure variations on configurations
of our interest generate unacceptable surface waves and distort the flow
field. Two closed circuit water tunnel facilities were designed and
constructed as described in the following section.

This study is based essentially on flow visualizations methods. It
was originally planned to investigate qualitatively and quantitatively
the immediate neighborhood of the point of separation. Flow visualization
is particularly attractive for flows that involve abrupt changes of the
velocity vector in magnitude or direction, such as separating flows.
Laser-doppler velocimetry was employed as a calibration tool. Some
measurements were also received by the LDV system, especially in oscil-
lating boundary layers. Both methods are described in the following
sections.

3.1 The VPI Water Tunnel

The basic specifications that the VPI water tunnel was expected to
meet were: a. Test sections appropriate for studying laminar or
turbulent boundary layers as well as the potential flow about simple
models. Reynolds numbers based on the length of the test section should
therefore range from 10^4 to 10^6 or more; b. Lowest possible volume so
that expensive fluids like glycerin-water mixtures, Dow-Corning Fluid

etc. could be used to fill the facility; c. Materials that would

sustain corrosive fluids as for example NaCl solutions, necessary for

hydrogen-bubble visualization, potassium permanganate and dilute acidic

solutions for dye visualization etc. It should be noted that no per-

manent dyes can be used, since the working medium is usually expensive

and cannot be disposed after a set of dye visualization experiments; d.

Operation free of vibrations. It is imperative that vibrations from the

pump and the driving motor or any device used to generate unsteady

hydrodynamic effects should not be transferred to the test section; e.

Total cost within the order of $15,000. This task appeared difficult to

meet due to unexpected rises of material costs.

To meet these specifications the tunnel shown in Fig. 3.1 was

designed. Long and carefully calculated diffusers were avoided in order

to meet the requirements of low cost and small total volume of working

medium. Synthetic materials resisting the corrosive chemicals were

chosen, namely plexiglass for the test sections and the settling chamber

and PVC pipes for the remaining sections of the tunnel.

A circular to rectangular converging section leads to the short

diffuser and the settling chamber. (see Fig. 3.1) Guide vanes situated

in the diffuser cut the size of large eddies and suppress separation

on the walls of the diffuser. At the upstream end of the settling

chamber two aluminum honeycombs are situated as shown in Fig. 3.1.

These honeycombs are made by Hexcel-Bel Air and have hexagonal openings

of approximately 3 cm^2 cross-sectional area and a diameter to length

ratio equal to 12. The diffuser, the settling chamber, the converging

section and the test sections are all constructed out of plexi-glass
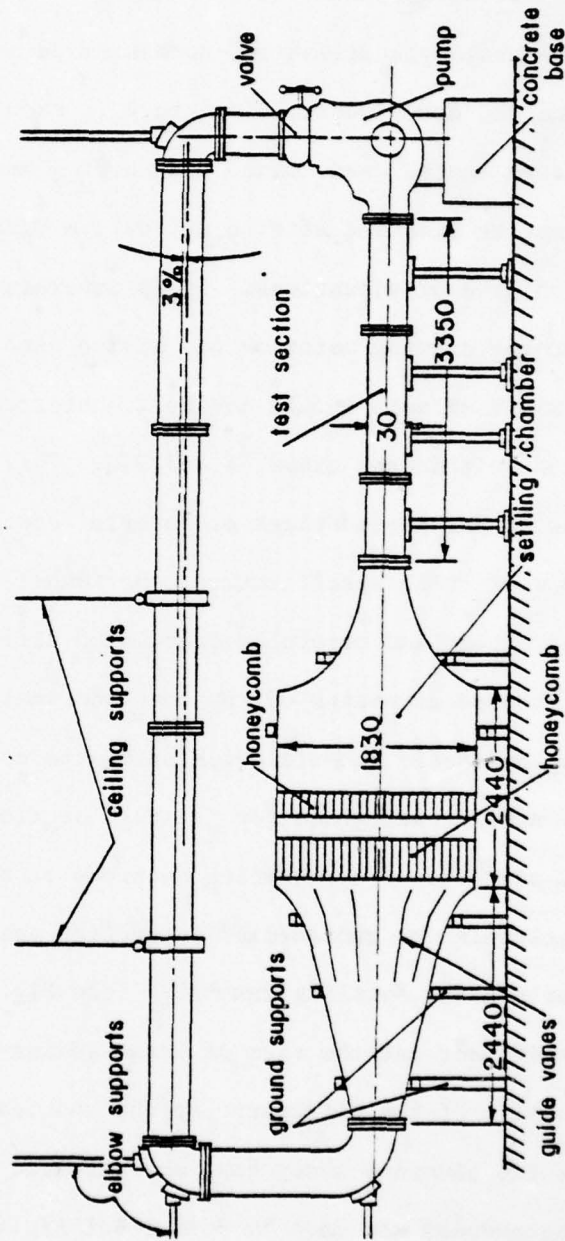
Fig. 3.1   The V.P.I. low speed water tunnel.

pieces of dimensions (3/4 in x 4 ft x 8 ft). A great effort was made to avoid large deflections of the side walls. This was accomplished by prestressed external steel reinforcements and tranverse aluminum bolts.

The converging section leads into a 25 cm x 30 cm (10 in x 12 in) rectangular test section. The test section is made up of interchangable units of 2.7 m (9 ft) total length. In this way large Reynolds numbers with not so large velocities can be achieved. A flexible shoot leads the flow into a low-head pump. The pump is made by Bell and Gossett (model: VSCS-PF, S&D 12 x 14 x 12 1/2) and has the following basic characteristics: 12 in discharge diameter, 8 ft head, and 2000 gpm flowrate. Chrome coating of the pump housing and the impeller appeared very expensive and time consuming. Instead it was decided to have these components cold-galvanized by Livingstore Coating Co. of North Carolina. Two motors are available to drive the pump. The first is a "Marathon Electric" 1170 RPM, 230V, 15 H.P. motor which can drive the system at full speed (3m/sec). To control the speed of the tunnel a DURCO BL-311 cast iron valve with a teflon lining and a stainless steel butterfly is connected to the discharge of the pump. For the low range of velocities a 2 H.P., 220 V variable speed motor (U.S. Electrical Motors with a U.S. varidrive) is also available. This motor can drive the pump with a range of 292-1170 RPM.

Elbows, transitions from rectangular to circular sections and piping that connects the pump to the settling chamber were manufactured out of PVC (Poly-Vinyl-Chloride).

A smaller facility was also constructed as shown in Fig. 3.2. This is a closed circuit tunnel with a free surface above the test section.
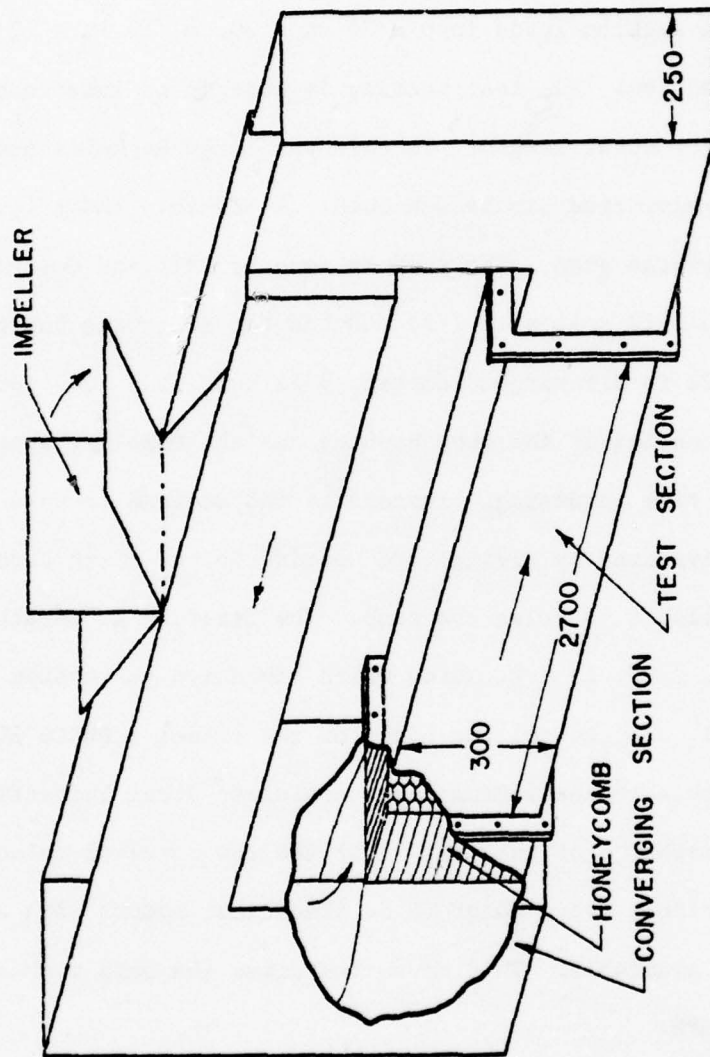
Fig. 3.2 The V.P.I. free-surface water tunnel (dimensions in mm)

The test section is totally submerged but the driving of the flow can be accomplished through a low-speed impeller at the free surface of the facility. This tunnel offers the advantages of very small volume of contained fluid, convenient exchange of the working mediums and as a result, access to the model and the sensing devices. The same test sections from our larger facility are received and therefore, preliminary tests can be performed with the small tunnel. Both facilities were calibrated with the flow visualization methods described in the sections that follow as well as by laser anemometry.

3.2 Optical Methods

To visualize the flow, we use pliolite and amberlite particles* that are dispersed in the fluid. The density of these substances is respectively ρ = 1.02 and 1.05 g/cm^3. These particles are separated by sieve-screening, according to their sizes, into particles of the order of 0.1 to 0.2 mm. Pliolite particles are bright white and should be preferred because of their higher reflectivity. However mixtures of glycerin and water are more dense than pure water and pliolite particles dispersed in such mixtures experience buoyancy forces that push them toward the top of the facility. Amberlite particles were found to be more useful for experiments with glycerin-water mixtures. The particles

---

*Pliolite is the commercial name of polyvinytoluene butadiene, made by Goodyear Chemicals.

Amberlite is the commercial name of a white ion exchange resin, IRA-93 made by Rohm and Haas Company.

to be used in a certain experiment are mixed in vertical columns and allowed to settle. The neutrally buoyant particles are withdrawn from the mixture, leaving behind the ones that either float to the top or sink to the bottom of the column.

The flow is visualized in planes parallel to the walls of the test section. All of the models tested are two-dimensional and the test section was scanned to check the two-dimensionality of the flow. A thin sheet of light is generated by a system of lenses as shown in Fig. 3.3, or by a parabolic reflector. The nearly parallel light so generated is passed through two successive slots of 5 mm width and then it is led into the test section. In front of the reflecting mirror and along the light path, a flash bulb is also situated, which may flash through the same slots into the test section.

Still pictures are taken with a 35 mm Olympus Camera and a 90 m; f 2.8 Vivitar Macro Lens. Time exposures of 1/2 up to 1/120 sec. are used. The images of particles expose the film over the time exposure interval by segments proportional to the average local velocity. This method of course has some limitations. The larger the speed of a particle, the shorter time its image exposes the film at a certain point and therefore the contrast is reduced. This drawback could be eliminated only if a very powerful source of light is used. It was also discovered that the method is not appropriate for recording flow fields with both large and small velocities. The proper camera speed is determined by the order of magnitude of the velocities that are expected in the region of interest. If a camera speed is chosen to reveal a small-velocity field then the faster moving particles expose almost the

entire width of the film and it is impossible to measure the lengths of individual path segments. Moreover the direction of the instantaneous velocity cannot be calculated with accuracy, since for unsteady flows the particle paths do not coincide with the instantaneous streamlines of the flow. Finally a minor error may be introduced due to the finite speed of the camera shutter. Details of the problem and a method for correcting the data received by this method are described in Appendix A.

The most important criticism may arise from the fact, that for large accelerations of the flow and for long time exposures (1/2, 1/4 sec.), the average velocity may be very far from the instantaneous velocity. For all the experiments performed, this effect was carefully considered and the error involved was estimated. A typical length for changes due to unsteady diffusion is the quantity $L_d = (\nu t)^{1/2}$ whereas the path traveled by a particle in the same period of time is $L_p = Ut$. The ratio of the two lengths $L_d/L_p = (\nu/U^2 t)^{1/2}$ is a dimensionless number indicative of the relative order of changes due to unsteady diffusion and convection. The smaller this number, the more accurate the representation of the unsteady flow by the present method. In our experiments this number was kept below the value of 0.05.

With the opening of the camera shutter, a flash may be triggered to direct an intense beam of light through the same optical path. (see Fig. 3.3) In this way the beginnings of particle path segments are marked on the film with brighter spots. A typical example is shown in Fig. 3.3a. This technique is particularly helpful if reversing flows are to be examined.
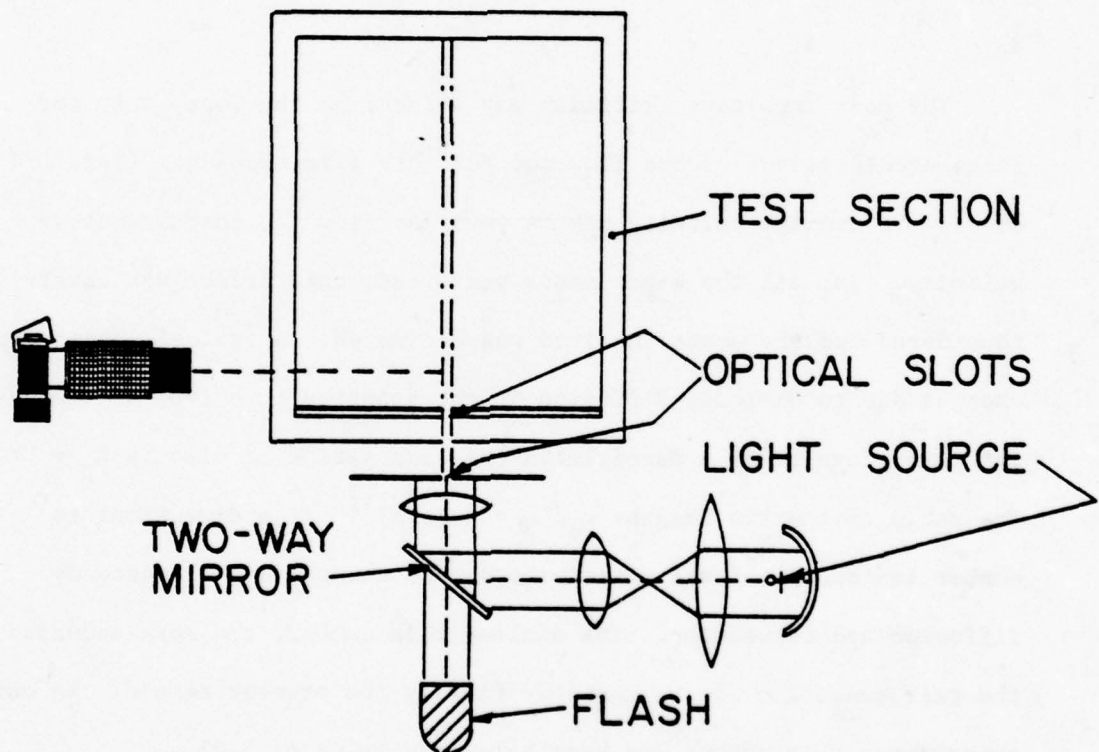
Fig. 3.3 The optical system for flow visualization.
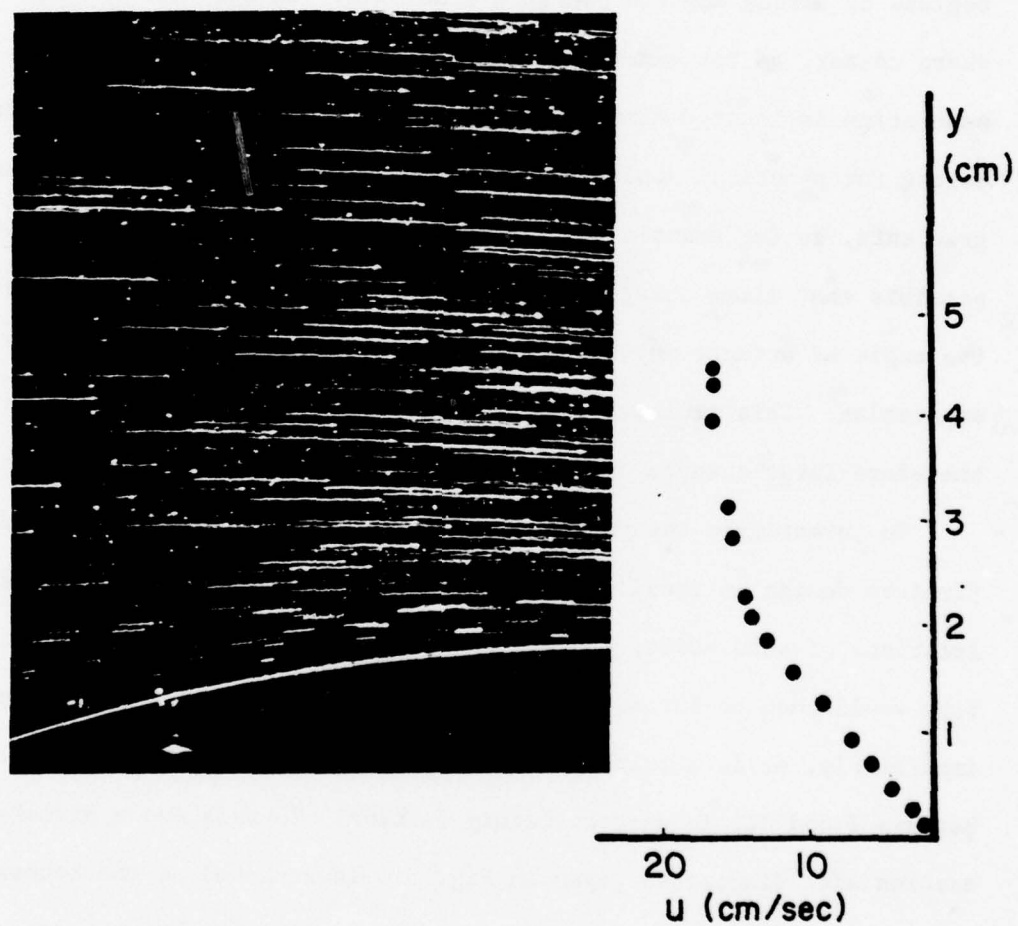
Fig. 3.3a   Typical example of flow visualization showing the direction and magnitude of the velocity and a velocity profile at approximately the middle of the frame.

3.3 The Models

Separation of the boundary layer is usually induced by adverse pressure gradients. However, its location is almost unaffected by changes of the outer flow conditions if the body configuration induces regions of strong adverse pressure gradients. In the extreme case of a sharp corner, as for example the flow over a backward facing step, separation is located almost always at the corner. A lot more interesting for practical applications are the cases of mild adverse pressure gradients, as for example the flow over airfoils. In these cases it is possible that minor changes of the outer flow, like a small increase of the angle of attack, may result in large excursions of the point of separation. This implies large changes in the pressure distribution and therefore large changes of integral quantities like drag, lift, etc.

To investigate the phenomenon of unsteady separation, we decided first to design an ideal situation where, for steady flows, two distinct locations of separation, at points say I and II could be achieved. The flow would then be forced to readjust from conditions I to conditions II impulsively, or in a transient manner or continuously, back and forth between I and II, in an oscillatory fashion. To this end a circular section with dimensions given in Fig. 3.4 is attached at the bottom of the test section. This model is made out of plexiglass to permit lighting of the flow on its surface. It will be referred to in the sequel as model A. A 7 mm deep hole was drilled and later filled with epoxy, to provide a length scale. This is shown in almost all of the flow visualization pictures that follow. It was later used to calculate the lengths of particle path segments as well as to define the axial
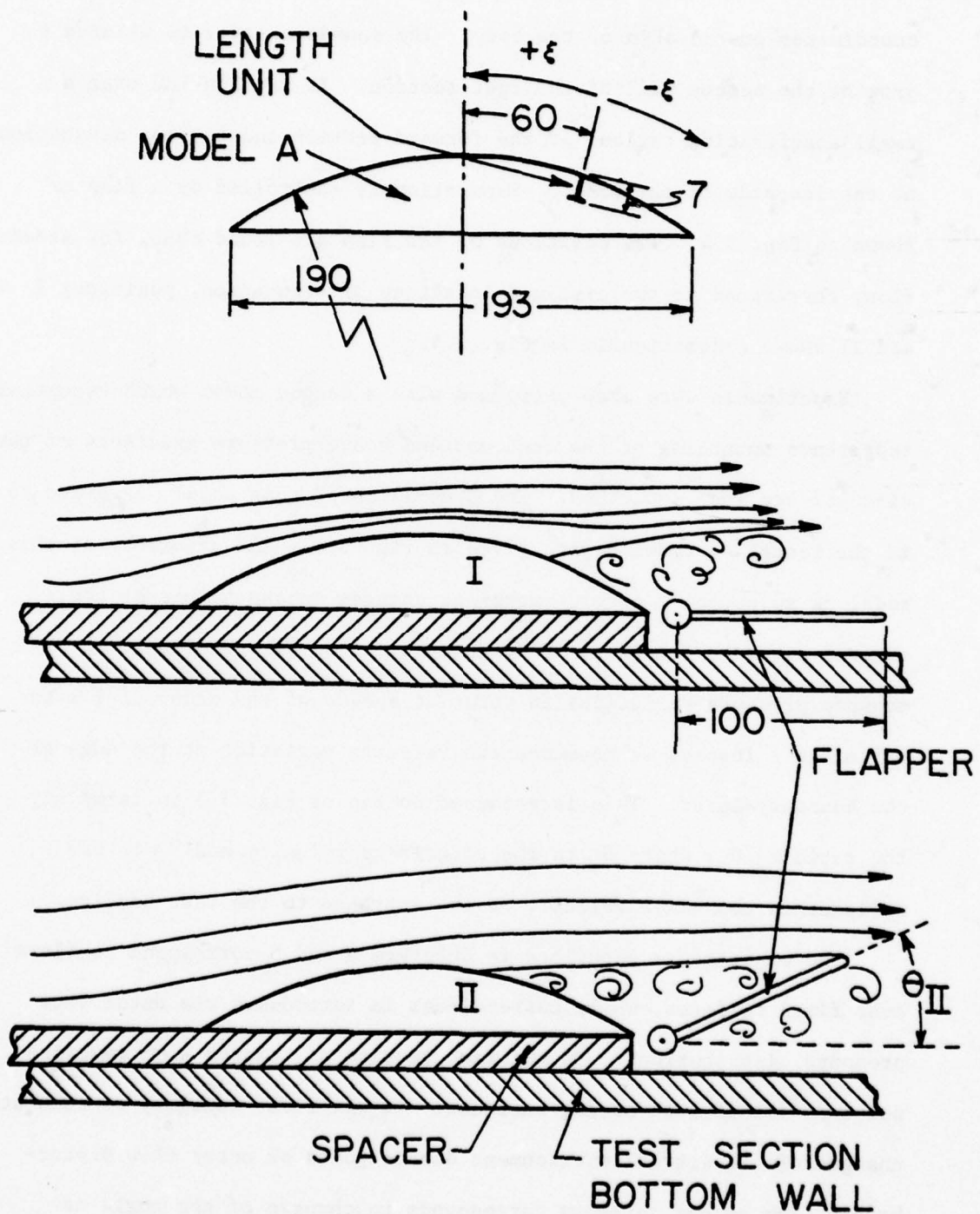
Fig. 3.4   The model A and the extreme flap positions. All the dimensions are in mm.

coordinates on the skin of the body. The boundary layer is allowed to grow on the bottom wall of the test section. It is then led over a small accelerating region, at the forward portion and towards separation at the lee side of our model. Separation is controlled by a flap as shown in Fig. 3.4. Two positions of the flap are found that, for steady flow, correspond to two distinct locations of separation, positions I and II shown schematically in Fig. 3.4.

Experiments were also performed with a second model which essentially represents smoothing of the contours and hence pressure gradients of the circular arc just described. The dimensions of this model, referred to in the sequel as model B, are given in Fig. 3.5. The afterbody of this model is adjustable, permitting minor changes in the values of the adverse pressure gradient. Unfortunately it is very difficult to measure pressure variations in water at speeds of the order of 0.1 to 0.5 m/sec. Instead we measured the velocity variation at the edge of the boundary-layer. This is recorded on top of Fig. 3.5 in terms of the ratio U_e/U_∞, where U_e is the outer-edge velocity and U_∞ is the undisturbed mean-flow velocity at the entrance to the test section.

The experiments described in Chapters 4 and 5 correspond to flows over fixed surfaces, while unsteadiness is introduced via outer flow pressure distributions. In the last section of Chapter 4 we describe our experiments with moving surfaces. In the first category we simulate changes of the airfoil environment due to gusts or outer flow disturbances. The second category corresponds to changes of the angle of attack of an oscillating blade.

41
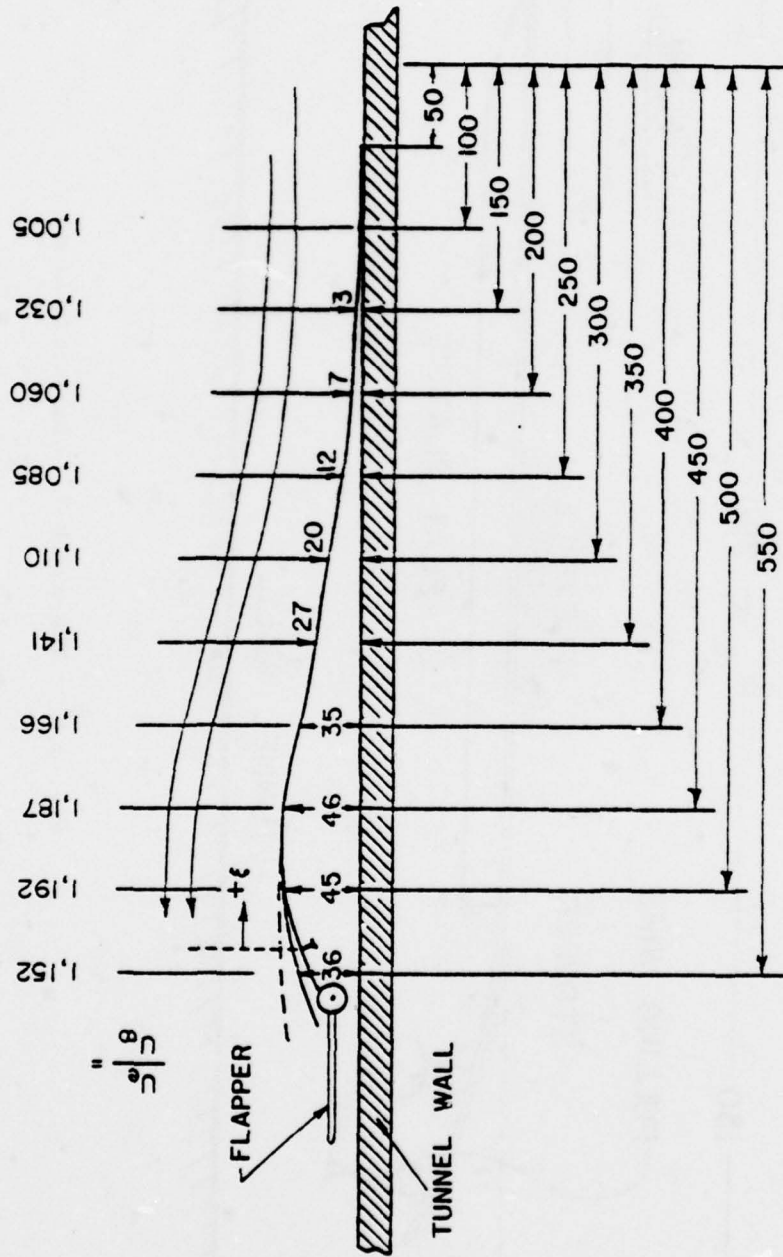
Fig. 3.5   The model B.   Dimensions in mm.

42
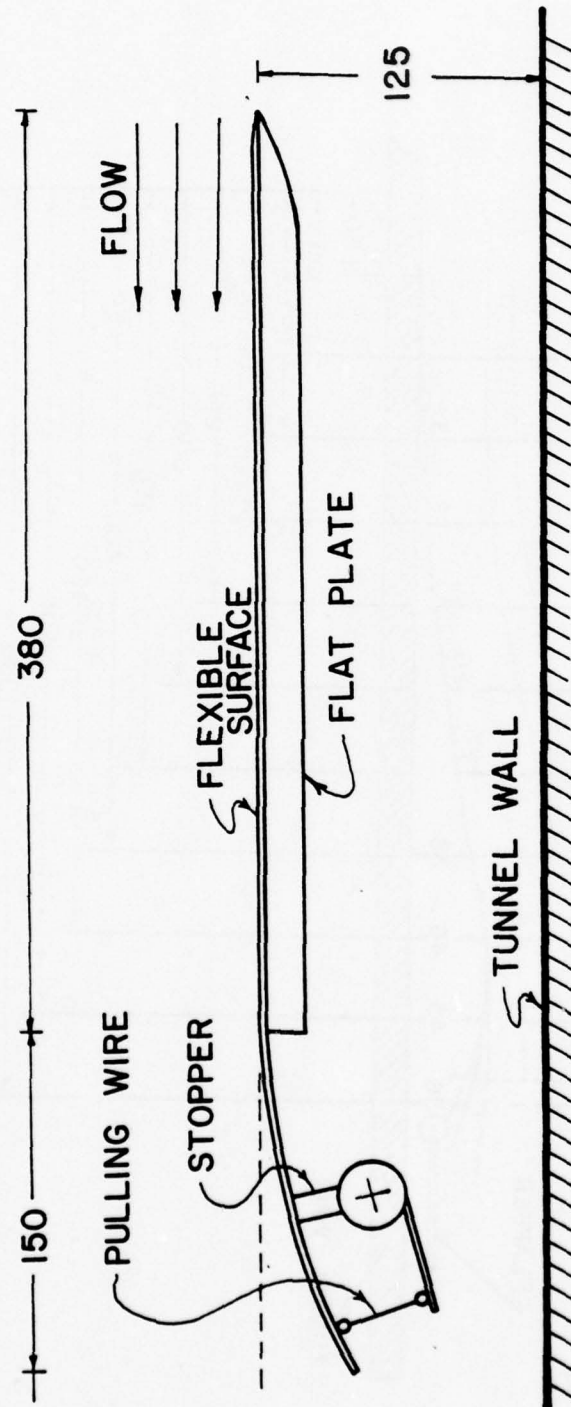
Fig. 3.6   The model C.   Dimensions in mm.

Changes of the shape and orientation of the model surface are accomplished with flexible surfaces. A flat plate is attached in the middle of the test section in order to provide some distance for the boundary layer to grow. The surface of the plate is covered by a thin flexible surface which extends further downstream as shown in Fig. 3.6. The flexible part of the model can be deflected downward thus generating a portion of adverse pressure gradients and separation.

The thin plate that extends downstream is essentially a cantilever beam. The bending moment distribution and therefore the curvature of the plate decrease from point F towards the point G at which the pulling wires are attached.

It is desirable to simulate the flow over a Howarth body i.e., a body over which the outer-flow distribution decreases linearly

$$U_e = U_\infty - kx$$

This implies that U_e starts decreasing right at the leading edge of the plate, and its curvature increases with x. This would be a very difficult flow to obtain experimentally. However in order to approach somewhat this distribution and achieve larger excursions of separation, the flexible plate is supported at one more point between F and G, the point H. In this way large curvatures in the neighborhood of point F are avoided.

3.4 Laser-Doppler Velocimetry

For the Laser Anemometry measurements a DISA LDA one-channel system (55L series) was used. The transparent walls of the test section permit the use of the forward scattering mode. The arrangement of the

equipment is shown in Fig. 3.7. A laser tube directs a laser beam into a DISA beam splitter (55L series). A system of brag cells is attached on the casing of the beam splitter to provide for frequency shifting. The two beams are then led into the test section and allowed to cross at the point of interest (measuring volume). A photomultiplier (55L10) is focused at the measuring volume as shown in the figure. The signal is directed to a preamplifier an oscilloscope and a DISA signal processor (55L20).

Only the component of the velocity parallel to the boundary of the model at a certain ξ-station is measured. The laser beam arrangement in space is shown in Fig. 3.8. The plane of the two beams p, is given an inclination with respect to the horizontal, equal to β, which is the slope of the model boundary at the point of interest. The two beams are shown in the figure crossing the vertical wall of the test section at the points A and B, crossing each other at M where the measuring volume is formed and penetrating the model boundary at the points A' and B' respectively. The bisector of AA' and BB' in the plane p, is also given a slight inclination α, with respect to the horizontal, say the generator of the model boundary at the point of interest. The fringes are thin planes parallel to the plane r, inclined by an angle β with respect to the vertical plane q. The normal to the plane of the fringes is dennoted by the vector $\bar{e}$ in Fig. 3.8 and it is parallel to the model boundary at this point. This arrangement permits the measurement of the velocity component in the direction $\bar{e}$ regardless of the value of the angle α.
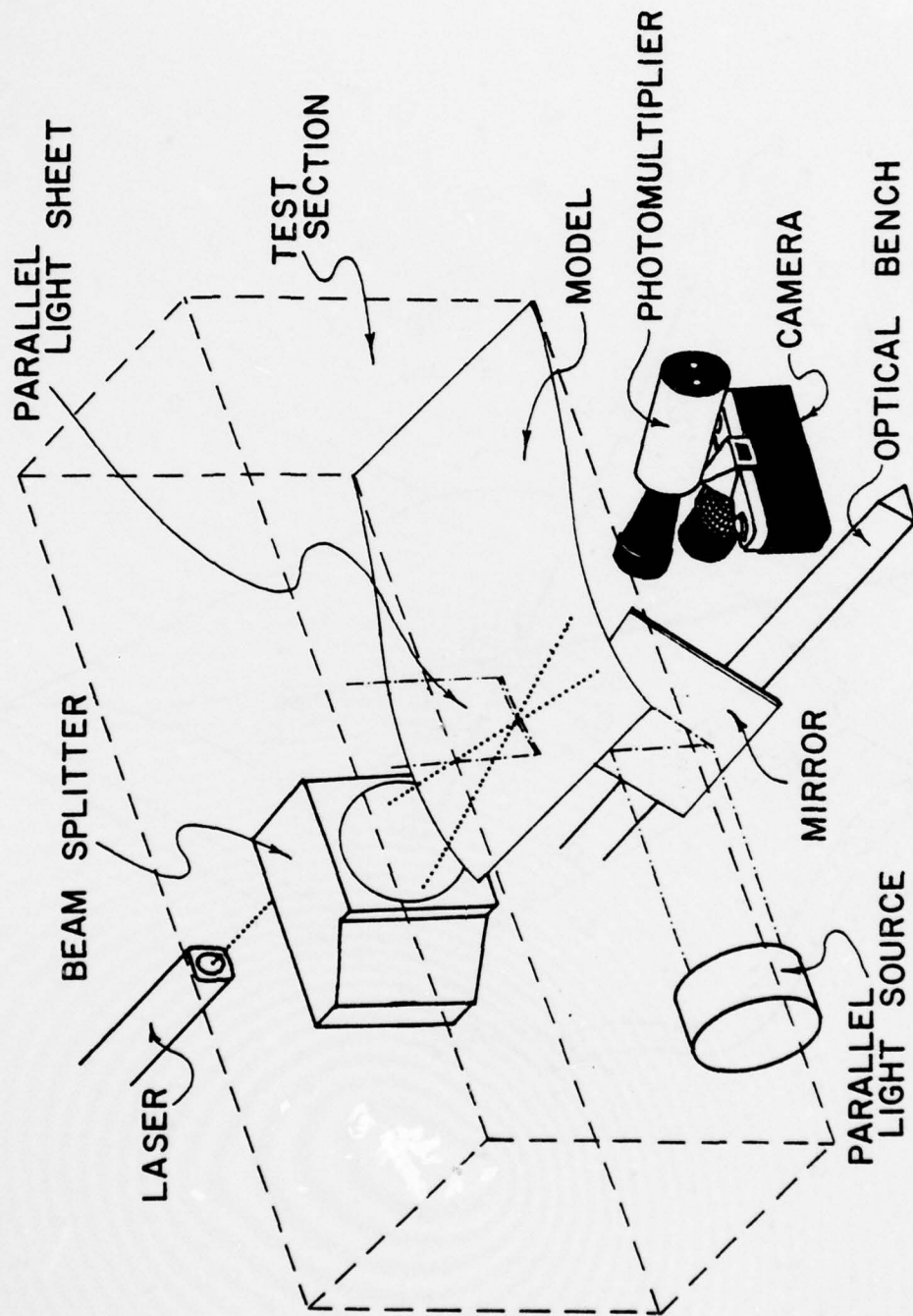
Fig. 3.7 The experimental arrangement for simultaneous flow
visualization and LDA measurements (reference beam mode)
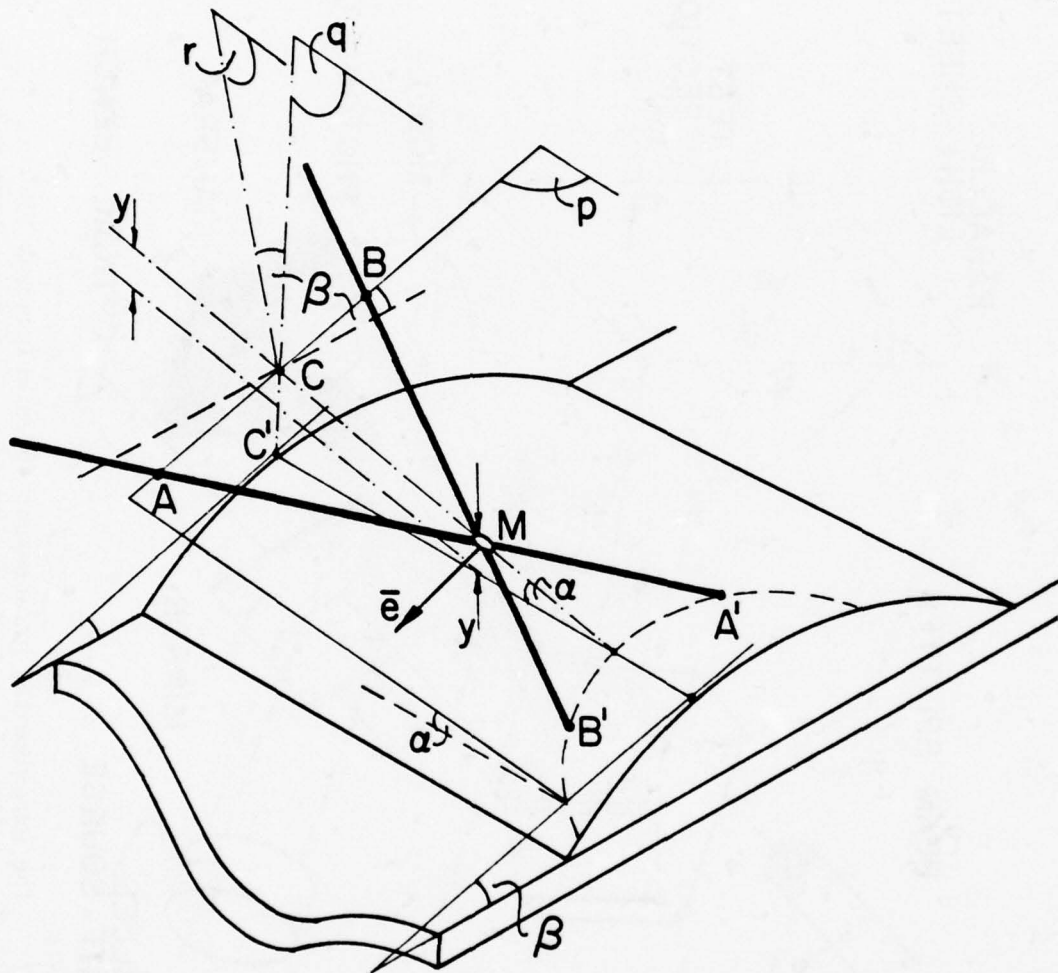
Fig. 3.8   Angles involved in laser anemometry.

To measure vertical distances and record the position of measure-ment the following procedure is followed. The optical bench is lowered until the points A' and B' coincide with the point M, that is until the two beams intersect exactly at the skin of the model. A scale is then located vertically on a side wall, with its zero at the point where one of the beams intersects the tunnel walls. From then on vertical dis-placements of the optical bench are read on this scale. The method is as accurate as possible for the determination of the point $y = 0$. Accuracy of y-readings is influenced by the ability of the experimenter to read visually the vertical scale.

Since the scattering mode permits maximum scattered light col-lection, the aperture of the photomultiplier collecting lens can be set to higher values (smaller diameters). This decreases the optical noise and permits better focusing on the photomultiplier's pinhole. This in turn results in better signal to noise ratios and less drop-out per-centages. It was found that frequency shifting further improves the signal to noise ratio.

The pliolite particles used in the photographical measurements of the flow provide a good Doppler signal clearly observable in the oscilo-scope. The addition of plain COFFEEMATE may slightly improve the quality of the Doppler signal.

During the initial tests of the system it was found that mechanical vibrations traveling through the concrete floor are transmitted all the way to the optical bench. This was discovered by projecting the fringes on a vertical wall. With the pump motor on, the fringes can be clearly

seen to jitter. As a result, a spurious noise is received which appears
on the recorder identical to a turbulent velocity measurement. These
vibrations were eliminated by supporting the optical beam on a 10 cm
thick styrofoam plate.

3.5 Tunnel Calibration

The velocity in the tunnel can be estimated roughly via a pitot
tube and a static probe attached on the vertical wall of the test section.
This device is useful of course for speeds above 0.6 m/sec since readings
less than 0.5 m/sec correspond to only a few mm of water. Speeds as
high as 2.5 m/sec have been achieved using the Marathon Electric motor.
This is a constant-speed motor and the speed of the tunnel can be controlled
only via the butterfly valve. A rough estimate of the speeds that can
be achieved in this way plotted against the position of the valve is
shown in Fig. 3.9.

Visual observations indicated that the 90°-turn, upstream of the
settling chamber generates a very uneven profile, strongly favoring the
lower part and directing the flow towards the bottom of the test sec-
tion. It was of course expected, that a diffuser with such a large
divergence would induce separation. The shearing effect thus generated
seems to persist all along the settling chamber. As a result, an uneven
profile is generated at the converging section and soon converts into
large scale eddies that are convected downstream in the middle of the
test section. These visual observations were corroborated with LDV
measurements. These measurements indicate that on top of the normal
free stream turbulence, there exists a disturbance with a period of the
order of 0.5 to 5 seconds. To remedy this unpleasant feature of the
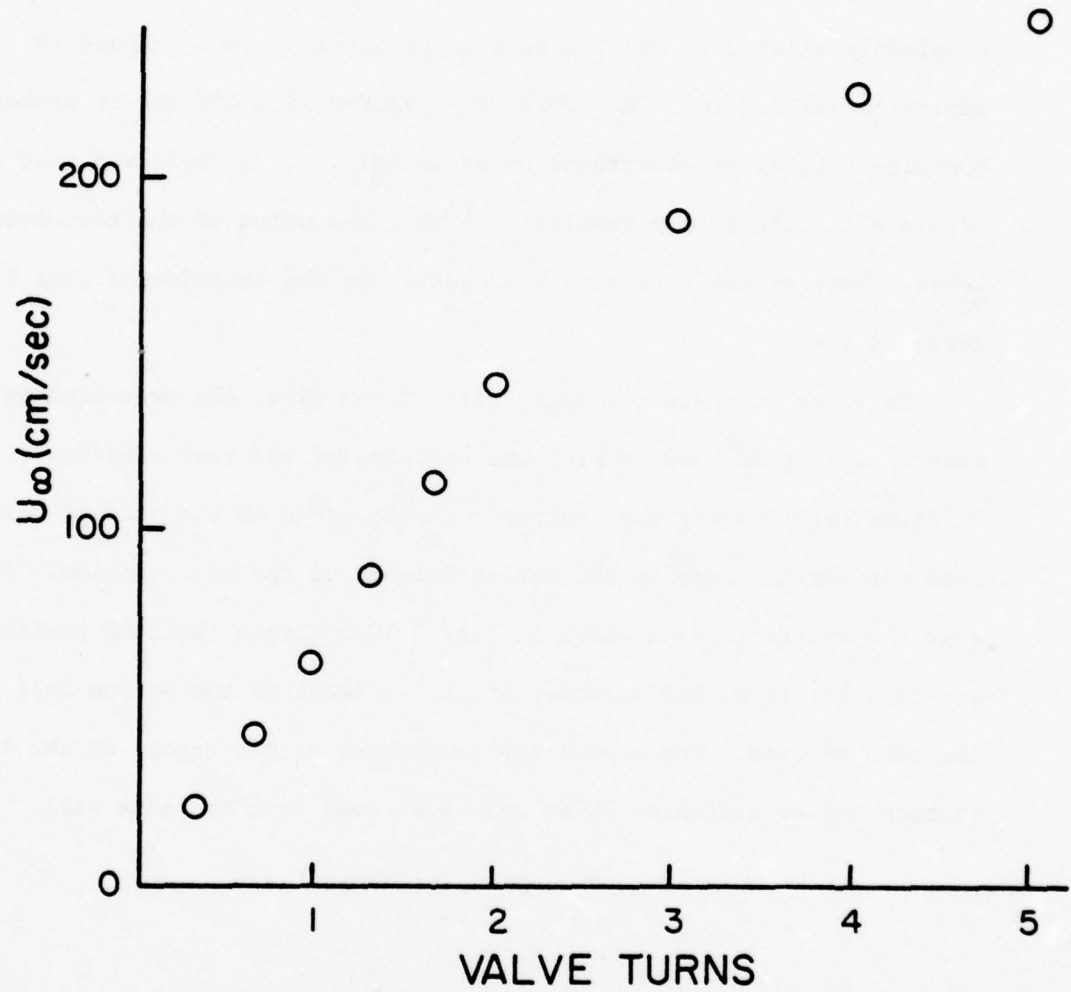
Fig. 3.9   Mean tunnel flow velocity as a function of butterfly valve position

flow it was decided to install turning vanes in the 90°-elbow and extend them in the form of expanding vanes in the diffuser, as shown in Fig. 3.1. This indeed forces the flow to be distributed more evenly in the settling chamber and improves its quality. Large-scale eddies are completely eliminated and the turbulence level is thus dropped to approximately 1.0 to 1.2%. This was measured with LDV and it probably contains optical or electronic noise as well. It is believed that a sequence of screens may result in further reduction of the turbulence level. However the facility is adequate for the experiments that it is designed for.

In order to check the uniformity of the flow, LDV measurements were made at a distance 100 cm from the entrance of the test section. Unfortunately the way the equipment is supported on the optical bench does not permit scanning the entire heighth of the test section. However the available data shown in Fig. 3.10 indicate that the profiles are parallel to within an order of 1%, at least in the bottom half of the test section. Three profiles are shown; at the center of the test section and at distances 70 mm and 10 mm away from the side wall.
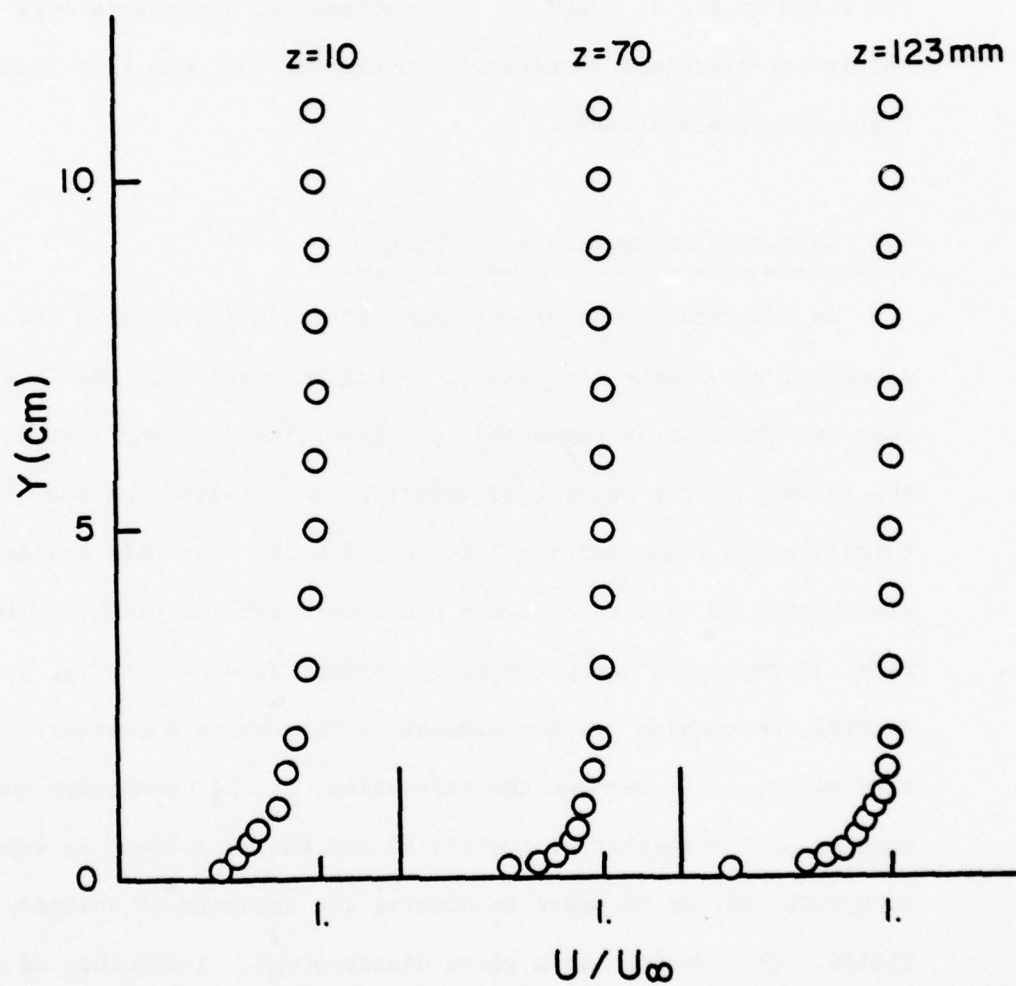
Fig. 3.10 Velocity distribution at $R_e = 10^5$ for three different lateral positions.

CHAPTER 4

TRANSIENT AND IMPULSIVE CHANGES OF THE
PRESSURE DISTRIBUTION

In this chapter we describe results of experiments performed with

the fixed models A, B and C. Unsteadiness is introduced here via im-

pulsive or transient changes of the flap or via mean flow accelera-

tions and decelerations.

4.1 Impulsive Changes $R_e = 10^5$ Model A

In the first phase of our experiments, using model A and water as

a medium, we examine the case of impulsive changes of the flow. To

this end the flap is connected to a lever and a strong spring. With

the release of the lever a microswitch is activated and the flap

quickly moves from position I to Position II. A simple system of

electronics is used to activate the camera and the flash. This was

first accomplished using the delay-circuit as shown in Fig. 4.1 to

control the opening and the closing of the camera's shutter. The

time delay, Δt in between the initiation of the phenomenon and the

opening of the shutter is controlled and the experiment is repeated

with different Δt in order to observe the sequence of unsteady velocity

fields. This system has a clear disadvantage. A sequence of photo-

graphs thus generated does not correspond to different instances of

the same transient phenomenon, spaced apart by equal time intervals.

It represents, instead, the flow field of repetitions of the same

transient phenomenon, viewed at different instances after its initia-

tion. The repeatability of the flow is therefore an important factor

52

53
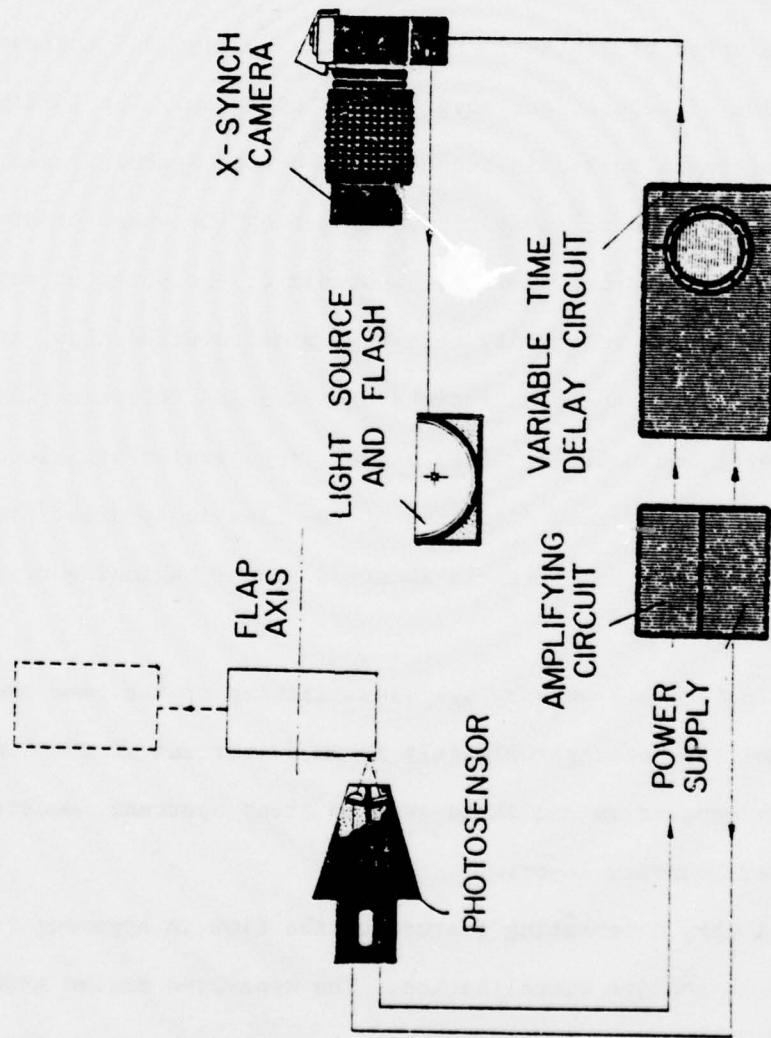
Fig. 4.1   Electronic circuit for triggering the disturbance generator and the camera.

and in fact some of the sequences of photographs indicate discrepancies.

One set of experiments was performed with model A, $R_e \cong 10^4$ and a sharp change of the flap inclination from $\theta_I = 0$ to $\theta_{II} = 40°$. In Fig. 4.2 we show four visualizations of the flow at times $t = 0.2, 0.4, 0.6,$ and 0.8 sec. after the initiation of the impulsive change, taken with a camera speed of 1/8 sec. The sequence in Fig. 4.2 indicates that the location of separation, moves slowly upstream. The initial station of separation is marked in these plates by the Symbol S_1 and the instantaneous station of separation, defined by the wake formation, is marked by an arrow. However, upstream of the point of separation, there exists a relatively thin region of reversed flow, in qualitative agreement with the descriptions of Sears and Telionis [15], Carr, McAlister and McCroskey [22] et. al. (see review article of Telionis, [24]). The reversed direction of the flow is apparent from the bright dots that mark the particle location at the beginning of the film exposure.

In Fig. 4.3 we show dye visualization of the same phenomenon. Dye is emmitted here approximately 10 mm downstream of the location of steady separation and it is seen to creep upstream, underneath the laminar boundary layer.

A very interesting feature of the flow is apparent from both particle and dye visualization. The separated region grows at the beginning in a controlled fashion but after a certain time it appears that it attains momentum and its thickness increases abruptly. The

t=0.2 sec

t=0.4

Fig. 4.2   Flow visualization of an upstream moving separation
with $R_e \sim 10^5$.
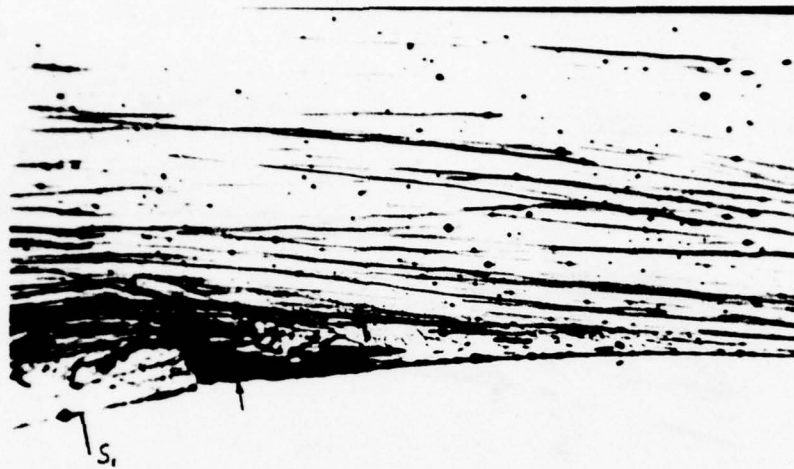
t=0.6 sec
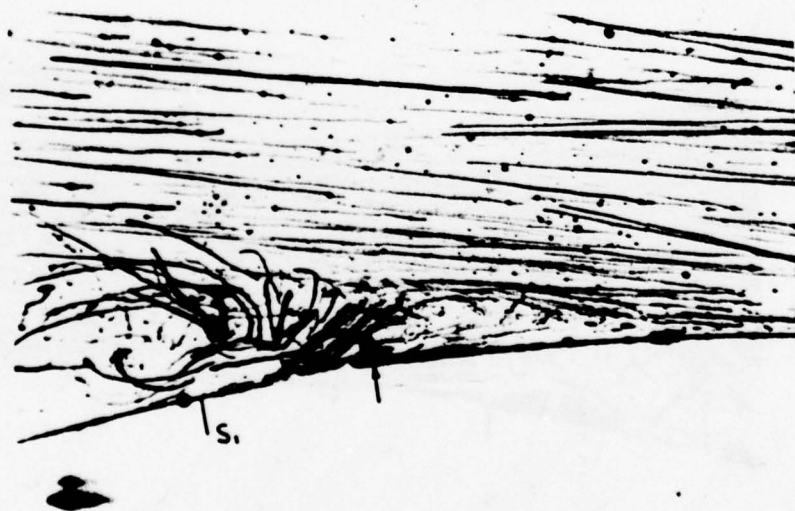
t=0.8 sec

Fig. 4.2 cont.

Fig. 4.3   Dye visualization of the phenomenon depicted in Fig. 4.2.

phenomenon is reminiscent of the bursting of the leading edge separation bubble. This is clearly shown in the last frame of Fig. 4.2. The momentum thus generated quickly takes the form of a well-organized vortex. The weak turbulent field of the wake is probably still present but the dominant motion appears clearly to be the vortical motion and the exchange of mass with the outer stream which is accomplished further downstream. This trend appears to persist in all the experiments performed and it is documented in many sequences of still frames some of which are contained in Ref. 25.

This was the first set of experiments performed in our facility and the outer flow appears in the visualization to be "non-laminar." It is true that 10^5 is the highest Reynolds number chosen for these experiments but still the flow theoretically should be laminar. The facility at that time was not totally free of destabilizing effects as for example sharp changes of the direction of the flow, vibrating motors, etc. For all these reasons one may suspect that the flows just described may have had some turbulence in the free stream. However, we felt that they should be included in the present report since they clearly indicate the spectacular explosion that occurs during the interval of unsteady motion.

4.2 Impulsive Changes, $R_e = 10^3$, Model A

Experiments performed with smaller Reynolds numbers indicate a characteristically different behavior. Such experiments were performed in the smaller facility, (Fig. 3.2) with a mixture of glycerin and water

in a ratio 60% by volume. The use of glycerin mixtures permits one to reduce the Reynolds numbers without simultaneous reduction of the velocities. It is therefore easier to observe the flow and capture a velocity field with reasonable film exposure time. Examination of low Reynolds number flows using water as a testing medium would require very small velocities and unrealistically small Δt's. However, the use of glycerin has some distadvantages as well. The dimensionless number $L_d/L_p = (\nu/U^2 t)^{1/2}$ which describes the ratio of distances of diffusion propagation to particle displacement, grows. As a result, the error involved when using the present method becomes larger. In the experiments performed with glycerin-water mixtures, L_d/L_p ranged between 0.05 and 0.12.

Transient flows are investigated again for low Reynolds numbers. A more sophisticated triggering system is now being used. It involves a KIM-1 microprocessor (see Fig. 4.4) which is programmed to receive the signal of the initiation of the impulse and then activate the flash and trigger the camera at specified intervals of time. Details on the programming of the microprocessor are described in Appendix B. In this way it is possible to receive snapshots of the same phenomenon at different times and thus capture the evolution of a single unsteady flow field. In Fig. 4.5 we show a sequence of velocity fields taken with a camera speed of 1/2 sec. and a Reynolds number equal to 1000. The first frame represents the steady flow for $\theta = 0$. The second frame is shot with a delay $\Delta t_o = 0.5$ sec. after an impulsive change of the flap angle from $\theta = 0$ to $\theta = 40°$. The following frames were received at
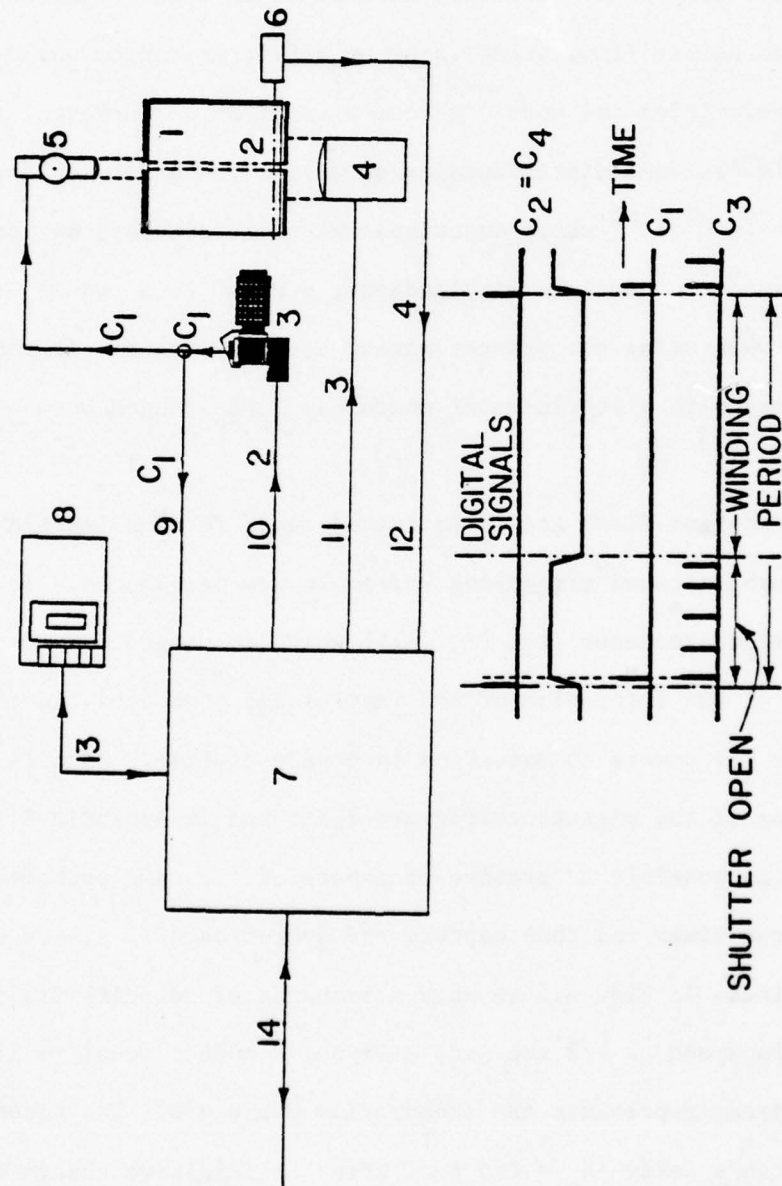
Fig. 4.4 The triggering system interfaced with a microprocessor.

CAPTION TO 4.4

1. TEST SECTION WITH TRANSPARENT WALLS (CROSS SECTION)

2. PLANE OF LIGHT (OBSERVATION PLANE)

3. OLYMPUS OM-1 MOTOR DRIVE CAMERA (3 FRAMES PER SECOND)
   WITH VIVITAR 90mm f2.8 MACRO LENS(1:1 MAGNIFICATION RATIO)

4. FAST RECYCLING XENON STROBE(UP TO 20 FLASHES PER SECOND)
   COMBINED WITH CONTINUOUS OUTPUT 1000W QUARTZ LAMP IN THE
   SAME HOUSING AND FOCUSED AT INFINITY BY A LENS

5. VIVITAR 283 STROBE (UP TO 3 FLASHES PER SECOND) FOCUSED
   AT INFINITY BY A LENS

6. OSCILLATOR (VARIABLE SPEED MOTOR OSCILLATING A SHAFT)

7. KIM-1 (MOS) MICROPROCESSOR (6502 ARRAY) WITH TWO 6530
   ARRAYS (ROMS), 1152 BYTES OF "READ" "WRITE" MEMORY, TWO
   PROGRAMMABLE INTERVAL TIMERS, SIX LED DISPLAY, KEYBOARD,
   AUDIO CASSETTE INTERFACE, TTY INTERFACE

8. AUDIO CASSETTE RECORDER INTERFACED WITH THE MICROPROCESSOR

9. CAMERA'S SHUTTER OPEN FEEDBACK THROUGH CAMERAS X SYNCH AND
   SLOW STROBE'S (5) CONTROL LINE

10. MOTOR DRIVE CONTROL LINE

11. FAST STROBE'S (4) CONTROL LINE

12. R.P.M. 2 PHASE FEEDBACK THROUGH A LED/PHOTOSENSOR

13. AUDIO CASSETTE INTERFACE

14. TTY INTERFACE WITH IBM COMPUTER (OPTIONAL)

intervals of $\Delta t = 1$ sec. The speed of exposure was kept rather low in order to reveal the properties of slowly moving flow at the bottom of laminar boundary layer and in the separated region. Immediately after the initiation of the impulsive change, the flow indicates a violent departure from the steady state configuration. Very soon, two distinct recirculating regions appear and a saddle point configuration is formed at approximately the station where steady separation occured. These flow patterns could be interpreted as "reversed flow upstream of separation," if separation is defined as the saddle point that is shown in this figure. The velocity fields shown in these frames are indeed fully contained in the viscous region of the flow. This becomes clear from velocity profiles derived from the visualization of Fig. 4.5 and shown in Fig. 4.6. However the first bubble seems to retain its identity even after the flow has arrived at its steady-state condition. It is therefore possible that such recirculating bubbles are part of the wake which for low Reynolds numbers, is usually made up of a few discrete vortices. It should be emphasized that with larger viscosities, viscous diffusion is increased and the response of viscous phenomena, including separation, is faster. The sequence of photographs shown in Fig. 4.5 could be interpreted therefore as follows. Separation immediately moves upstream. The temporal rearrangement of the vortices then represents the familiar unsteadiness contained in the wake. This would be the interpretation that the numerical analyst would probably offer (Mehta and Lavan [26] and Mehta [27]). Indeed, for low Reynolds numbers, reversing of the flow direction could be defined as separation.

63

t = 0 sec

t = 0.5

t = 1.5
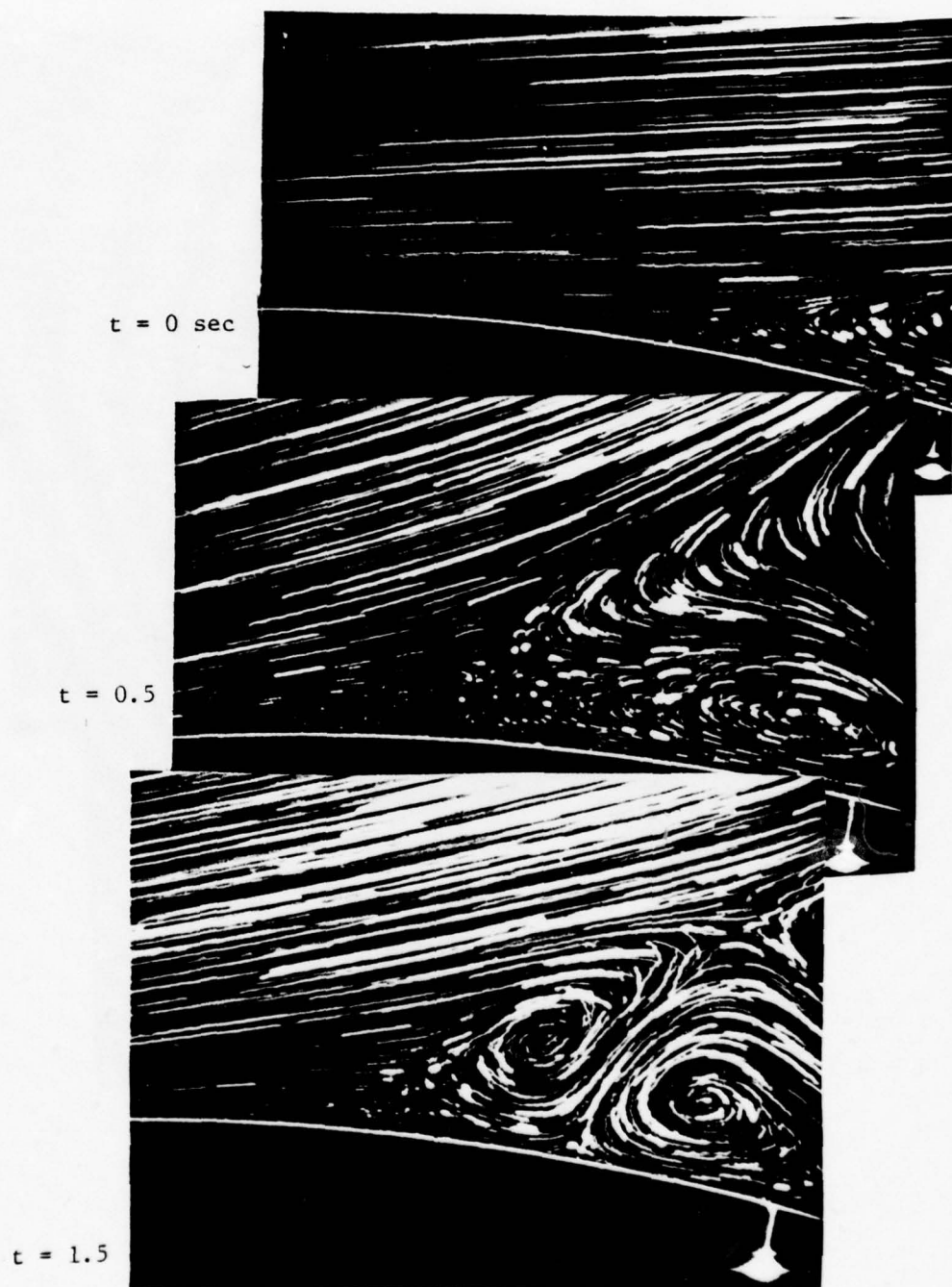
Fig. 4.5   Flow visualization of instantaneous velocity fields
            for an impulsive change $\theta_I = 0$ to r_{II} and $R_e \cong 1000$.
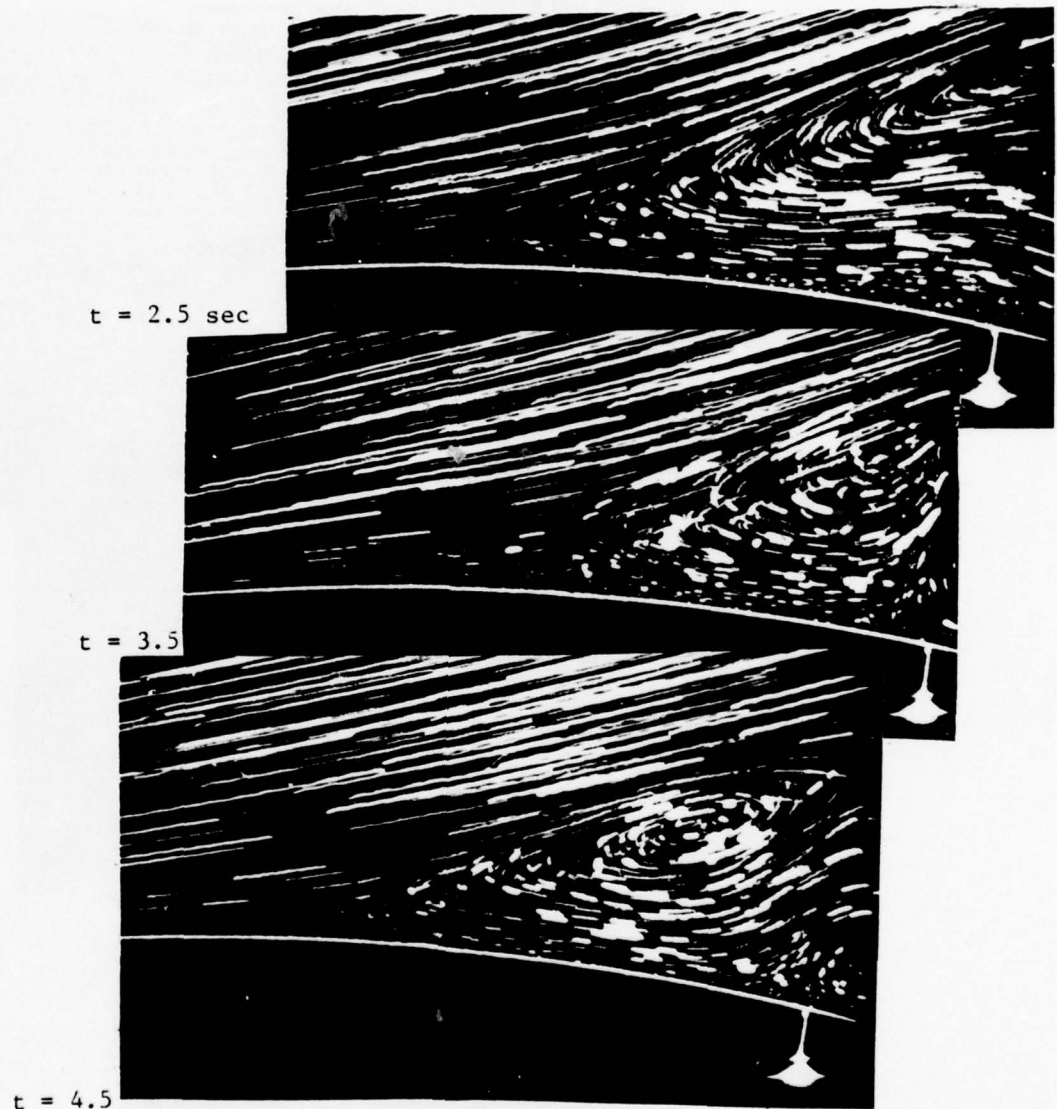
64

t = 2.5 sec

t = 3.5

t = 4.5

Fig. 4.5 (continued)

65
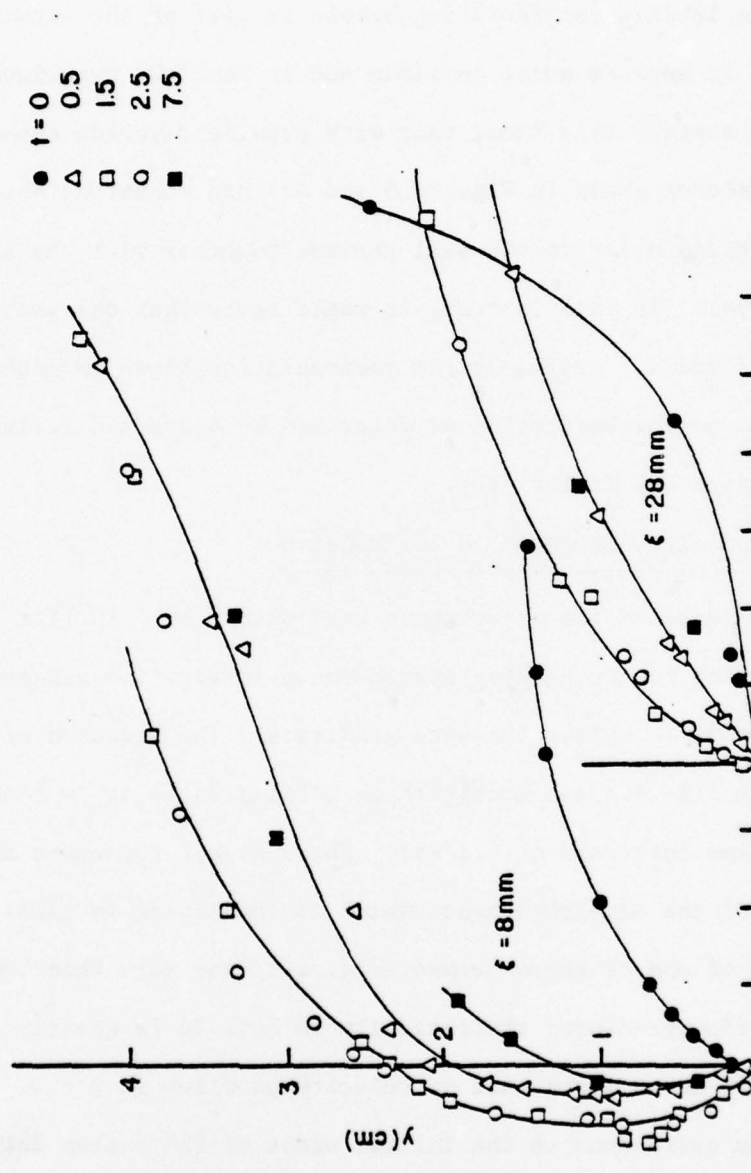
Fig. 4.6   Velocity profiles at stations ξ = 8428 (see Fig. 3.4) derived from the flow visualization of Fig. 4.5.

In Fig. 4.7 we show a sequence of velocity fields again for $R_e \cong$ 1000 but with a final flap inclination $\theta_{II} = 30°$. The general characteristics of the flow are similar. In fact it is now easier to accept that the leading recirculating bubble is part of the attached boundary layer. It appears quite possible and in fact our experimental data seem to support this idea, that with growing Reynolds numbers, the flow patterns shown in Figs. 4.5 and 4.7 are conserved but their dimension perpendicular to the wall shrinks together with the laminar boundary layer. If this is true, it would imply that the patterns of Fig. 4.5 and 4.7 represent the recirculating flows in front of an upstream moving separation as described by Sears and Telionis [15] and Despard and Miller [10].

4.3 Impulsive Changes $R_e = 10^4$ Model B

We repeated the experiments with water ($R_e \cong 10^4$) for transient flows using the triggering system shown in Fig. 4.4 and model B which provides milder pressure gradients. The sequence of frames shown in Fig. 4.8 was made with an initial delay $\Delta t_o = 1$ sec. and subsequent time intervals $\Delta t = 1$ sec. These plates represent average flow fields of the same phenomenon which is developing in time. In the blow up of one of these frames (Fig. 4.9) the very thin layer of reversed flow predicted theoretically in Ref. 26 is clearly shown. Fig. 4.10 shows a sequence of velocity profiles at $\xi = 0$. These profiles correspond to the initial steps of the motion during which the flow is well ordered and the wake appears in the form of a recirculating bubble. The sequence of plates of Fig. 4.8 indicates

Fig. 4.7 Flow visualization of instantaneous velocity fields for an impulsive change $\theta_I = 0$ to $\theta_{II} = 30°$ and $R_e = 1000$

68

t = 2.5

t = 3.5
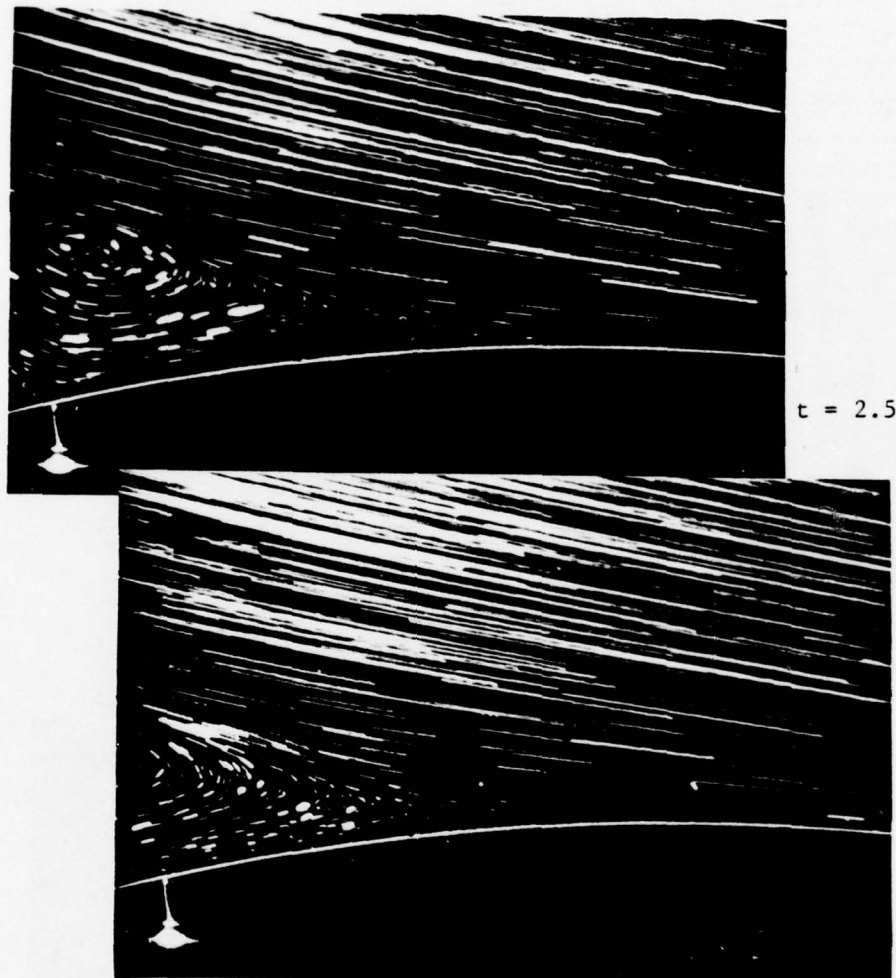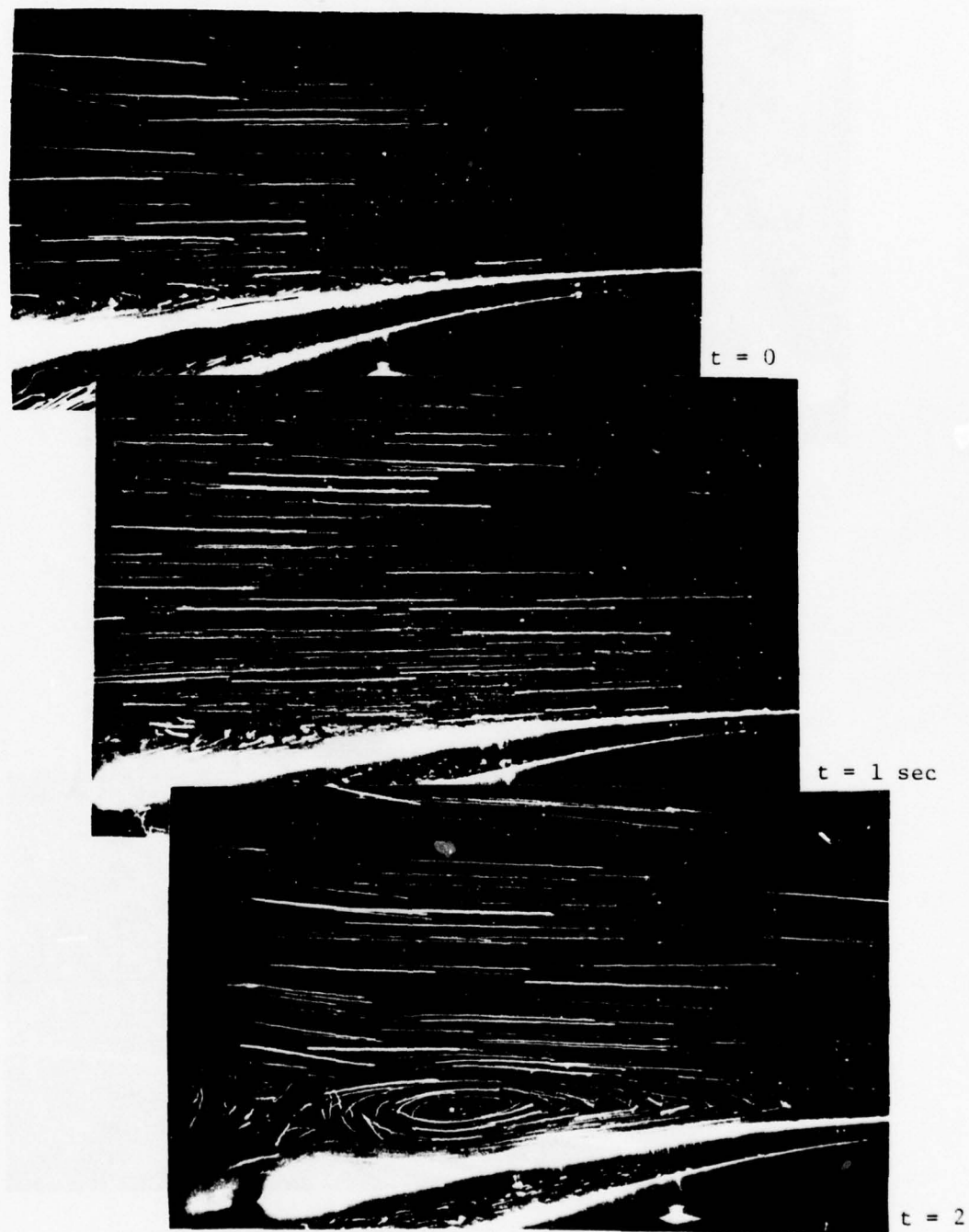
Fig. 4.7 (continued)
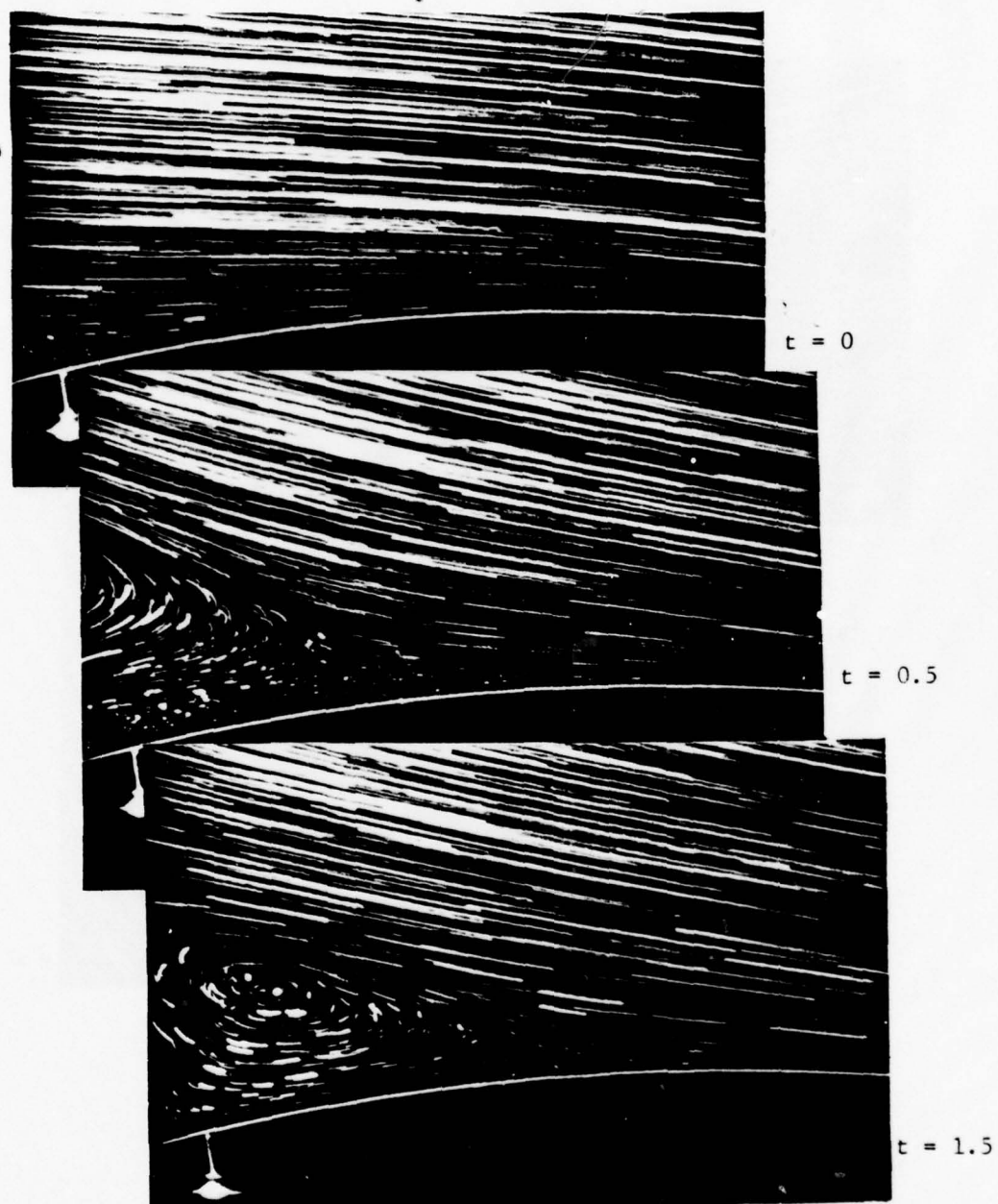
Fig. 4.8   Flow visualization of instantaneous velocity fields over model B for an impulsive change $\theta_I = 0$ to $\theta_{II} = 35°$ and $R_e = 10^4$.

t = 4 sec

t = 5

t = 7
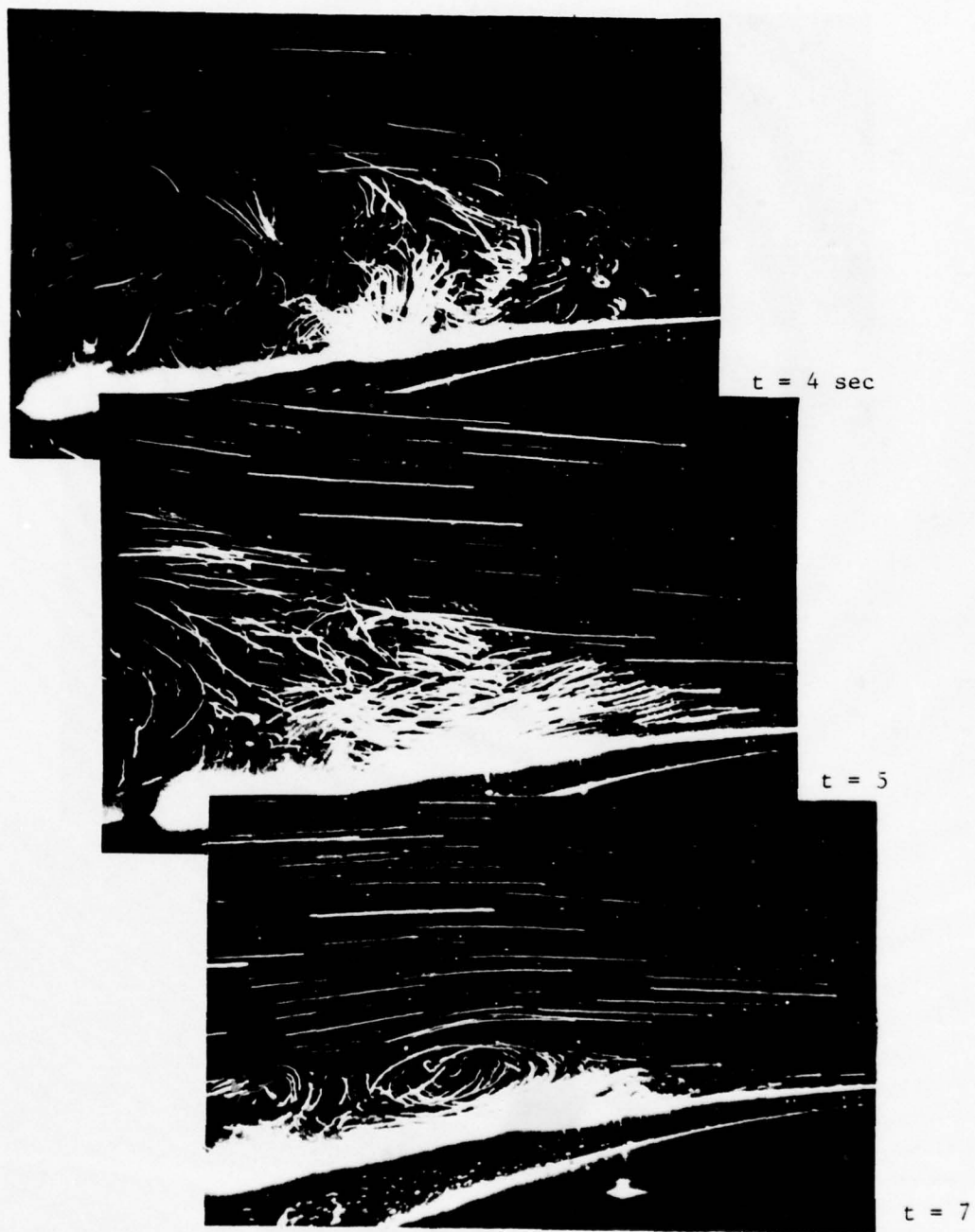
Fig. 4.8 (continued)

Fig. 4.9 Detail of Fig. 4.8 (frame t = 1 sec) magnification
5.7 x life size

72
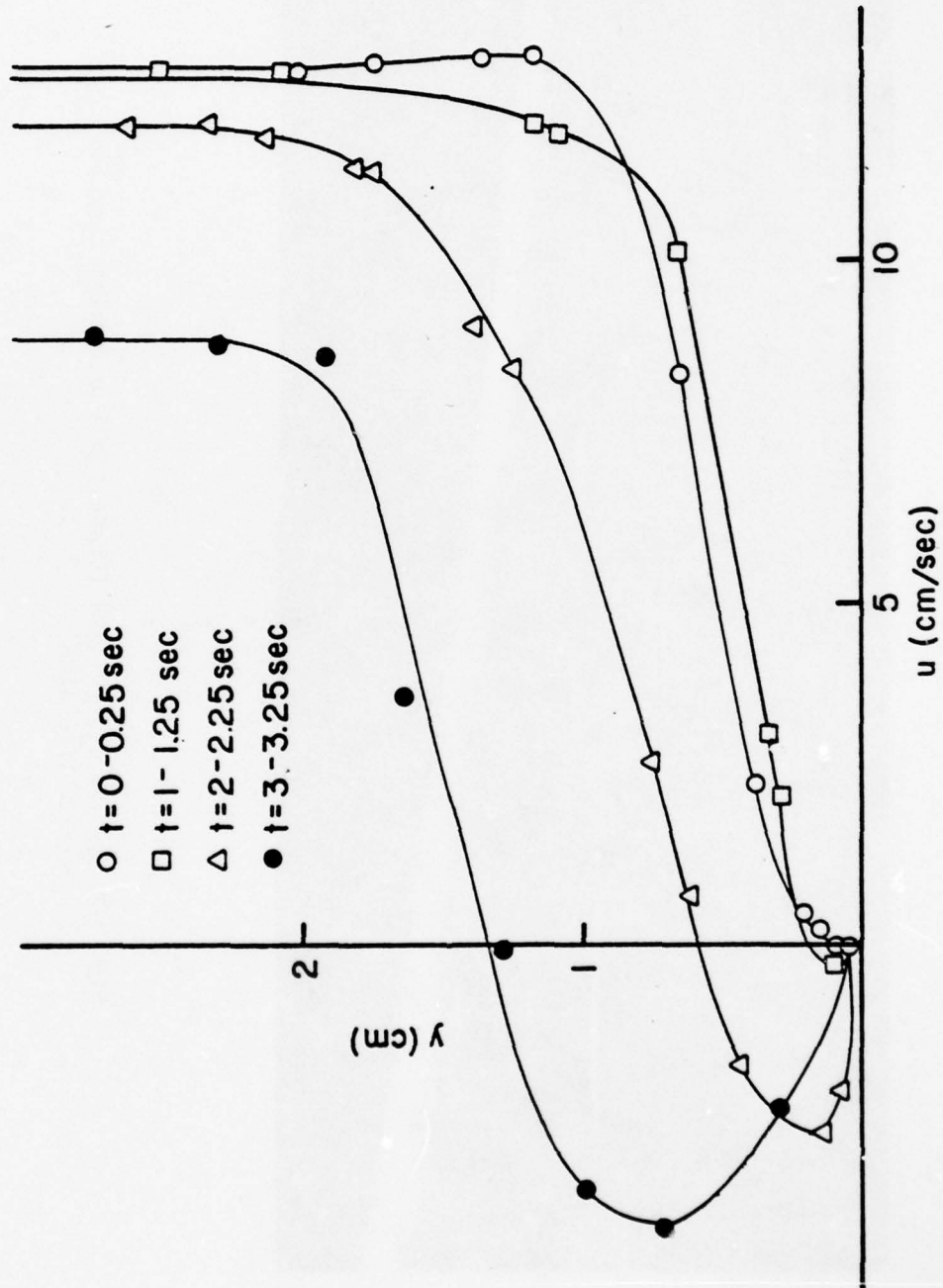
Fig. 4.10 Velocity profiles at station ξ = 15 derived from the flow visualization of Fig. 4.8.

73

that at t = 4 sec. a spectacular explosion occurs in the wake and the
particles of the wake, including the ones that reside next to the wall
are jettisoned into the flow. Subsequently this erratic motion sub-
sides and the configuration approaches the steady flow that corresponds
to the final flap angle.

4.4 Mean-Flow Accelerations

In another set of experiments we studied the response of laminar
separation to accelerating and decelerating outer flows, for $R_e \approx 10^4$.
In these experiments the disturbing flap was completely removed and
unsteadiness was introduced only via the change of the magnitude of the
outer flow. It should be noted here that potential flow is unaffected
by such changes and the streamline configuration of inviscid flow should
remain undisturbed. The flow is governed by Laplace's equation

$$\nabla^2 \phi = 0$$

with ϕ the potential function. Time is introduced via the boundary
conditions, in this case the free-stream velocity. However, in inviscid
flow the pressure is given by Bernoulli's equation

$$\frac{\partial \phi}{\partial t} + \frac{V^2}{2} + \frac{dp}{\rho} = f(t)$$

where V, p and f(t) are the velocity, pressure and an arbitrary function
of time respectively. Clearly time variations of ϕ generate pressure
disturbances which in turn influence to location of separation.

In Fig. 4.11 we show a sequence of velocity fields for a flow
accelerating from $U_\infty = 12$ cm/sec to $U_\infty = 25$ cm/sec. The visualization

at t = 0 corresponds to the undisturbed flow. The flow at an initial interval Δt_o = 0.5 and subsequent intervals Δt = 1 sec. after the initiation of the acceleration is shown until Δt = 3.5 sec. An inspection of the outer flow is enough to convince that during the acceleration process the outer flow essentially "washes away" the separated region. Indeed separation is displaced downstream and eventually moves out of the frame of observation. Subsequently and after the outer flow has achieved the new steady velocity of 25 cm/sec, the point of separation moves slowly again into the picture and at t = 6 sec it arrives at almost its initial position. This was expected since for $R_e \approx 1000$ or above, the location of separation in steady flow is insensitive to the magnitude of the outer flow velocity.

Velocity profiles received from these visualizations are shown in Fig. 4.12. These profiles correspond to the stations AA and BB, that is, the point above the scale marker and 60 mm upstream, as shown in Fig. 4.11. The flow at point AA is probably a very small distance downstream of the point of steady separation. The velocity profile at this point clearly shows a vanishing of the skin friction, or perhaps a small region of slow reversed flow. After the acceleration of the outer flow begins, the wall shear becomes positive and increases sharply. The inflection point of the profile disappears and only after the outer flow achieves its final value, do we observe a sharp decrease of the velocity, the appearance of a point of inflection and a vanishing value of the velocity at the same distance from the wall as for t < 0. Normalized velocity profiles are shown

BB

AA

60 mm

7 mm

190 mm

t = 0

t = 0.5 sec

t = 1.5

t = 2.5

t = 3.5
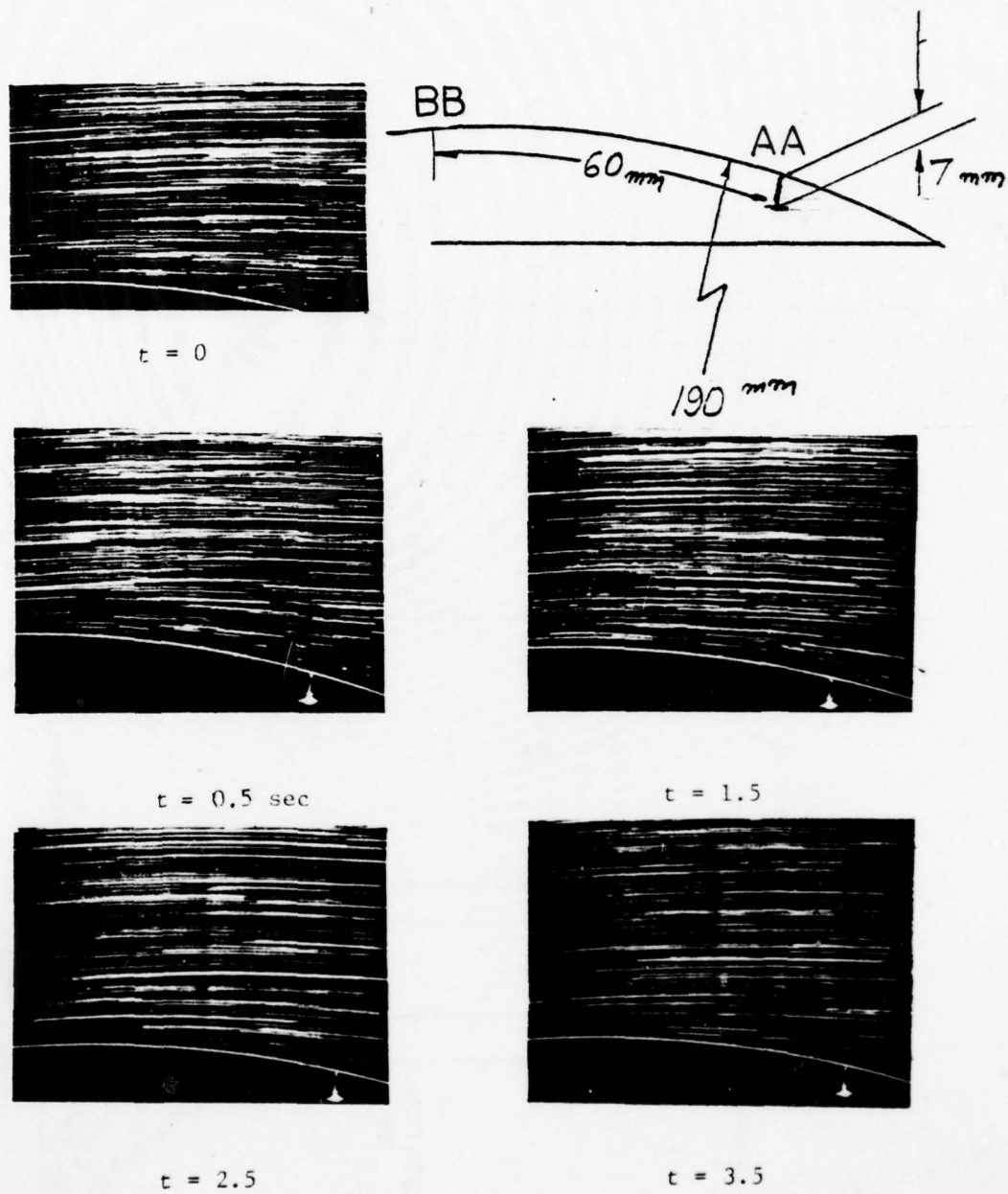
Fig. 4.11   Flow visualization for flow over model A accelerating
in magnitude from U_∞ = 12 cm/sec to U_∞ = 25 cm/sec.

76
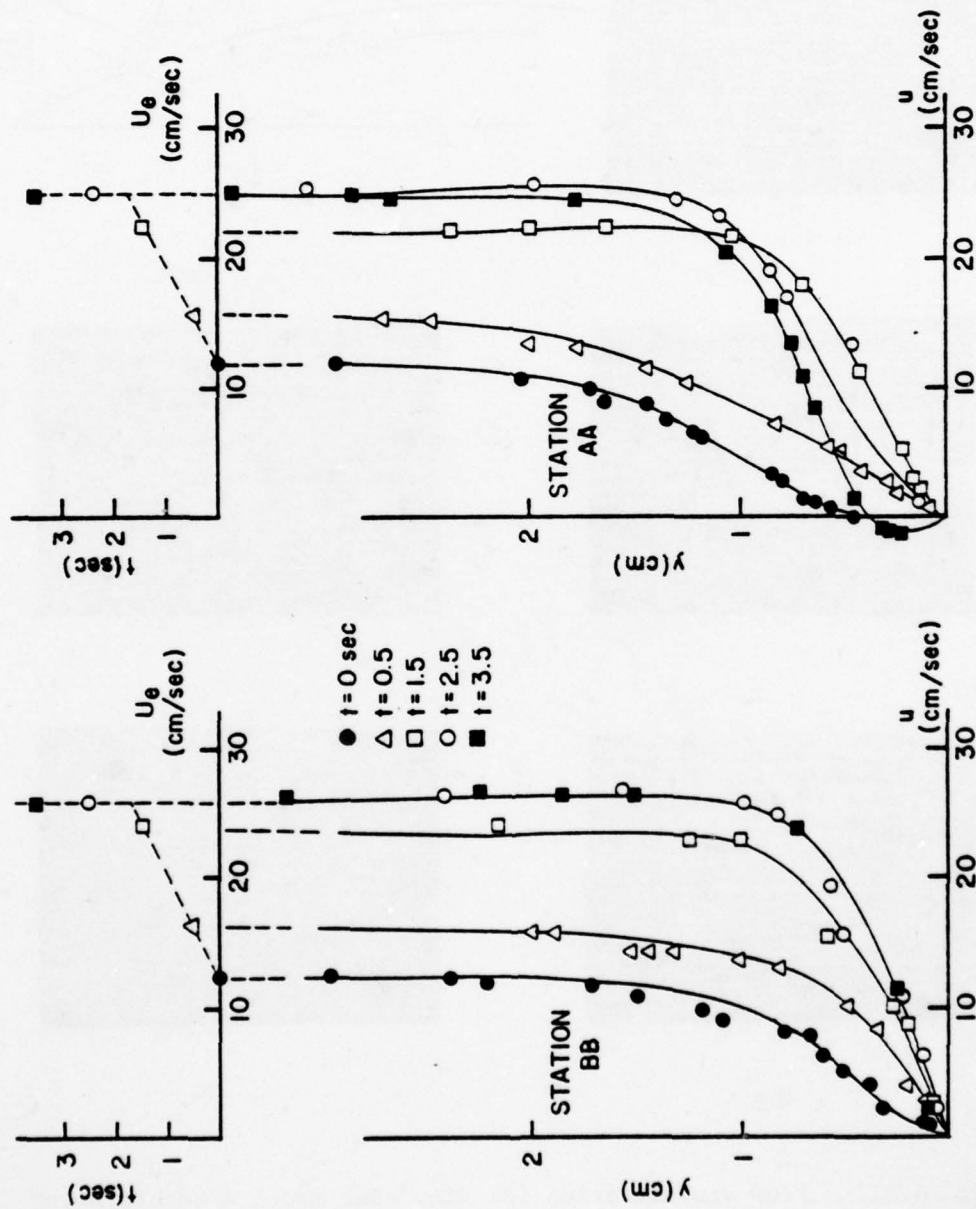
Fig. 4.12 Velocity profiles at stations $\xi = 0$ (station AA) and $\xi = 60$ (station BB) (see Fig. 3.4) derived from the flow visualization of Fig. 4.11.
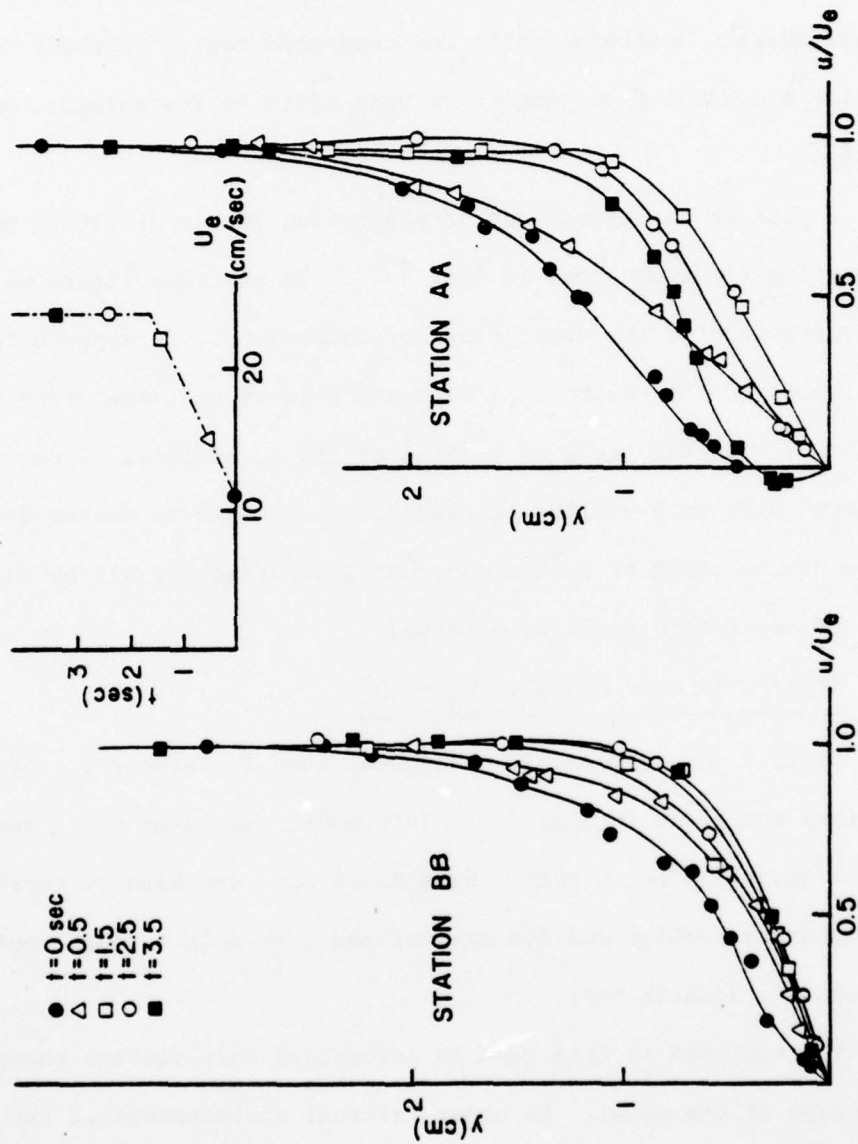
Fig. 4.13   Dimensionless velocity profiles for stations AA and BB derived from the data of Fig. 4.12.

in Fig. 4.13.

A sequence of instantaneous velocity fields for decelerating flows is shown in Fig. 4.14. In this case the point of separation is displaced sharply upstream, while the separated region thickens abruptly. As time grows the flow pattern returns again to its original configuration.

A plot of the excursions of separation for accelerating and decelerating flows is shown in Fig. 4.15. In the same figure we show the variations of the outer flow for comparison. It appears that the time scale of the response of separation is of the same order of magnitude with the scale of changes of the outer flow. Experiments repeated with much smaller accelerations resulted in weaker displacements of the point of separation, until no effect at all on the location of separation could be observed.

4.5 Separation over Model C, $R_e = 10^4$

Model C is the flexible model described in Chapter 3. Its dimensions are given in Fig. 3.6. This model was essentially designed with a Howarth flow in mind. Such flows are very hard to reproduce, as explained earlier and the present model is only a rough approximation to a Howarth body.

Unsteadiness in this case is introduced only via the change of the shape of the model. No other external disturbances of the flow are involved. The deformation of the model, from a flat surface to the shape shown in Fig. 3.6 simulates for example, a sharp change of the angle of attach of an airfoil.

t = 0,5 sec

t = 1,5

t = 2,5

t = 3,5
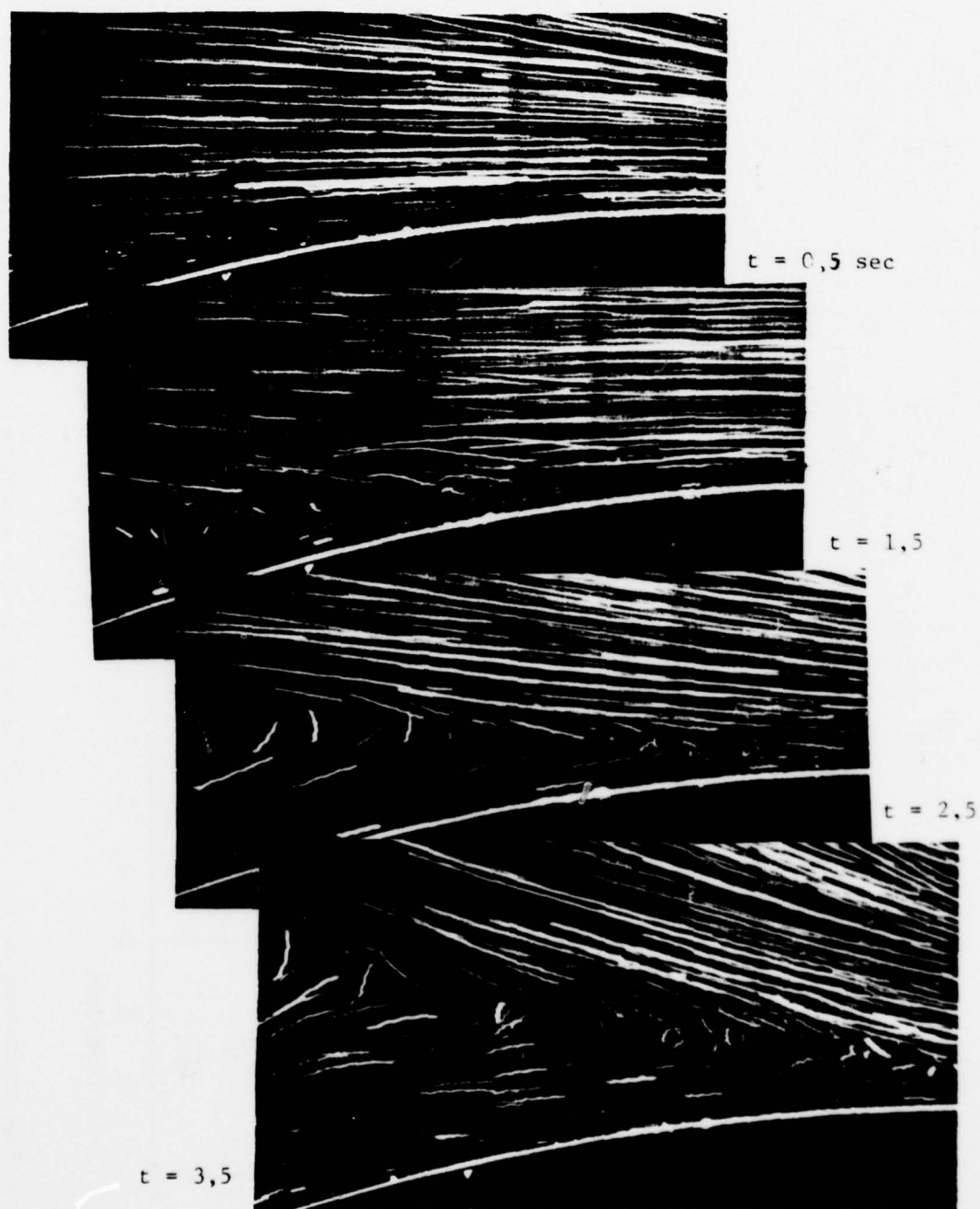
Fig. 4.14   Flow visualization for flow over model B decelerating in magnitude from U_∞ = 20 cm/sec. to U_∞ = 12 cm/sec.

80
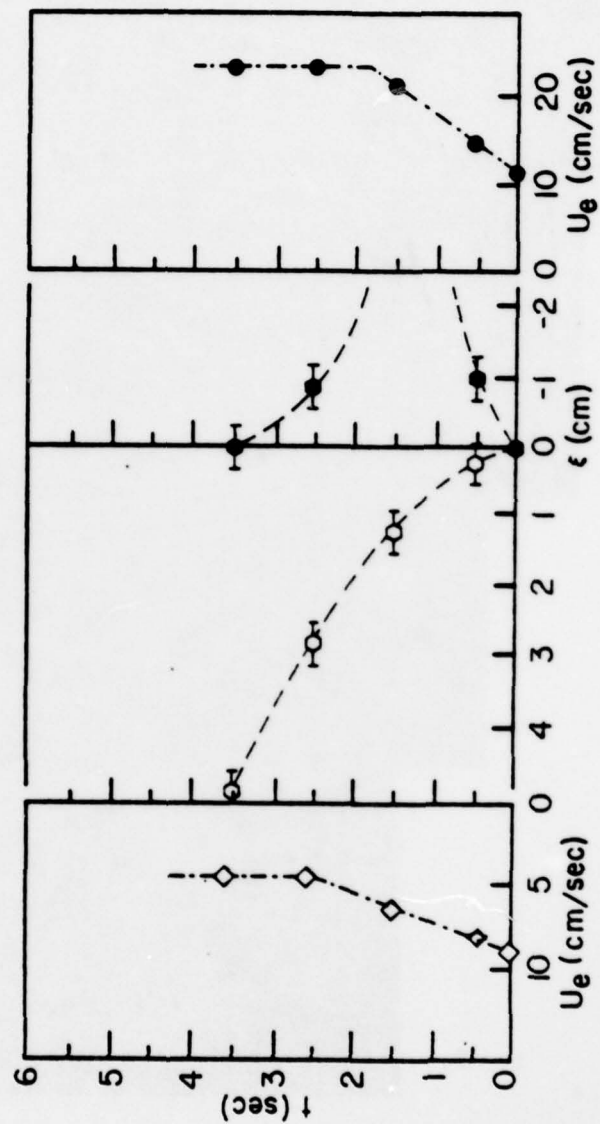
Fig. 4.15   The excursions of the point of separation for accelerating (open symbols) and decelerating (closed symbols) flows.

The experiments are performed as follows. The lever that drives the flexible surface is turned up so that the surface GHF (see Fig. 3.6) is lifted to become an extension of the flat plate. Laminar attached flow and a Blasius steady boundary layer are allowed to develop on the flat plate. At a certain instant t_o, the lever is given a sharp displacement and the flexible surface deforms to its new position as shown in Fig. 3.6. The microprocessor is programmed to trigger the camera at t_o and at $t_o + n\Delta t$ so that again a sequence of frames are taken as shown in Fig. 4.16.

At first the flow is fully attached as shown in the first frame of Fig. 4.16. This clearly demonstrates the inertia characteristics of the phenomenon. Shortly after the impulsive change, a portion of the skin of the body is covered with a very thin layer of reversed flow. However, the outer flow remains attached. The activity of flow reversing and vortex forming is confined at first to a very thin layer at the bottom of the boundary layer. The streamlines of the flow follow very closely the contour of the body. Therefore very small pressure disturbances should be expected at this time level.

Soon, two distinct vortices are formed. One, that extends upstream seems to be the oldest. The second, further downstream is historically younger but already develops into a thicker vortex, clearly showing the potential to develop into a disturbance of larger scale. The subsequent development is a little confusing and we were unable to follow an orderly upstream propagation of the

t = 0 + sec

t = 0.4

t = 0.8
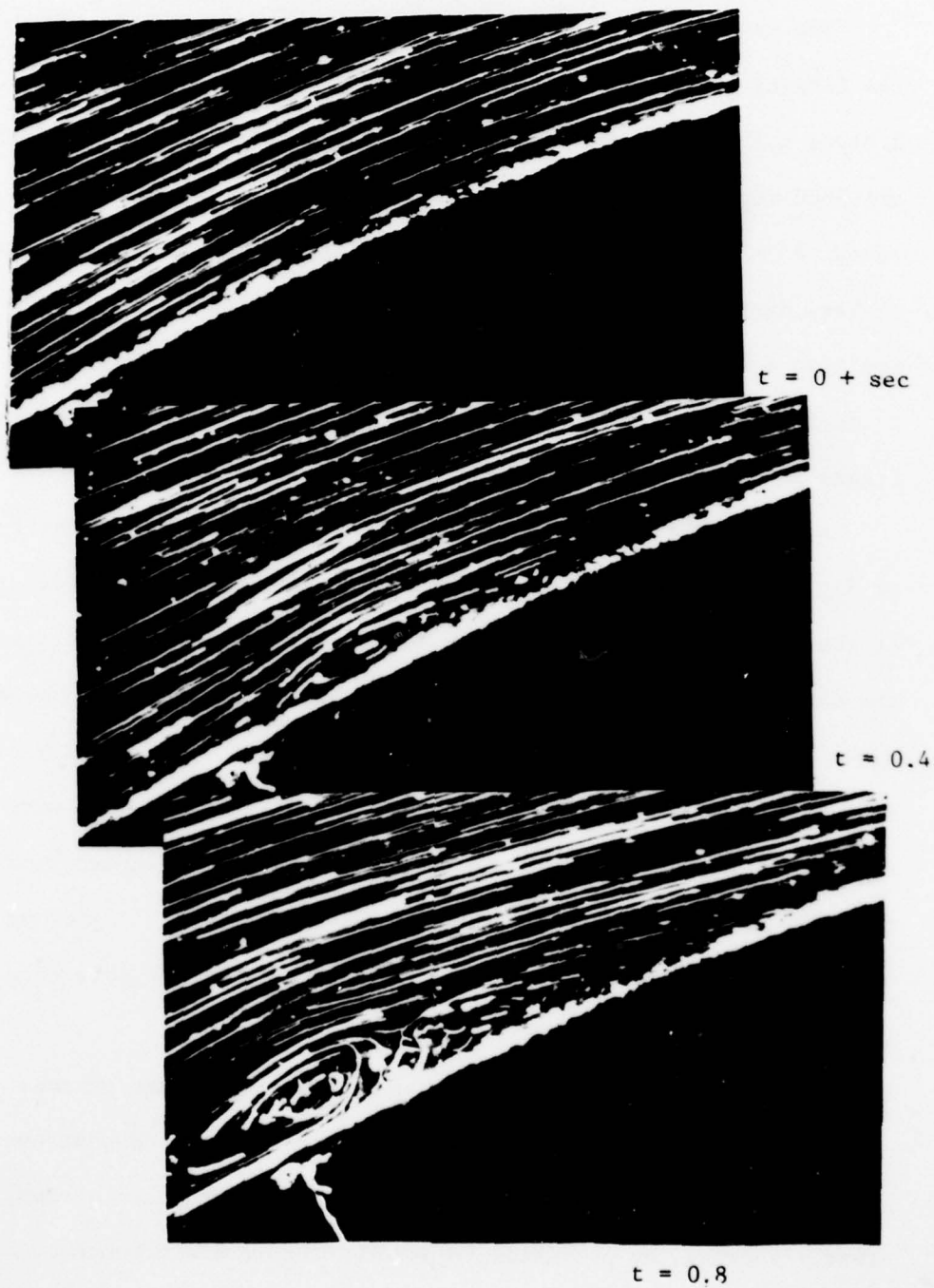
Fig. 4.16   Flow visualization for flow over C and impulsively
bending as in Fig. 3.6, $R_e = 10^4$.
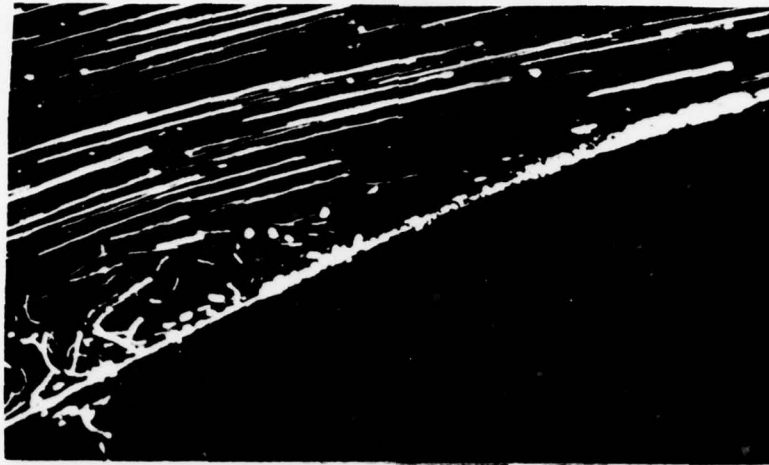
t = 1.2

t = 1.6

Fig. 4.16   cont.

phenomena under consideration: flow reversal and separation. We attribute this fact to the geometrical properties of the model we have constructed, which does not have a monotonically increasing curvature.

CHAPTER 5

PERIODIC DISTURBANCES OF THE OUTER FLOW

In the present paper we report only on some preliminary findings in the area of oscillatory flows. Disturbances are again generated via flaps of different sizes at the downstream end of the models as shown in Figs. 3.4 and 3.5. The flap is driven by a variable-speed motor via pushing rods in the shape of a parallelogram. In this way, no external unbalanced forces are transmitted and the test section is free of vibrations. The mechanism that drives the parallelogram is a classical crank-connecting-rod system with a relatively long rod, so that harmonic oscillations can be approximated. The range of frequencies thus accomplished is 0.5 - 5 Hz. Experience derived from the present experiments and earlier analytical and experimental investigations indicates that separation responds to unsteady disturbances with a characteristic inertia-like behavior. It was thus expected that the domain of interest would rather be in the lower part of the range of frequencies.

The triggering device of Fig. 4.4 is used to signal all the events. A photosensor receives a signal at a specified phase of the rotating disk which drives the flap (see point 6 in Fig. 4.4). This message is fed into the microprocessor, which in turn sends a signal to the camera (line 10) with a delay time Δt, after one cycle is completed. Thus, during the nth cycle, the signal arrives at the camera delayed by $n\Delta t$. If the quantity $n\Delta t$ exceeds the period of oscillation, then the process is repeated starting from zero delay. A schematic representation of the events is shown in Fig. 5.1. More details and the computer program can

85
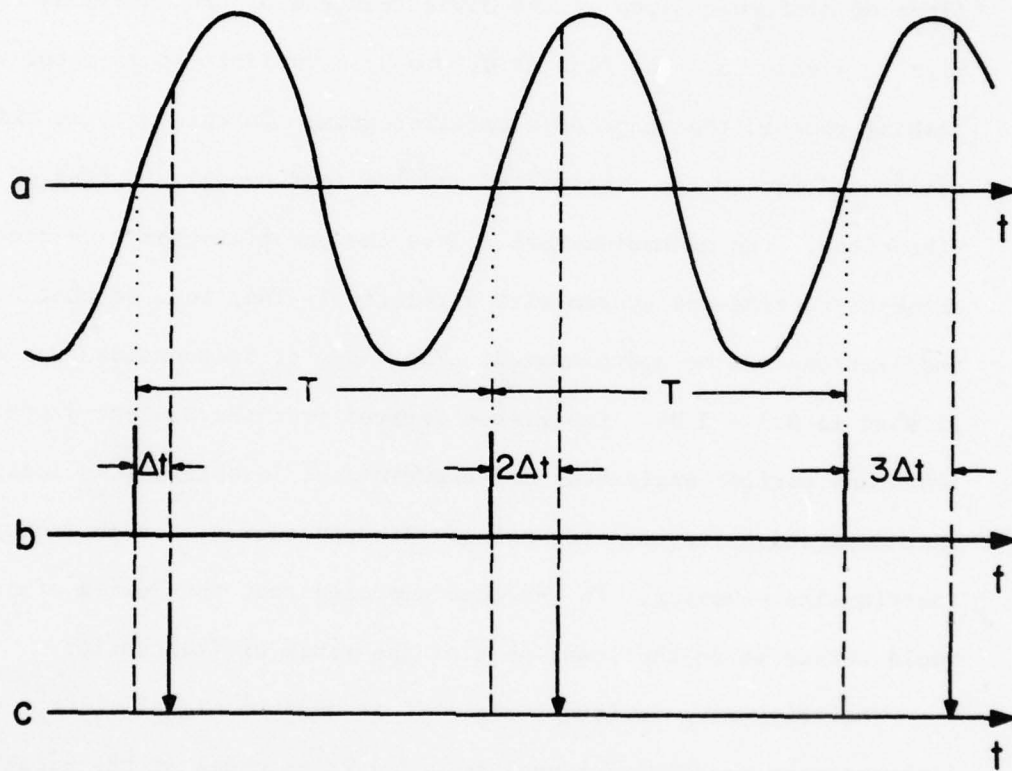
Fig. 5.1   Schematic representation of signals.   a.   Amplitudes of oscillating flap.   b.   Signal received from the LED and led into the microprocessor.   c.   Signal sent to sensing equipment (camera).

1·0 2·8 2·5

5·0 3·15 2·2

5·6 3·5

1·1 4·0 2·0

4·5

1·8

1·25 1·4 1·6
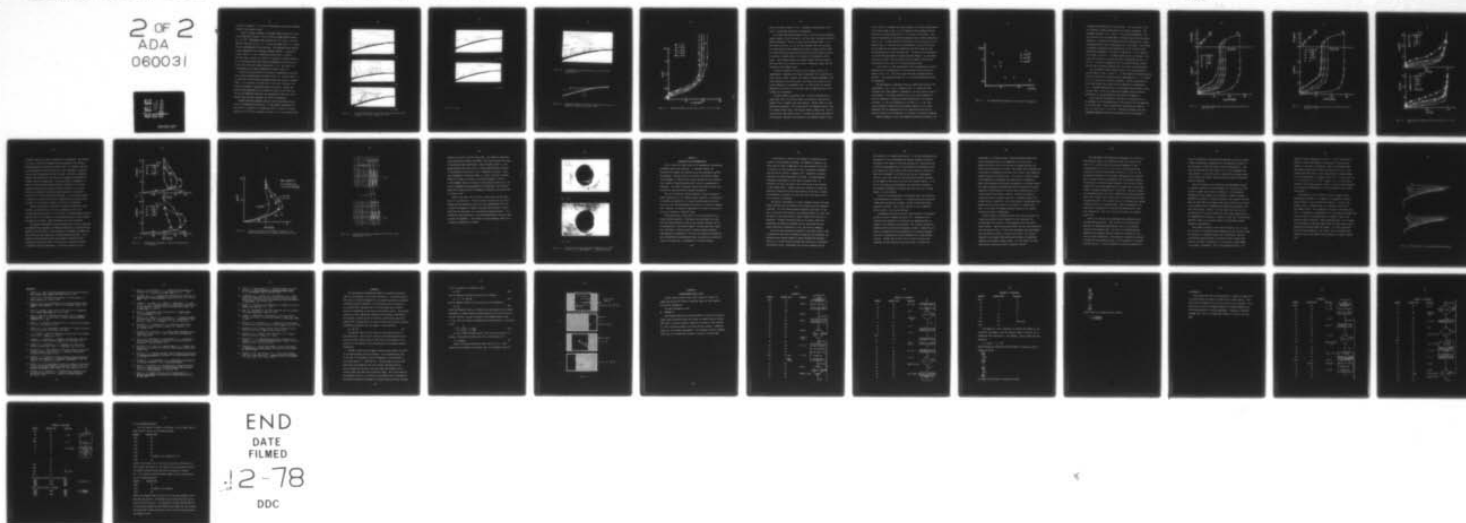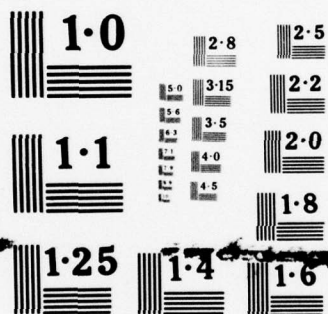
NATIONAL BUREAU OF STANDARDS
MICROCOPY RESOLUTION TEST CHART

be found in Appendix B. In this way measurements are taken at different phases of the periodic motion.

Figure 5.2 shows a sequence of averaged velocity fields of a flow oscillating with a period $T = 0.6$ sec and an average Reynolds number $R_e = 5 \times 10^5$. Measurements were received for $\Delta T = 0.1$ sec. The film exposure time was $1/15$ sec. At $t = 0$ the flap angle was $\theta = 0$. A phase delay of approximately $60°$ was detected. The separated region appears to gain momentum and its thickness increases sharply. A relatively violent vortex is in fact propagating upstream until it engulfs the whole wake. However the location of separation is barely affected by the oscillatory motion and remains approximately at the position $\xi = 15$ mm, that is two unit lengths upstream of $\xi = 0$. The steady flow corresponding to the same configuration is shown in Fig. 5.3.

Velocity profiles measured at the point of separation as detected from the flow visualizations are shown in Fig. 5.4. In this figure it is shown that the wall shear fluctuates between the zero and a negative value. It is therefore concluded that for the case considered, the criterion proposed by Despard and Miller [10] is met. Despard and Miller define separation as the location at which, as one traces the wall in the downstream direction, one encounters for the first time a negative skin friction throughout the cycle of oscillation.

Despard and Miller measured velocity profiles and detected separation by inspecting the outer flow. In the present experiments the outer flow is visualized in considerable detail. However, our interpretation can of course be rightly criticized. It is very possible here

t = T/6
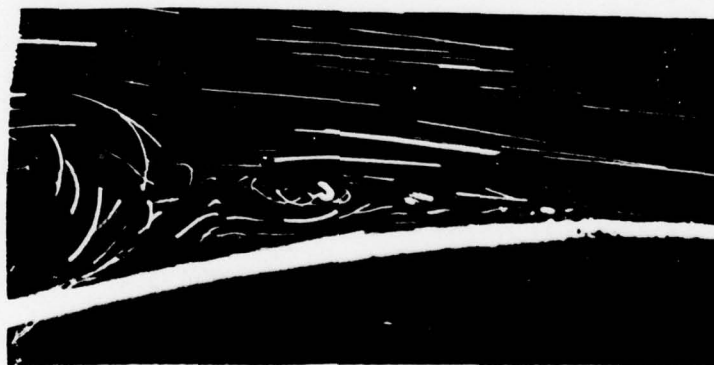
t = 2T/6

t = 3T/6

Fig. 5.2   Flow visualization for oscillatory flow over model A with
a period T = 0.6 sec. and R_e = 5 x 10^5.
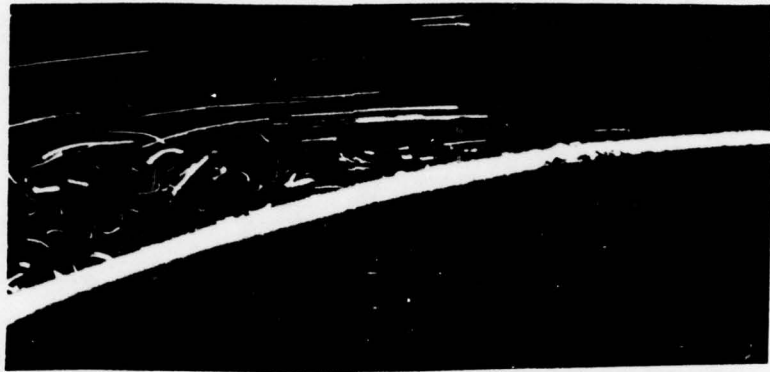
t = 4T/6
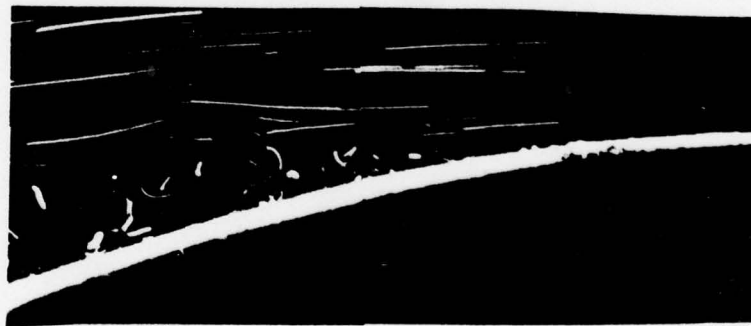
t = 5T/6

Fig. 5.2 cont.

Fig. 5.3a   Visualization of steady flow at $R_e = 10^5$ with flap
positioned at I
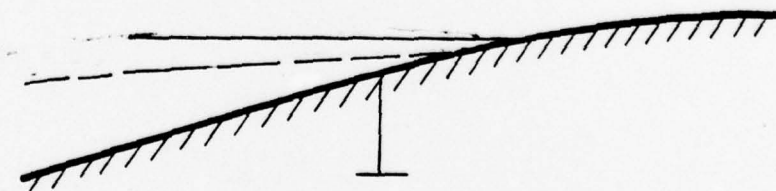
Fig. 5.3b   Boundaries separating recirculating from outer flow. — —
frame T/6 from Fig. 5.2;——Fig. 5.3a.
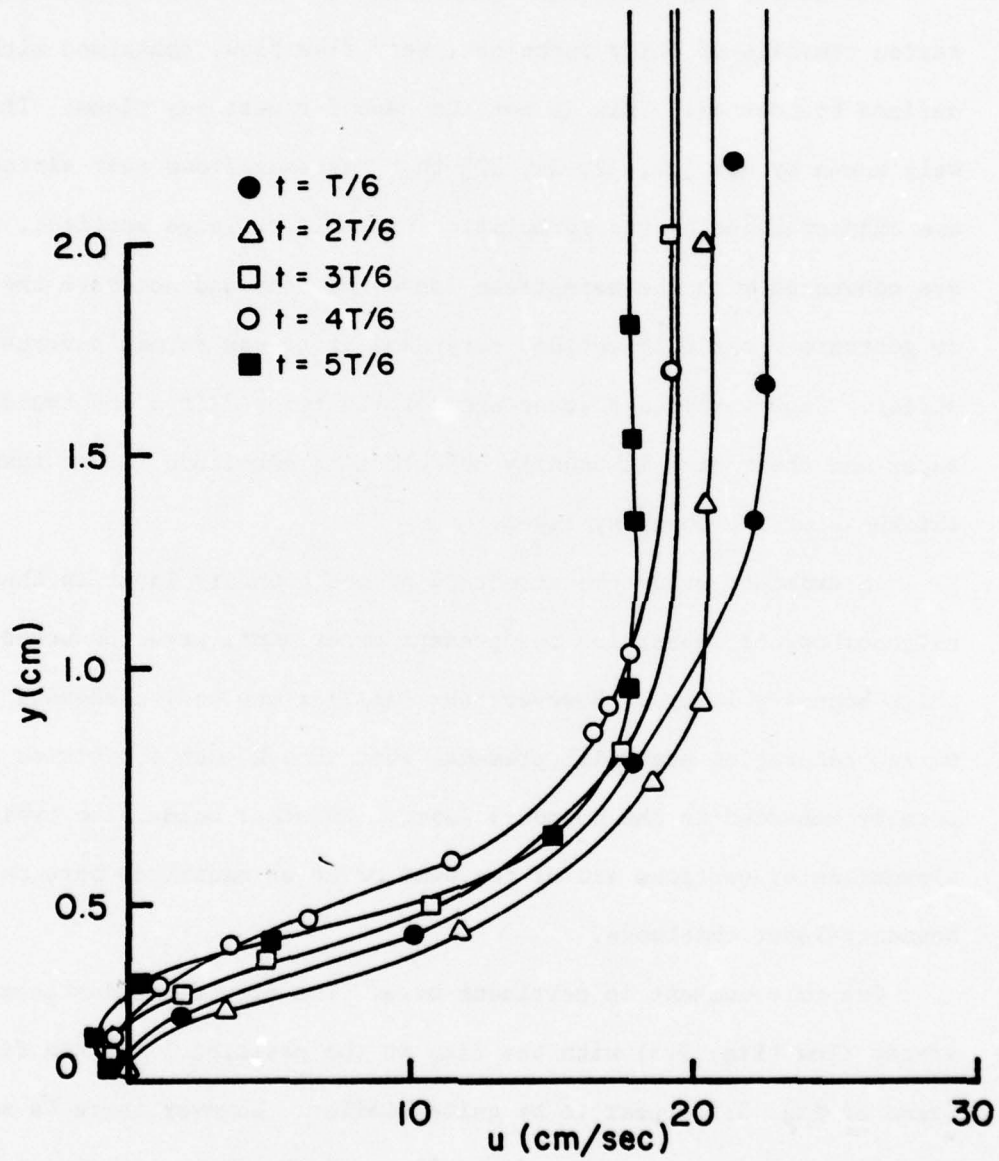
Fig. 5.4   Velocity profiles of the flow of Fig. 5.2 at $\xi = 15$ mm.

that we see what we wanted to see. A different interpretation can be based on alternative definitions of separation.

For steady high Reynolds number flows it is true that the separated region consists of fully turbulent, very slow flow, contained within well defined boundaries. This is not the case for unsteady flows. It is well known by now [21, 22, 36, 37] that unsteady flows over airfoils, are characterized by the formulation of small or large vortices, which are convected with the mainstream leave the body and activate the wake to generate a periodic motion, very similar to von Karman's vortex street. Such vortices however are totally removed from the boundary layer and their size is usually one order of magnitude larger than the thickness of the boundary layer.

In order to study the structure of the boundary layer in the neighborhood of separation the present experiments were conducted with thick boundary layers. However, the familiar unsteady phenomena of the vortex generation are still present, even though such activities are totally embedded in the boundary layer. In other words, the typical dimensions of vortices are of the same order of magnitude here as the boundary-layer thickness.

One more comment is pertinent here. The flow visualizations of steady flow (Fig. 5.3) with the flap at the position I and the first frame of Fig. 5.2 appear to be quite similar. However there is a very significant difference. The first 30 mm of the separated region in Fig. 5.3 contains "dead" fluid. The velocity there is almost zero. On the other hand the same region in Fig. 5.2 contains activated flow which is recirculating. Moreover, the boundary of the separated region in Fig.

5.3 is close to a straight line almost parallel to the free stream whereas in the first frame of Fig. 5.2, the "boundary" that separates the free flow from the recirculating flow is a lot closer to the surface. This could be interpreted as attached non-separated flow as shown schematically in Fig. 5.3b. In other words the dotted line of Fig. 5.3b and the first frame of Fig. 5.2. indicate that the disturbance of the outer flow may be very small and the pressure distribution may not be very far from the distribution of a fully attached flow. It would be very interesting to run the same experiments for higher Reynolds numbers. If the present conjecture is right, then the region below the dashed line should get thinner, since this is part of an attached boundary layer.

In the spirit of these observations it may be appropriate to define separation as the leading point of the energized vortical flow which appears in Fig. 5.2. This vortex grows and moves upstream during the upstroke. Its strength decreases and it is convected downstream during the downstroke.

The displacement of separation from its steady-state position that corresponds to $(\theta_{II} - \theta_I)/2$, is shown in Fig. 5.5. These data were collected from a large number of experiments, ran with various values of the frequency. This figure indicates that in all cases examined the point of separation is displaced further downstream as the frequency increases. In fact for frequencies of the order of $n = 5$ Hz, separation disappears completely from the models examined in this study. Comparison with the experimental data of Despard and Miller was not possible because of the differences in the range of frequencies examined.

Laser velocimetry of such flow appeared inconclusive because of the
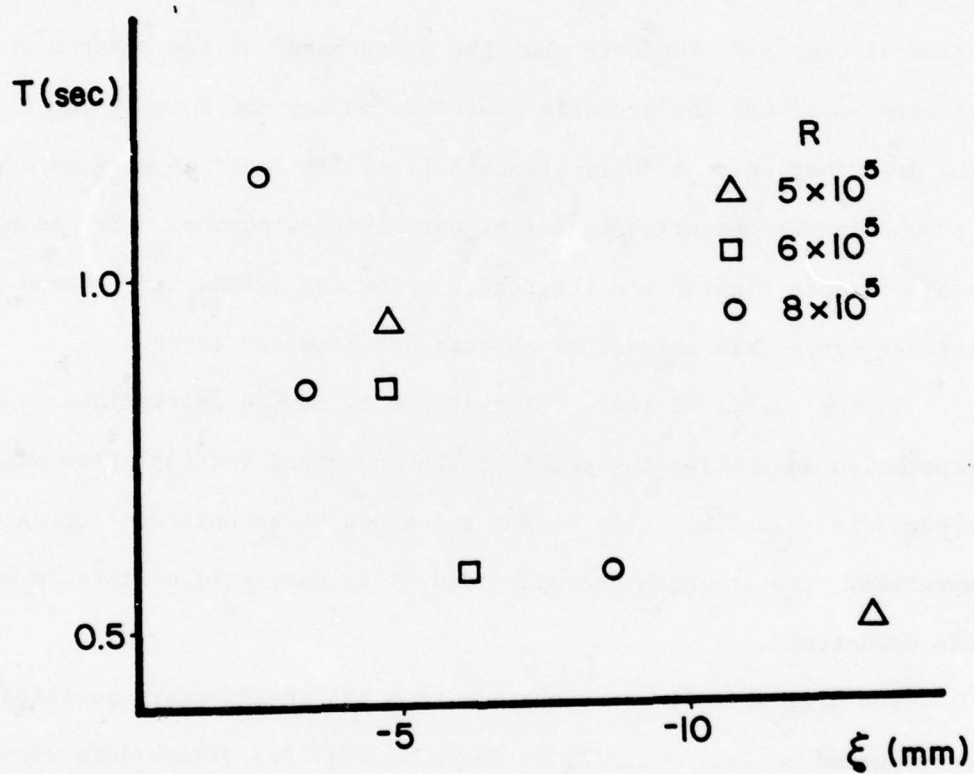
Fig. 5.5   The downstream displacement of the point of separation.

confusing and random motion of the wake flow.   For such flows it will

be necessary to measure simultanously two velocity components.   The

equipment available is not capable of making such measurements.   The

LDV system was used for measurement of boundary-layer flows upstream of

separation.   Oscillatory-flow experiments were conducted with a larger

disturbing flap but with a fixed mean speed of the tunnel.   This results

in stronger accelerations and decelerations of the flow and further

downstream displacement of the point of separation.   This is shown on

top of Figs. 5.6 and 5.7.   In these Figures we plot the average of the

outer flow velocities U_e and the amplitude of variation ΔU_e for $\xi = 0$

and -12.   It should be emphasized that the flowrate remains constant

and the flap disturbances generate only local mean flow accelerations.

The acceleration effect appears clearly in the average absolute

profiles shown in Figs. 5.6 and 5.7.   In these figures the steady velocity

profiles indicate that separation may be approximately at $\xi = 0$, whereas

at $\xi = -12$ the flow is definitely separated.   Optical observations of

such flows indicate that indeed the flow separates at approximately

$\xi = 0$.   Averaged reduced profiles of oscillatory flow are shown in Figs.

5.8a and 5.8b.   In the last figures the averaged values of velocity

derived with an optical method are also shown for comparison.

One of the most characteristic features of oscillatory flow is

an overshoot of the fluctuating part of the velocity over the amplitude

of the outer flow.   Velocity amplitude of oscillation are shown in

Fig. 5.9 a and b for $\xi = 0$ and -12.   Telionis and Tsahalis [38] have

calculated amplitude profiles and indicated that the percentage of
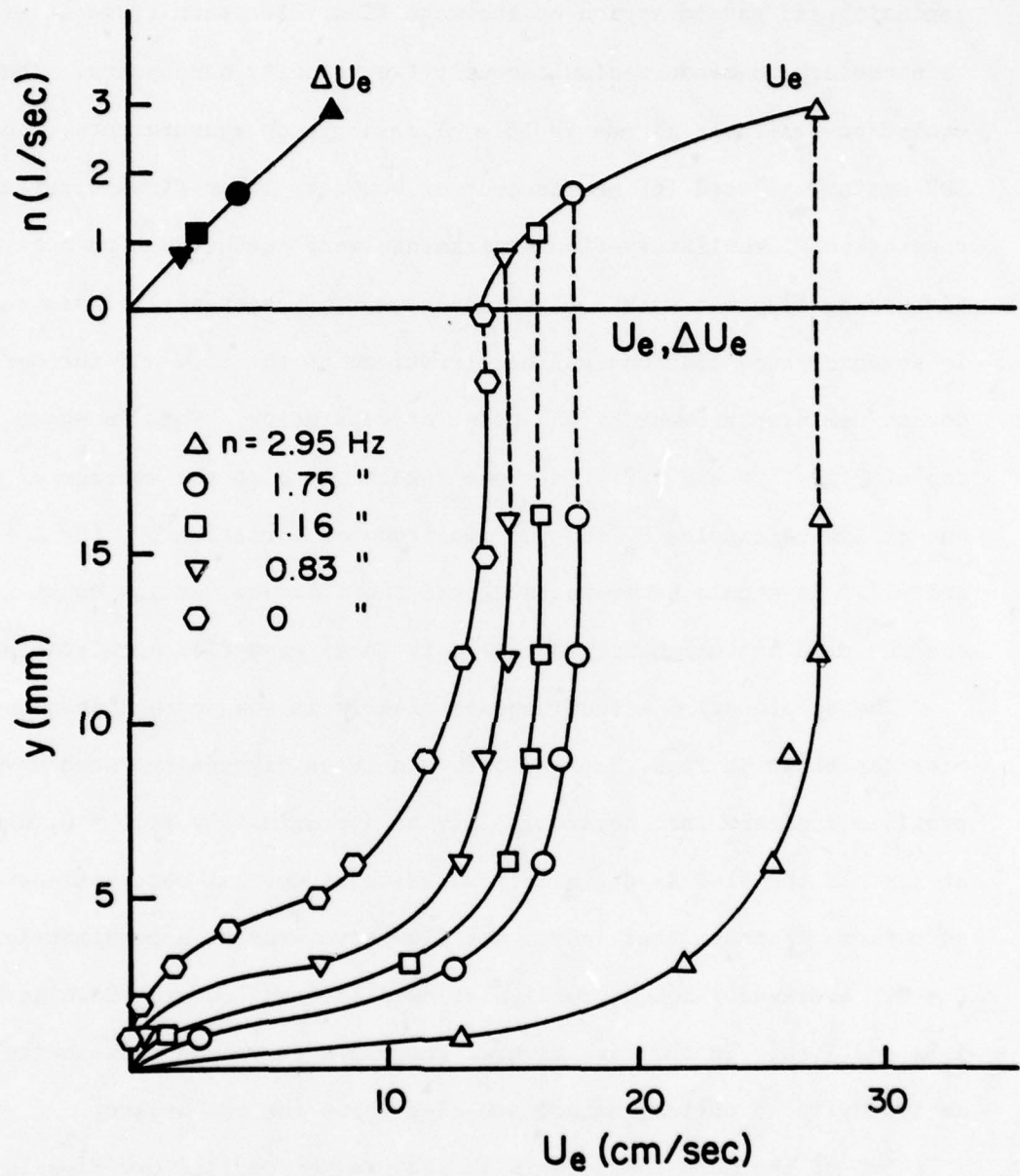
Fig. 5.6   Averaged boundary-layer velocity profiles obtained by
LDV, at ξ = 0.
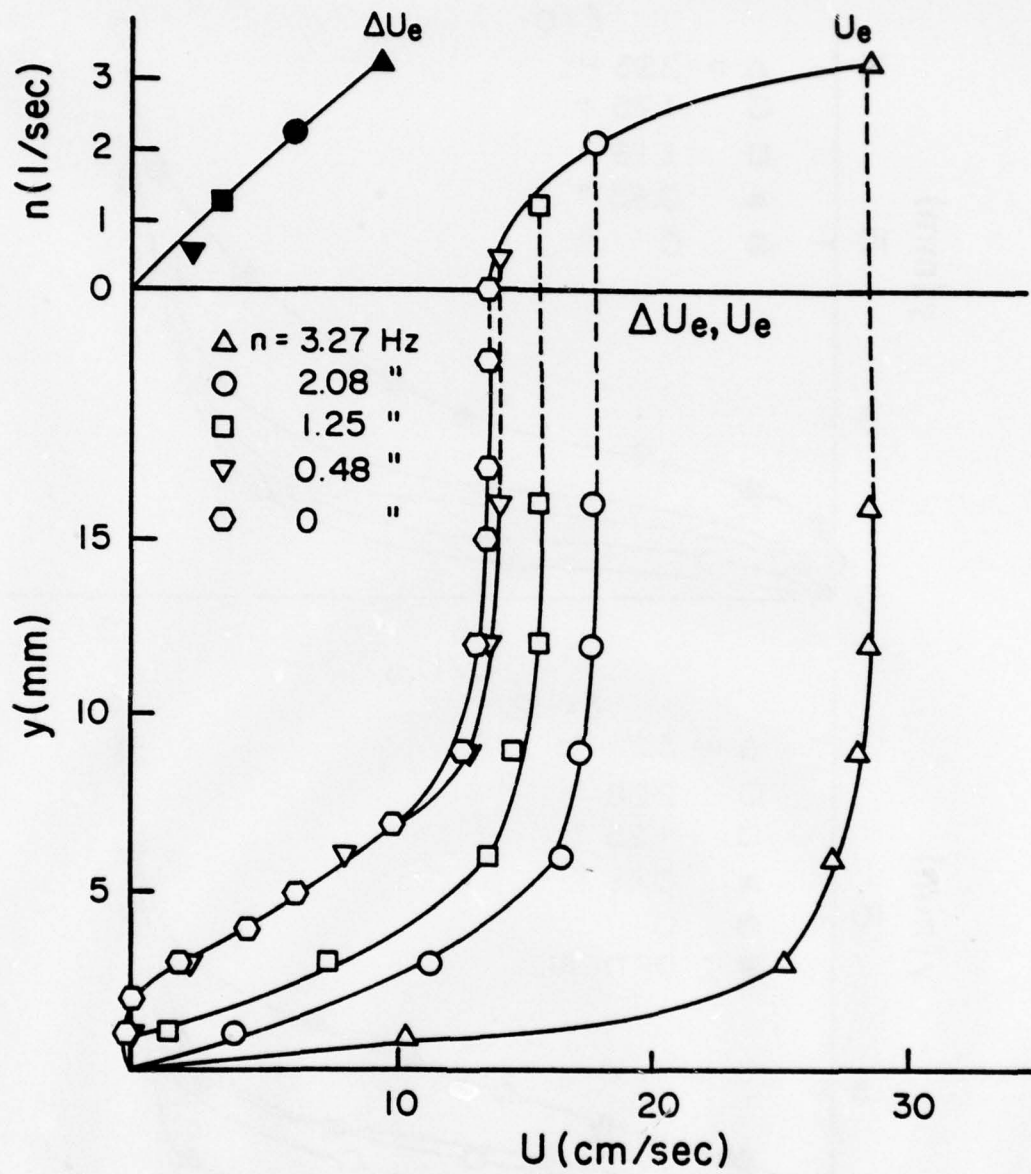
Fig. 5.7   Averaged boundary-layer velocity profiles obtained by LDV, at ξ = -12.
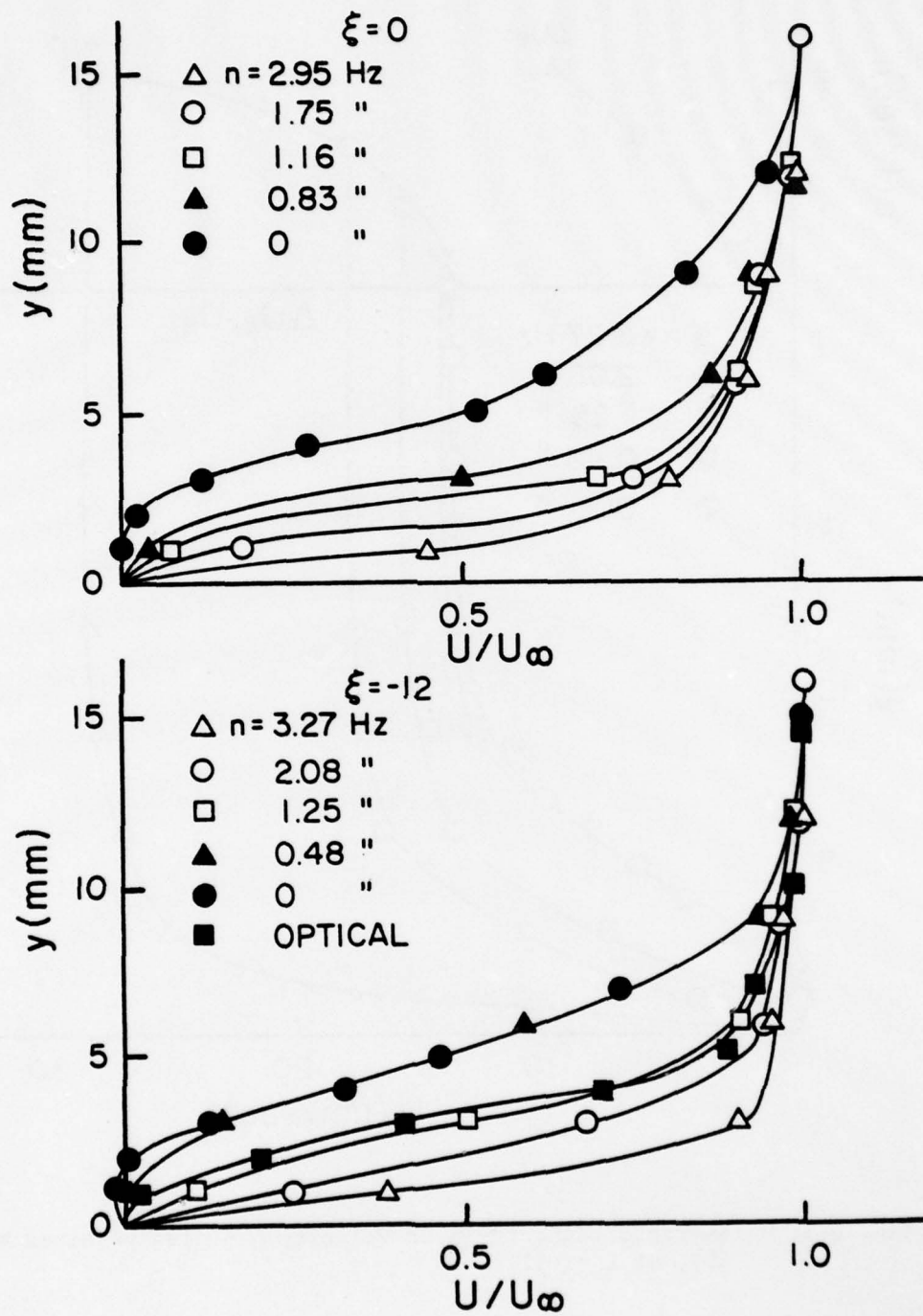
Fig. 5.8   Nondimentional averaged velocity profiles at ξ = 0 and
            -12.

overshoot grows as the point of separation is approached. The theoretical curve of Telionis and Tsahalis that corresponds to the furthest downstream points calculated are shown in Fig. 5.9c together with some of the experimental points obtained with laser anemometry. Admitedly the two body configurations are not the same. The contour assumed by Tsahalis and Telionis has curvature which continuously increases with distance from the leading edge. The present model is preceded by a region of mild favorable pressure gradient followed by a an adverse pressure gradient over a contour with fixed curvature. It was very difficult to determine the proper scaling factors for the vertical scale as well as the distance from separation. It was finally decided to choose as a length scale for both configurations the distance from the point of zero pressure gradient to the point of separation.

Typical LDV results, as recorded on a Hewlett Packard strip chart recorder, are shown in Fig. 5.10, for a frequency of 3.27 Hz ξ = -12 and vertical position of y = 1 and 9 mm. The driving signal received when the flap is in the middle of the upstroke position is also recorded and shown on the figure. Phase differences can also be detected.

The present investigation clearly indicates that, for the conditions investigated here, separation is displaced downstream if oscillations are imposed on the outer flow. This contradicts the findings of Despard and Miller who found that separation is always displaced upstream. In an attempt to bypass special effects that probably interfere with the experimental lay-out described in this section, we decided to design a completely different experiment. To this end a sphere 15 cm in
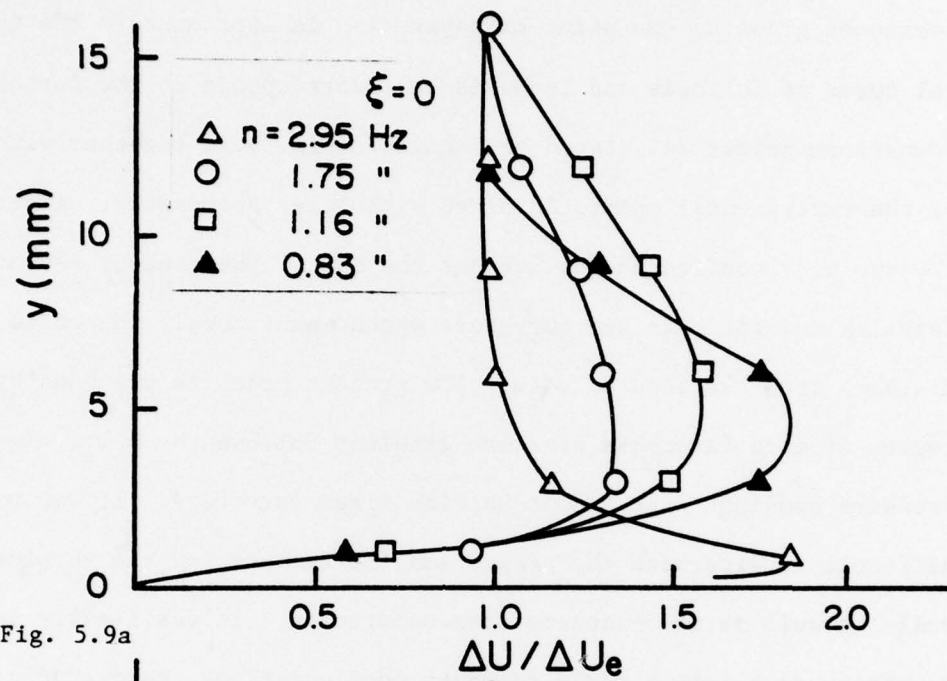
Fig. 5.9a
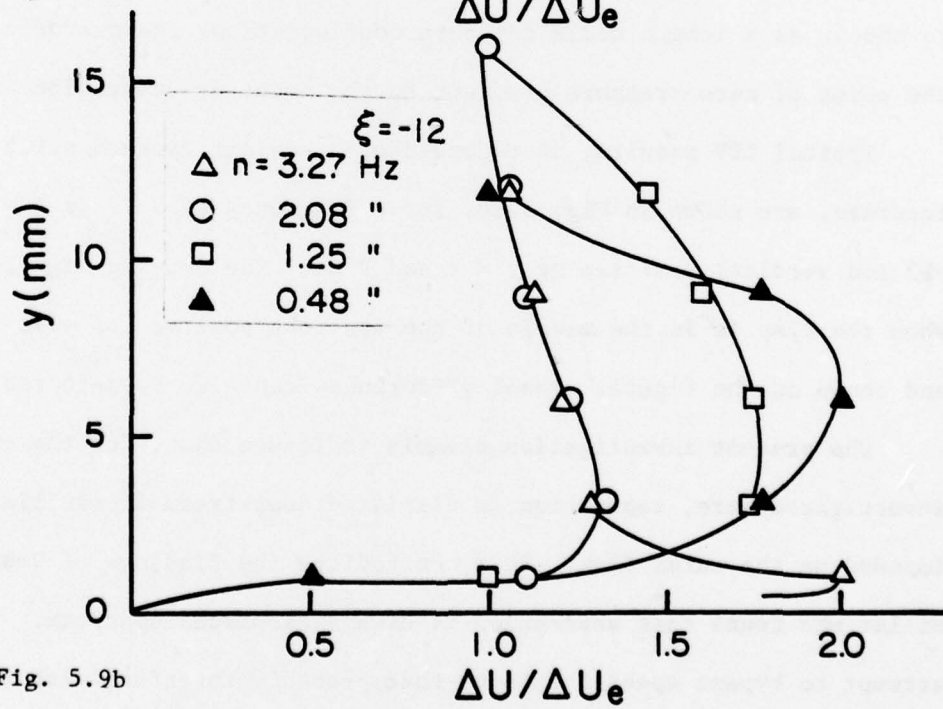
Fig. 5.9b

Fig. 5.9   Dimensionless amplitude of velocity fluctuation for
           $\xi = -12$ and 0.
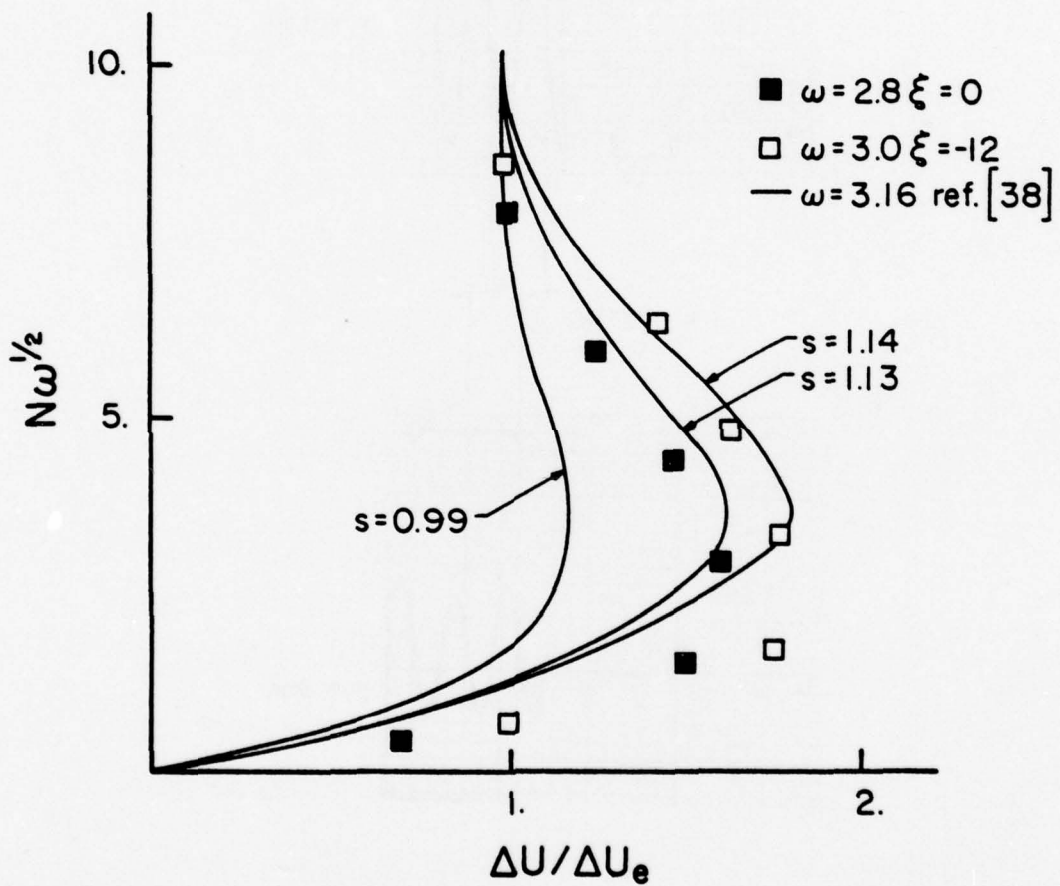
Fig. 5.9c   Velocity amplitude of oscillations compared to the theoretical predictions of Tsahalis and Telionis [38].
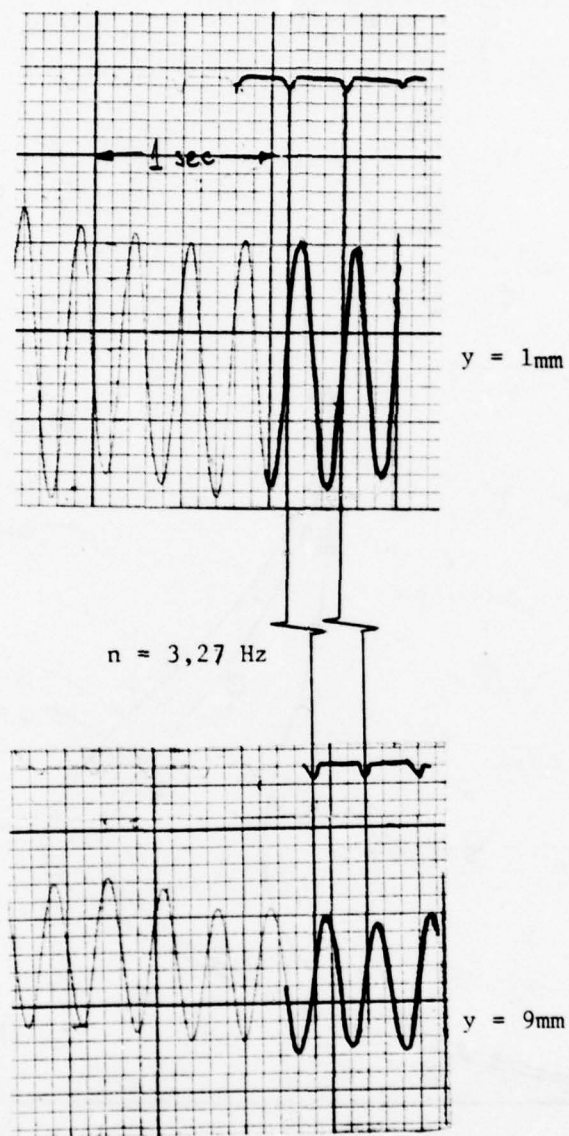
Fig. 5.10   Typical LDV results as recorded on a HP strip chart
recorder for $\xi = -12$.

diameter was towed in the VPI towing tank. Two different supporting struts were used to support the sphere. The first was heavy and rigid. The second was light and flexible. With the sphere towed at a submerged position the system with the second supporting strut vibrated in the direction of the motion with a frequency of 2.5 Herz. These data correspond to a Reynolds number $R_e = U_\infty D/\nu = 10^5$ and a Strouhal number, $St = \omega D/U_\infty = 3.2$, based on the sphere diameter. The flow in the boundary layer was visualized by dyes emitted from ports at the point of stagnation and approximately 45° downstream. The azimuthal angle of 90° from the point of stagnation is marked on the sphere with a continuous line.

Figure 5.11a shows the flow about a sphere towed with the heavy strut at a uniform speed. The dyes clearly indicate that the flow is laminar and that separation occurs on a line approximately 80° from the point of stagnation. Figure 5.11b shows the flow about a sphere towed with the same speed, but oscillating as described before. It is clearly seen that separation is displaced downstream to almost 90° from the point of stagnation. The boundary layer has remained laminar and no signs of transition are evident.
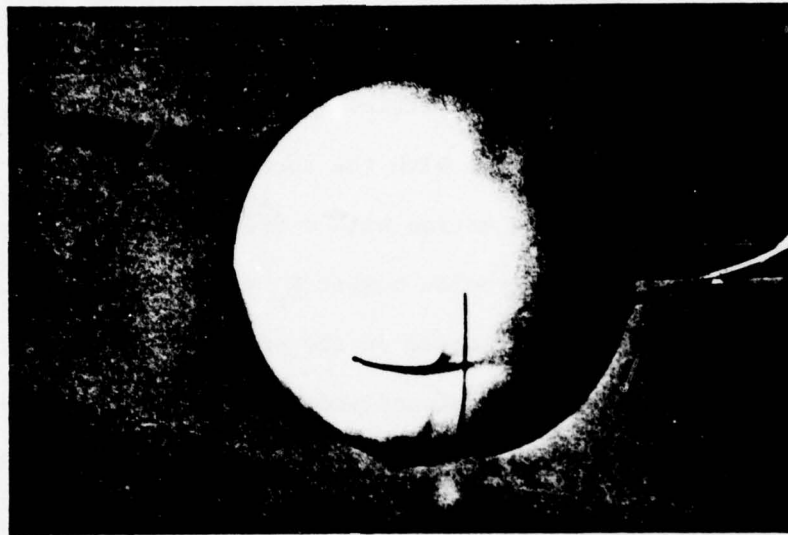
Fig. 5.11a
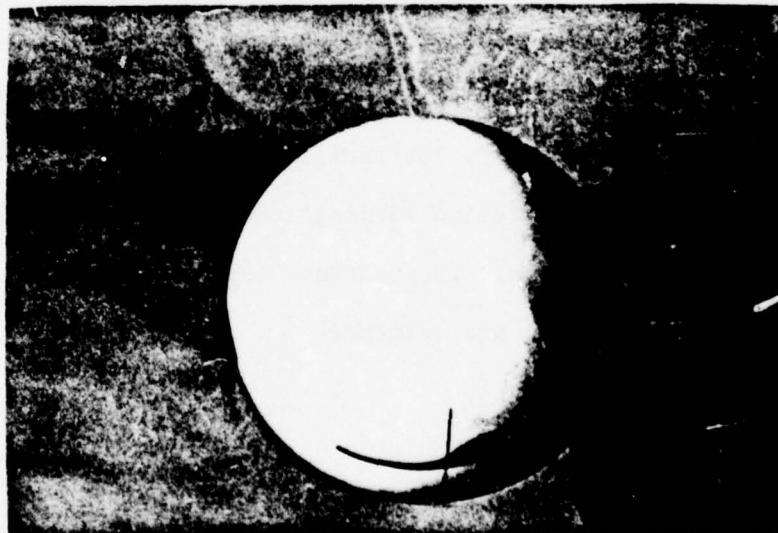
Fig. 5.11b

Fig. 5.11   Visualization of the flow about a sphere for $R_e = 10^5$,
St = 3.2.   a. Fixed sphere, b. oscillating sphere.

CHAPTER 6

CONCLUSIONS AND RECOMMENDATIONS

This is the first formal report on an experimental investigation undertaken almost four years ago. It describes briefly the facilities we designed and constructed and the experimental methods we developed. The main thrust of our effort was directed towards the development of effective and accurate methods of flow visualization, capable of supplying qualitative as well as quantitative information. Our target is unsteady viscous flows and both these characteristics pose particularly irksome difficulties.

The flow visualization method developed, unlike the method of smoke visualization or the hydrogen bubble technique, is nonintrusive. It provides the capability to visualize without special provision, any part of the flow and permits the detection of forward or reversed flow. Moreover, the method is applicable for viscous or inviscid as well as for laminar or turbulent flows.

The ultimate goal of this effort was the investigation of unsteady laminar separation. Experiments were performed with rigid and fixed solid surfaces as well as with flexible surfaces that deform dynamically to the desired shapes. Various models were tested that correspond to varying values of adverse pressure gradients. Time-dependent disturbances of the outer flow pressure distributions were accomplished using downstream flaps, accelerations and decelerations of the mean flow, or deformation of the body contours.

105

A characteristic inertia in the response of separation was observed in the experiments performed. For impulsive changes of the outer flow the order of magnitude of the time required for the flow to arrive at its new flow pattern is L/U_∞ in qualitative agreement with the work of Telionis & Tsahalis [38]. Separation is usually detected by an abrupt thickening of the wake. An upstream-moving separation is preceded by a thin layer of reversed flow. On occasions this layer was found to be as thin as 5% of the thickness of the boundary layer. However, even then, methods that detect separation by measuring the wall shear directly, would fail to predict the phenomenon in unsteady flow since the sign of the skin friction is not related to separation.

The present investigation of actual streamline patterns and wake-shapes indicates that the problem is more complex than was originally conceived. For mild adverse pressure gradients which should be the case in flows over thin airfoils, the separated region is so thin that the point of flow reversal may be easily confused with the point of separation. Pressure variations would not be greatly affected by separation and perhaps the argument and the controversy over the proper definition of separation in this case loses its meaning.

One of the most interesting findings of the present study is that a considerable time after an impulsive change has been performed, the separated region appears somehow to gather momentum and eventually erupts into a violent motion which may later develop in a strong and well-ordered vortex. Subsequently, this activity subsides and the

flow returns to its steady-state pattern. It is very interesting that the pattern of the flow generated by abruptly changing the shape of the body is very similar to the flows generated by a disturbing flap. It should be emphasized that such explosion-type disturbances evolve into large scale vortical wakes, much thicker than the steady-state wakes that correspond to the initial and the final configuration. This is in fact true, even for very mild adverse pressure gradients, as for example in the case of the flow over lifting airfoils. It is due to such large scale disturbances that spectacular overshoots and hysteresis phenomena of integral quantites like lift, pitching moment, etc. are observed.

The study of accelerating or decelerating outer flows indicates a strong influence on separation. A uniform acceleration essentially "washes away" separation altogether, whereas deceleration pushes separation upstream. After a small interval of time, separation slowly returns to its original position.

Preliminary work with oscillatory flows resulted in conclusions similar to those of Despard and Miller [10]. Separation is not affected by the amplitude of oscillation but responds quickly to changes of the frequency of oscillation. The criterion proposed by Despard and Miller is met with reasonable accuracy. However for the range of frequencies and the configuration of the models examined, the point of separation is shifted downstream of its quasi-steady location. Perhaps this is due to the fact that our outer-flow dependence in axial distance varies with time, a situation that

corresponds to a pitching airfoil, whereas Despard and Miller gen-
erated disturbances only in the magnitude of the outer flow.
Despard and Miller [10] do not provide any information about the
shape size and location of the wake. The present study indicates that
the periodic disturbances of the outer flow, induce a well organized
periodic motion in the wake as well. As a result, a vortex is gene-
rated downstream of the Despard and Miller point of separation,
grows, moves upstream and eventually disappears in a periodic fashion.
Once again alternative interpretations may be provided but the most
significant characteristics of the flow may be resolved only if re-
liable pressure data become available. Finally with regard to
oscillatory flows, we should recall that in unsteady airfoil stall
studies [36,37], periodicity quite often leads to leading edge stall,
whereby the whole upper surface of the airfoil is covered with a
wake. In this case the Despard and Miller model and the present
observations would be inapplicable.

Earlier studies of unsteady viscous flows [18-23] indicate that
large scale descrete vortices emanate from the leading or the
trailing edge of an airfoil, or even sometimes from a relatively
smooth surface. These vortices grow quickly and very soon extend deep
into the potential flow. In fact their development has been modeled
quite accurately in terms of inviscid flow theory. The vortices
captured in the present flow-visualization studies are completely
embedded in the laminar boundary layer. Yet they exhibit the same
characteristic properties found in potential vortices.

This experimental investigation was undertaken in an effort to shed some more light to the theories of Sears [2], Moore [3] and Rott [5], to clarify some of the physical arguments of later contributions [10, 14, 15, 16, 22, 26, 28, 35] and provide some evidence for the most recent numerical work [14, 16, 24, 34, 38]. An objective evaluation of the present findings and their relationship to earlier theories and numerical data is therefore necessary. To begin with, it has been always advocated [2-5] and most recently proved [16], that steady separation over a moving wall can be transformed to unsteady separation over a fixed wall. The first problem was investigated here first and the saddle points predicted theoretically, were captured for the first time, for both upstream and downstream moving walls. The evidence of Fig. 2.8 indicates that the MRS criterion is met for a downstream wall, since the branches of the saddle point configuration are parallel and perpendicular to the wall respectively. This is not true for the case of an upstream moving wall.

Most of the unsteady flow experiments were performed with an upstream moving separation. This is easier to realize and more important for engineering applications, since it is intimately connected with unsteady stall. The case of a downstream moving separation was attempted and some results were included here but they are rather inconclusive. Unfortunately no extensive excursions of separation were possible without a total breakdown of the separation-wake pattern. It was not possible to observe and measure the

speed of propagation of separation and therefore it was not possible
to make a quantitative comparison with the definition of Sears [2]
and the theory of Sears and Telionis [28] and Williams [16]. How-
ever the qualitative patterns appear to be in full agreement with
these theories. A very thin layer of reversed flow precedes indeed
a more violent wake region, where substantial pressure disturbances
should be expected.

One of the objectives of theoretical and experimental studies
of unsteady separation is the development of a crtierion that could
be used to signal the location of separation. In the numerical
integration of the boundary-layer equations, a method is needed to
determine the location of unsteady separation and therefore the point
where the wake begins and probably large scale vortices are initiated.
It was proposed that the boundary-layer separation singularity could
serve this purpose. However it is well known, that real life and
as expected, the full Navier Stokes are free of any singularities in
the neighborhood of separation. Except for large scale visualizations,
therefore, there is no available method for determining unsteady
separation experimentally.

The evidence contained in this report indicates that, at least
for the case of an upstream moving separation and for the early stages
of the motion, a consistent pattern can be identified. The thin
recirculating region upstream of separation, forms a bubble which
closes at the point of separation. At this point a second bubble,
a lot larger, is generated. This is the separation bubble. The

pattern is shown schematically in Fig. 6.1. Both vortices have a

sense of rotation that matches the direction of the outer flow.

However, at the point of separation a small recirculating bubble

with opposite sense may be formed, as shown in Fig. 6.1.b. Such

patterns have been found in a very large number of frames obtained

by flow visualization; for example in Fig. 4.16, $t = 8$ sec; Fig. 4.8,

$t = 2$ sec and Fig. 5.2, $t = 2T/\sigma$. Figure 4.5, $t = 1.5$ sec may be

thought of as a pattern similar to Fig. 6.1.b with a scale stretched

in the direction perpendicular to the wall, because of the low Rey-

nolds number.

This behavior of the flow may be used as a signal for the

approaching catastrophe. For example the v-component of velocity

should indicate a very characteristic behavior. As long as the

boundary layer is attached there is a continuous outflow from

the boundary layer. The v-component of velocity is therefore posi-

tive. Its separation is approached and in the process of passing from

the first vortex to the second vortex, a change in sign of this

quantity should be detected. These properties should not be thought

of as describing low Reynolds number flows for which distinct and or-

ganized recirculating bubbles are common. It is well established

by now and was documented in this report, that in unsteady flows,

organized vortices may emerge from the region of a steady turbulent

wake.
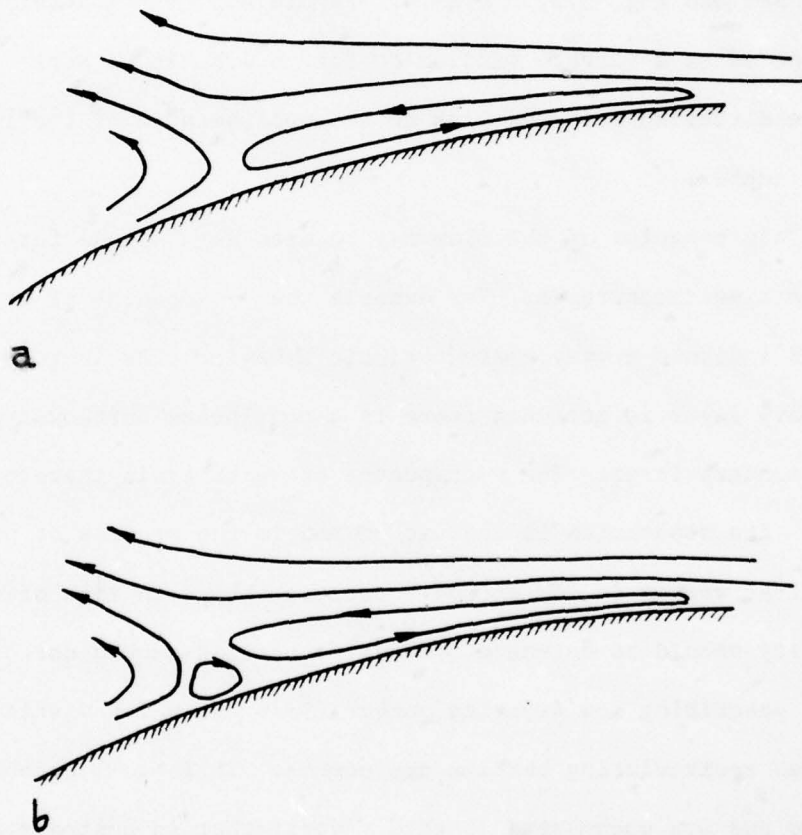
Fig. 6.1 Flow patterns for an upstream moving separation.

References

1. Prandtl, L., "Uber Flussigkeitsbewegung bei sehr kleiner Reibung", Proc. Intern. Math. Congr. Heidelberg, 484-91, 1904.

2. Sears, W. R., "Some Recent Developments in Airfoil Theory", J. Aero. Sciences, 23, 490-499, 1956.

3. Moore, F. K., "On the separation of the Unsteady Boundary Layer", Boundary Layer Research, H. Gortler, ed. Springer, Berlin, 296, 1958.

4. Rott, N., Unsteady Viscous Flow in the Vicinity of a Stagnation Point, Quart. Appl. Math. 13, p. 444, 1956.

5. Rott, N., Theory of Time Dependent Laminar Flows, in Theory of Laminar Flows, F. K. Moore (ed.), Princeton University Press, Princeton, N.J., 1964.

6. Vidal, J. R., "Research on Rotating Stall in Axial-Flow Compressors, Part III", WADC TR-59-75, 1959.

7. Ludwig, G. R., "An Experimental Investigation of Laminar Separation From a Moving Wall", AIAA Paper 64-6, 1964.

8. J. S. Tennant, "A Subsonic Diffuser with Moving Walls for Boundary-Layer Control", AIAA J. 11, 240-242.

9. Tennant, J. S. and Yang, T., "Turbulent Boundary-Layer Flow from Stationary to Moving Surfaces" AIAA J., 11, 1156-1160, 1973.

10. Despard, R. A. and Miller, J. A., "Separation in Oscillating Laminar Boundary-Layer Flows", J. Fluid Mech., 47, 21-31, 1971.

11. Sandborn, V. A., "Characteristics of Boundary Layers at Separation and Reattachment", Res. Memo. No. 14, College of Engineering, Colorada State University, 1969.

12. Simpson, R. L. "Features of Unsteady Turbulent Boundary Layers as Revealed from Experiments", in Unsteady Aerodynamics, AGARD PRE-PRINT No. 227, paper No. 19, 1977.

13. Kenison, R. C., "An Experimental Study of the Effect of Oscillatory Flow on the Separation Region in a Turbulent Boundary Layer", in Unsteady Aerodynamics AGARD PREPRINT No. 227, paper No. 20, 1977.

14. Telionis, D. P., and Werle, J., "Boundary-Layer Separation from Downstream Moving Boundaries", Journal of Applied Mechanics, 95, 389-374, 1973.

114

15. Sears, W. R. and Telionis, D. P., "Boundary Layer-Separation in Unsteady Flow", S.I.A.M. J. of Appl. Math. 28, 215-   , 1975.

16. Williams, III, J. C., Incompressible Boundary-Layer Separation, in Annual Review of Fluid Mechanics, Annual Reviews Inc., 9, 113-144, 1977.

17. Schraub, F. A., Kline, S. J., Henry, J., Rumstadler, P. W., and Littel, A., "Use of Hydrogen Bubbles for Quantitative Determination of Time Dependent Velocity Fields in Low-Speed Water Flows", J. of Basic Eng., 87, 429-444.

18. Werle, H. "Hydrodynamic Flow Visualization" in Annual Review of Fluid Mechanics, 5, 1973.

19. Ruiter, G. H., Nagib, H. M., and Fejer, A. A., "Unsteady Boundary-Layer Separation over Oscillating Airfoils", Proceedings of SQUID Workshop, Atlanta, ed., Marshall, F. J., pp. 423-425, 1971.

20. McCroskey, W. J., "Dynamic Stall on a Helicopter Rotor Blade", Proceedings of SQUID Workshop, Atlanta, ed., Marshall, F. J., pp. 346-350, 1971.

21. McAlister, K. W. and Carr, L. W., "Water-Tunnel Experiments on an Oscillating Airfoil at R_e = 21,000", NASA Technical Memorandum 78446, March 1978.

22. Carr, L. W., McAlister, K. W. and McCroskey, W. J., "Analysis of the Development of Dynamics Stall Based on Oscillating Airfoil Experiments", NASA TN D-8382, 1977.

23. McAlister, K. W., Carr, L. W. and McCroskey, W. J., "Dynamic Stall Experiments on the NACA 0012 Airfoil", NASA Technical Paper 1100, January 1978.

24. Telionis, D. P., "Unsteady Boundary Layers-Attached and Separated", in Unsteady Aerodynamics, Proceedings of an AGARD Symposium, Paper No. 17, 1977.

25. Telionis, D. P. and Koromilas, C. A., "Experimental Investigation of Unsteady Separation", VPI & SU Engineering Report.

26. Mehta, U. B. and Lavan, Z., "Starting Vortex, Separation Bubbles and Stall-a Numerical Study of Laminar Unsteady Flow aroung an Airfoil, J. Fluid Mechanics, 67, 227-256, 1975.

27. Mehta. U. B., "Dynamic Stall of an Oscillating Airfoil, in Unsteady Aerodynamics, Proceedings of an AGARD Symposium, Paper No. 23, 1977.

28. Sears, W. R. and Telionis, D. P. "Unsteady Boundary-Layer Separation", in Recent Research of Unsteady Boundary Layers, E. A. Eichelbrenner (ed.) 1, 404-447, 1971.

29. Pruppacher, H. R., LeClair, B. P. and Hamielec, A. E., "Some Relations Between Drag and Flow Pattern of Viscous Flow past a Sphere and a Cylinder at Low and Intermediate Reynolds Numbers", J. Fluid Mech., 44, 781-790, 1970.

30. Homann, F., Einfluss grosser Zähigkeit bei Strömung um Zylinder Forsch. Geb. Ing. Wes., 7, 1, 1937.

31. Fage, A., Photographs of Fluid Flow Revealed with an Ultramicroscope Proc. Royal Soc. A 144, 381, 1934.

32. Taneda, S., Experimental Investigation of the Waves Behind Cylinder and Plates at low Reynolds Numbers J. Phys. Soc. Japan, 11, 302.

33. Fansler, K. S. and Danberg, J. E., "Boundary-Layer Development on Moving Walls Using an Integral Theory", AIAA J. 14, 1137, 1976.

34. Tsahalis, D. TH., "Laminar Boundary Layer Separation from an Upstream Moving Wall," AIAA J., 15, 561-566, 1976.

35. Telionis, D. P., "Boundary Layer Separation", Ph.D. Thesis, Cornell University, Ithaca, N.Y., 1970.

36. McCroskey, W. J., "Some Current Research in Unsteady Fluid Dynamics - the 1976 FREEMAN SCHOLAR LECTURE", Journal of Fluids Engineering, Vol. 99, pp. 8-38, 1977.

37. McCroskey, W. J., "Recent Developments in Rotor Blade Stall", in Aerodynamics of Rotary Wings, AGARD Conference Proceedings No. III, 17, 1972.

38. Tsahalis, D. Th., and Telionis, D. P., "Oscillating Boundary Layers with Large Amplitude", in Unsteady Flows in Jet Engines, F. O. Carta (ed.), pp. 407-416, 1974.

APPENDIX A

The visualization and measuring method of recording the particle paths on film requires a focal plane type shutter. A leaf-type shutter will result to uneven illumination of the particle path due to apperture variations during the exposure. The focal-plane shutter consists of two curtains both traveling close to the film plane with a uniform velocity V independent of the value of the shutter speed S. This uniform velocity for most commercially available 35 mm cameras is 3600 mm/sec. The distance d between the end of the first curtain which starts the exposure and the beginning of the second curtain which ends the exposure, determines the exposure time the image of a still particle.

$$\Delta t_o = \frac{1}{S} = \frac{d}{V} \tag{A1}$$

The exposure time is not the same for still particles and for moving particles. This is due to the fact that a moving particle will meet the closing curtain sooner or later than a still particle if its motion is in the opposite or the same direction as the moving curtains respectively.

Consider a particle whose image is moving on the plane of the film in the same direction with the curtains. Let its exposed path, that is the path of its image be ℓ and its component in the direction of the curtain motion ℓ'. (See Fig. A2). This path has its tail at the point where the boundary of the first curtain coincides with the particle image and its head at the point where the boundary of the second curtain coincides with the particle image. For a still particle the exposure time is $t_o = 1/S$ which is the nominal time of the shutter. Now since the particle is moving in the same direction with the curtains

116

it will be exposed by a additional time

$$\Delta t = \frac{\ell'}{V} \qquad (A2)$$

The real exposure time for this particle is therefore

$$t_p = t_o + \Delta t = \frac{1}{S} + \frac{\ell'}{V} \qquad (A3)$$

and the average velocity of the particle can be determined by

$$V_p = \frac{\ell}{t_p} \qquad (A4)$$

Since this exposure time t_p is different for each particle in the same photograph, to achieve absolute proportionality of the particle path to the flow velocity, t_p must be reduced to the nominal exposure time $t_o = \frac{1}{S}$. This can be done by multipling the particle path by a correction factor

$$C = \frac{t_o}{t_p} = \frac{\frac{1}{S}}{\frac{1}{S} + \frac{\ell'}{V}} = \frac{1}{1 + \frac{S\ell'}{V}} \qquad (A5)$$

It can be shown *following similar steps that if the particle is* moving in the opposite direction then the correction factor is

$$C = \frac{1}{1 - s\ell'/V} \qquad (A6)$$

Typical correction facotrs may range from 0.9 to 1.1. This method was used whenever C was larger than 1.05 or smaller than 0.95.

118

d

1st curtain

2nd curtain

v   V = 3600mm/sec   24mm

Exposed area of the film

Focal plane shutter

$\text{exposure} = \frac{1}{s} = \frac{d}{v}$ (sec)

1

36mm

particle

$t = 0$

exposure starts

2a

ℓ_0

particle path

$t = t_0 = \frac{1}{s}$

2b

d

ℓ'

$t = t_0 + \Delta t = \frac{1}{s} + \frac{\ell'}{v}$

2c
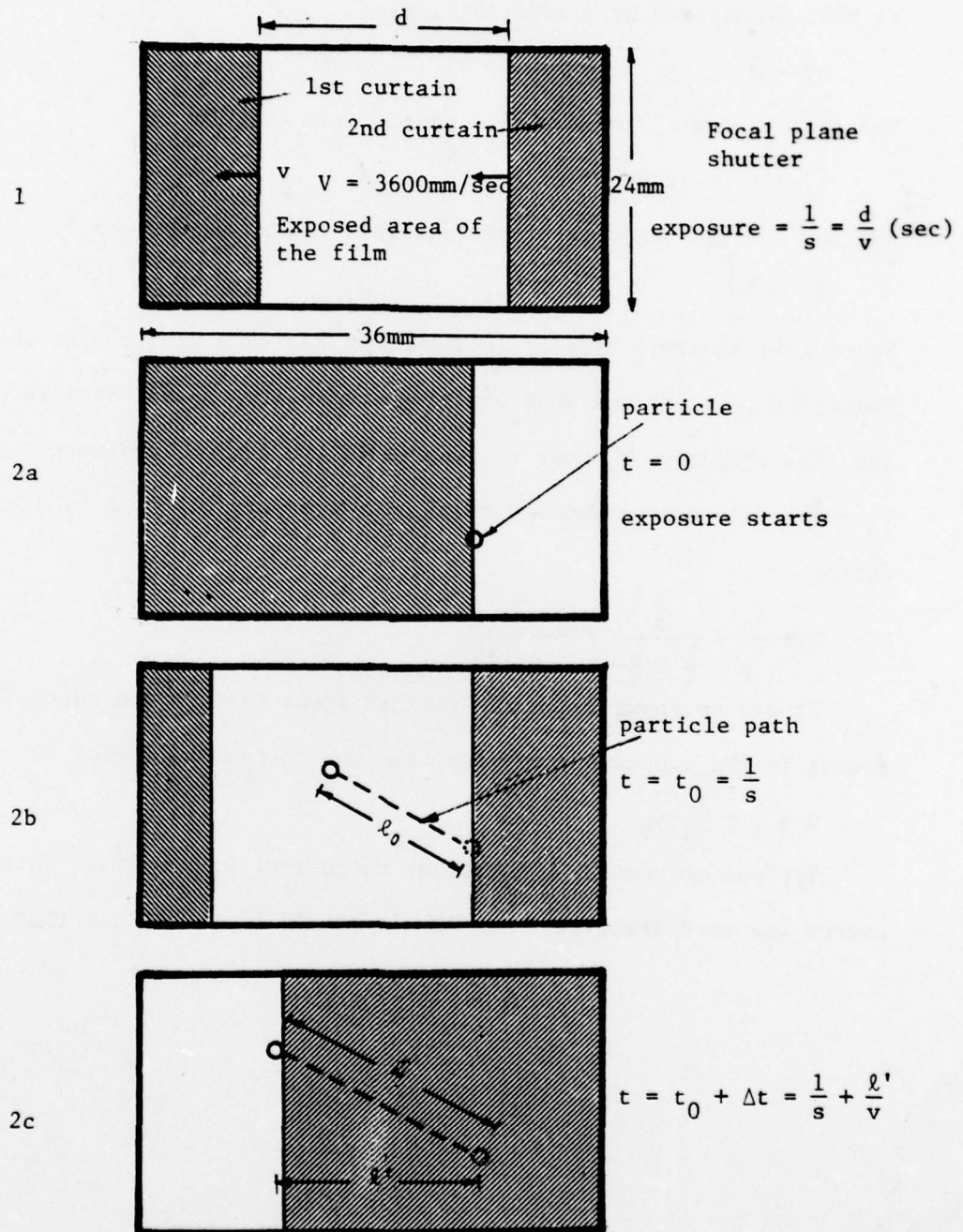
Fig. A

APPENDIX B

MICROPROCESSOR USER'S GUIDE

A KIM-1 microprocessor (series G530) is used to trigger the camera and activate the flash at specified times for both transient and periodic experiments.

Two basic programs are used:

B1. PROGRAM 01

This program instructs the microprocessor to receive an initiation signal from an external sensor then triger the camera after an initial time delay t_o and then continue trigering the camera at time intervals Δt_1 until a specified number of pictures has been exposed. Program 01 applies to the transient experiments. This program in machine language form, that is in hexadecimal notation is listed on the next page.

PROGRAM 01

ADDRESS	MACHINE CODE	OPERATION
0000	8C	
01	03	Y→1703
02	17	
03	8E	
04	01	X→1701
05	17	
06	A9	(FB)→A
07	FB	
08	CD	
09	00	A-1700
0A	17	
0B	F0	Branch on zero
0C	F9	
0D	A9	(32) → A
0E	32*	
0F	8D	
0010	07 time	A → 1707
11	17 base number	
12	EC	
13	06	X-1706
14	17	
15	D0	Branch on zero
16	FB	

START

Initialize
Port 1702 output
Port 1700 input

Accumulator = FB

is input ≠ FB? NO
yes

Load the number of the time base to the timer (1707) through the accumulator

is timers count zero? NO
yes
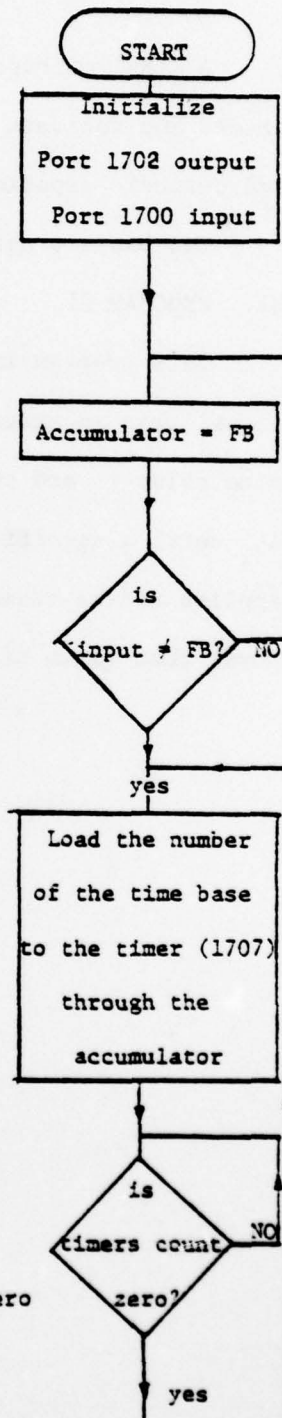
PROGRAM 01 (CONTINUED)

ADDRESS	MACHINE CODE	OPERATION	
17	C6	D6 → D6-1	Decrement memory
18	D6		F6 by1
19	E4	X-D6	is
1A	D6		D6 = 0? NO
1B	D0	Branch on zero	
1C	F0		yes
1D	A5	D7 → A	
1E	D7		transfer D7 to D6
1F	85	A → F6	
0020	D6		
21	EE		Increment output
22	02	1702 → 1702 +1	(1702) by 1(signal)
23	17		
24	C6	D8 → D8 - 1	Decrement D8 by 1
25	D8		
26	E4	X - D8	is
27	D8		F8 = 0? NO
28	D0	Branch on zero	
29	E0		yes
2A	4C		
2B	4F	GO TO START	Return to the START
2C	1C		STOP

PROGRAM 01 (CONTINUED)

ADDRESS	MACHINE CODE	OPERATION
00D6	a	n_o
D7	b	n_1
D8	c	x_2
D9	c	x_2
F4	01	y
F5	00	x
17FA	00	NM1 Vector
17FB	1c	

The symbols a, b and c represent the initial time number n_o, the continuous time number n_1 and the required number of pictures, x_2 in hexadecimal form respectively. The numbers n_o and n_1 define the time intervals:

$$t_o = n_o \Delta t/2, \quad t_1 = n\Delta t$$

Before running the program the desired number of pictures x_2 may be changed as follows

AD

00F8

DA

c

AD

0000

GO

To change the time base Δt, proceed as follows

AD

OODE

DE

m

000

GO

where m can be calculated from the formula

$$m = \frac{1}{2}\left[\frac{\Delta t (sec)}{0.001024}\right]$$

B2 PROGRAM 02

This program instructs the microprocessor to receive a signal from an external sensor and triger the camera after a delay time Δt. This delay time is increased by Δt after the first cycle is completed. Thus during the nth cycle, the signal arrives at the camera delayed by $n\Delta t$. This program applies to periodic experiments. Program 02 in machine language form, that is in hexadecimal notation is listed on the next page.
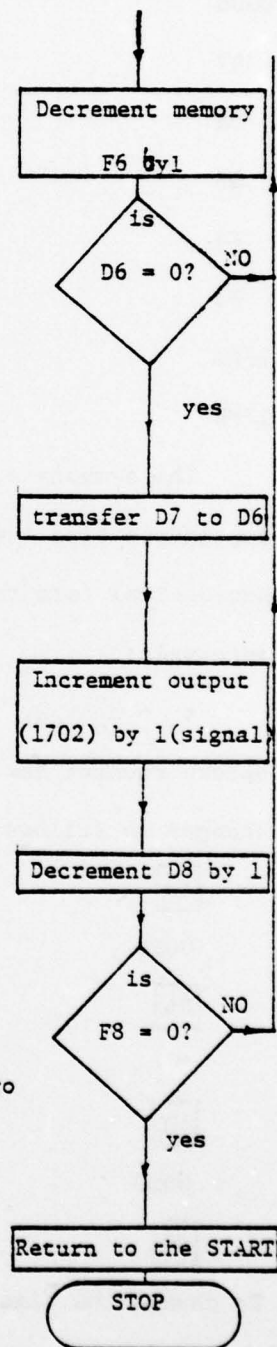
PROGRAM 02

ADDRESS	MACHINE CODE	OPERATION	
0000	8C	y 1703	START
01	03	y → 1703	Initialize
02	17		Port 1700 input
03	8E		Port 1702 output
04	01	x → 1701	
05	17		
06	A9	(FB) → A	Accumulator = FB
07	FB		
08	CD		
09	00	A − 1700	is input ≠ 0
0A	17		
0B	F0	Branch on non zero	
0C	F9		
0D	EE		yes
0E	02	1702 → 1702 + 1	Increment output by 1 (RESET)
0F	17		
0010	A9	(62) → A	Load the time
11	m=(64)*	Δt=0,1sec	base to the timer
12	8D		through the
13	07	A → 1707	accumulator
14	17		
15	EC		
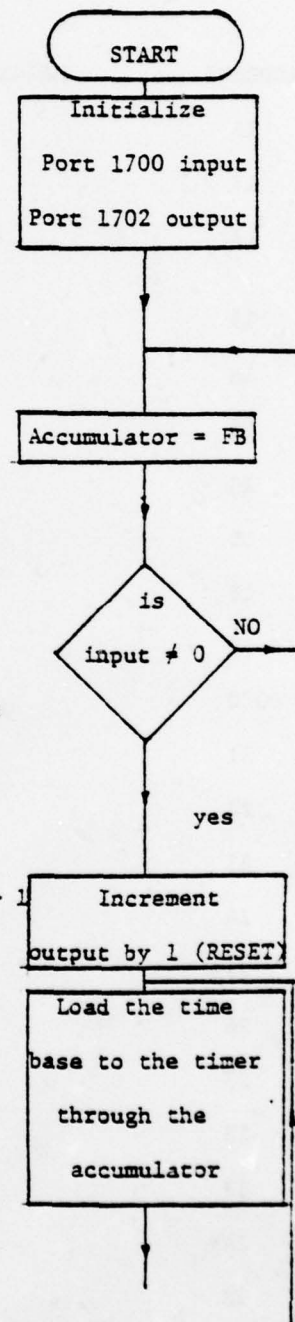
PROGRAM 02 (CONTINUED)

ADDRESS	MACHINE CODE	OPERATION
16	06	x-1706
17	17	
18	D0	Branch on zero
19	FB	
1A	C6	D6 → D6-1
1B	D6	
1C	E4	x-D6
1D	D6	
1E	D0	Branch on zero
1F	F)	
0020	EE	
21	02	1702 → 1702+1
22	17	
23	E6	D7 → D7+1
24	D7	
25	A5	D7 → A
26	D7	
27	85	A → D6
28	D6	
29	C9	A-(08)
2A	(08)*	#of pictures +1
2B	D0	Branch on zero
2C	D9	

is timers count = 0? NO

yes

Decrement D6 by 1

is D6 = 0? NO

yes

Increment output by 1(SIGNAL)

Increment D7 by 1

Transfer D7 to D6

is D7 = (08) NO

yes
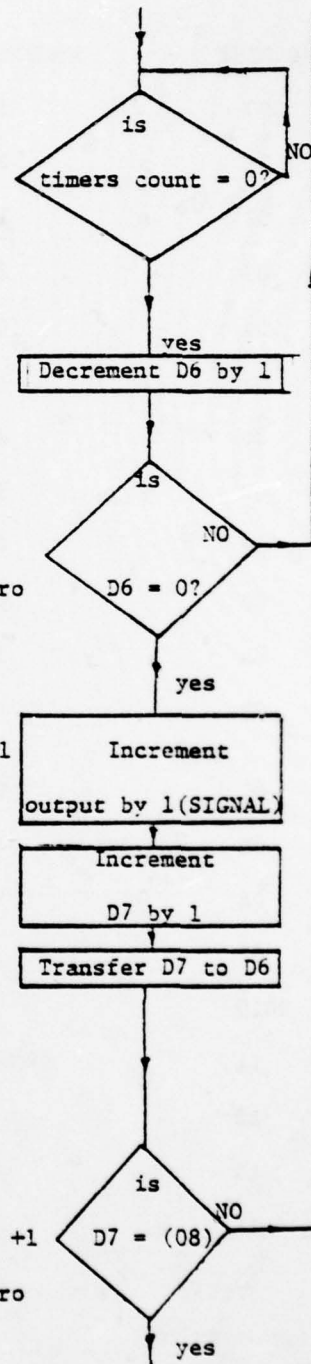
PROGRAM 02 (CONTINUED)

ADDRESS	MACHINE CODE	OPERATION
002D	84	
2E	D6	y → D6
2F	84	
0030	D7	y → D7
31	4C	
32	4F	GO TO START
33	1C	
	01	
	01	
00F4	01	y
00F5	00	x
17FA	00	NM1 Vector
17FB	1C	

```
        cont
   ┌─────────────┐
   │   D6 = 1    │
   │             │
   │   D7 = 1    │
   └─────────────┘
          │
   ┌─────────────┐
   │ RETURN TO THE│
   │    START    │
   └─────────────┘
          │
      (  STOP  )
```
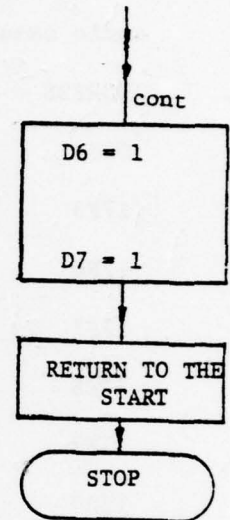
Each time the desired # of pictures changes

AD	002A	DA	# of pictures + 1
AD	0000	GO	

Each time the desired Δt changes

AD	0011	DE	$\# \; m = \dfrac{\Delta t(sec)}{0,001024}$
AD	C000	GO	

B3 TAPE RECORDER OPERATION

Once the program is loaded in the memory it can be dumped onto an audio cassette tape by the following procedure

ADDRESS	MACHINE CODE
00F1	00
17F5	00
17F6	00
17F7	FF
17F8	00
17F9	ID number of the program 01 or 02
1800	xx

Connect the microphon jack to the port M and start recording in the tape recorder then press GO. The display will go dark and as soon as the display relights showing 0000 XX the recording is finished.

B.3.2 For loading the microprocessors memory from the tape recorder use the following procedure

ADDRESS	MACHINE CODE
00F1	00
17F9	ID number of the program
1873	XX

Connect the earphone jack to the port 1 put the tape recorder in the play node and press GO. The display will go dark and as soon as the data record has been read. The display will relight showing 0000 XX. If the display relights and shows FFFF XX this means that the selected record has been located and read but that an error has occured during the reading of data.